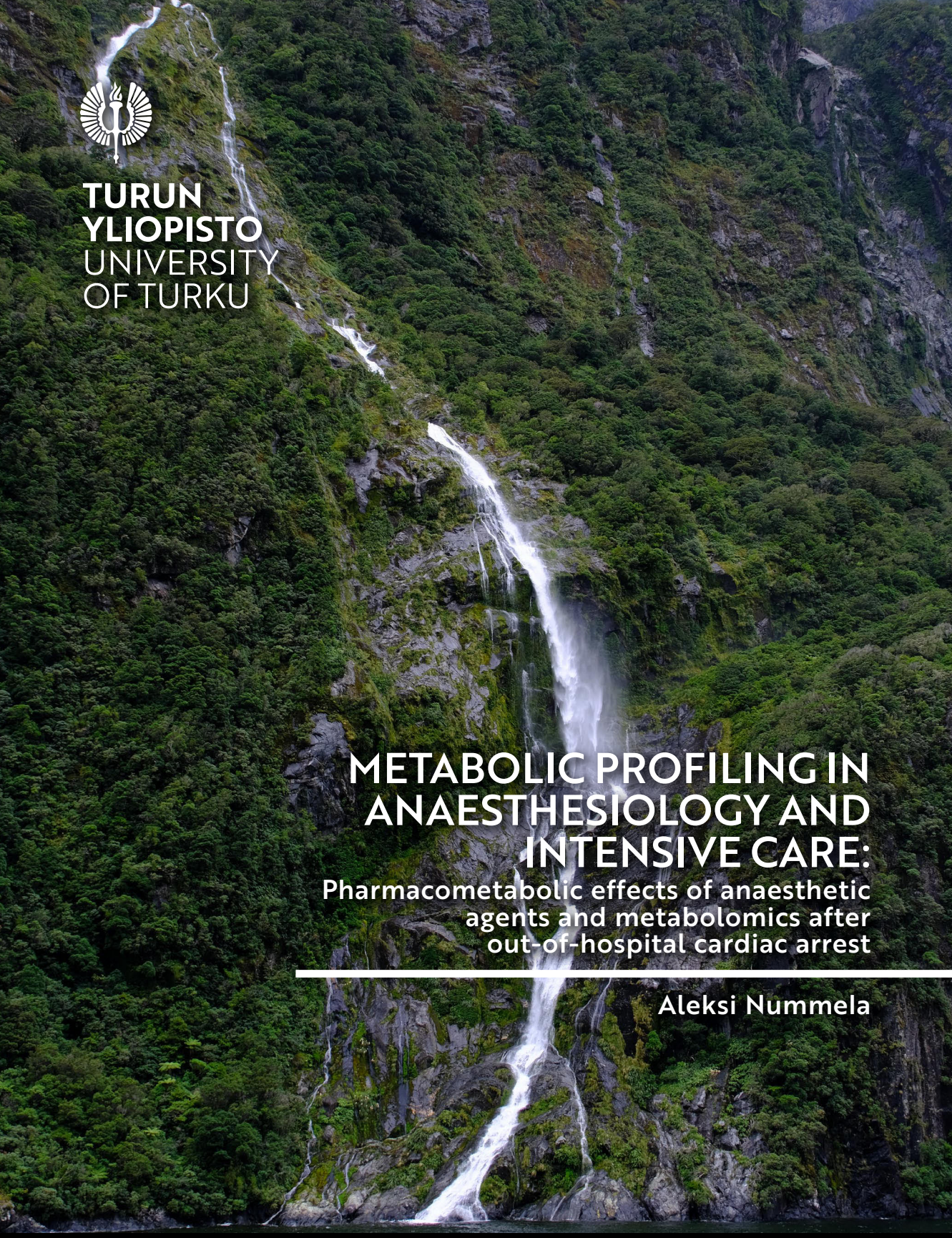

TURUN YLIOPISTO
UNIVERSITY OF TURKU

METABOLIC PROFILING IN ANAESTHESIOLOGY AND INTENSIVE CARE:

Pharmacometabolic effects of anaesthetic agents and metabolomics after out-of-hospital cardiac arrest

Aleksi Nummela

TURUN YLIOPISTON JULKAISUJA – ANNALES UNIVERSITATIS TURKUENSIS
SARJA – SER. D OSA – TOM. 1887 | MEDICA – ODONTOLOGICA | TURKU 2025

TURUN
YLIOPISTO
UNIVERSITY
OF TURKU

METABOLIC PROFILING IN ANAESTHESIOLOGY AND INTENSIVE CARE:

Pharmacometabolic effects of anaesthetic agents and metabolomics after out-of-hospital cardiac arrest

Aleksi Nummela

TURUN YLIOPISTON JULKAISUJA – ANNALES UNIVERSITATIS TURKUENSIS
SARJA – SER. D OSA – TOM. 1887 | MEDICA – ODONTOLOGICA | TURKU 2025

University of Turku

Faculty of Medicine
Department of Clinical Medicine
Anaesthesiology, Intensive Care, Emergency Care and Pain Medicine
Doctoral Programme in Clinical Research

Supervised by

Associate Professor Harry Scheinin

Integrative Physiology and Pharmacology
Institute of Biomedicine
University of Turku
Turku, Finland

Professor Timo Laitio

Anaesthesiology and Intensive Care
University of Turku
Turku University Hospital
Turku, Finland

Reviewed by

Associate Professor Tuomas Lilius

Division of Pharmacology and Pharmacotherapy
University of Helsinki
Helsinki, Finland

Department of Emergency Medicine and Services
University of Helsinki
Helsinki University Hospital
Helsinki, Finland

Professor Tuulia Hyötyläinen

School of Science and Technology
University of Örebro
Örebro, Sweden

Opponent

Professor Johanna Hästbacka

Anaesthesiology and Intensive Care
Tampere University Hospital
Tampere, Finland

Faculty of Medicine and Health Technology
University of Tampere
Tampere, Finland

The originality of this publication has been checked in accordance with the University of Turku quality assurance system using the Turnitin OriginalityCheck service.

Cover Image: Aleksi Nummela

ISBN 978-952-02-0219-4 (PRINT)
ISBN 978-952-02-0220-0 (PDF)
ISSN 0355-9483 (Print)
ISSN 2343-3213 (Online)
Painosalama, Turku, Finland 2025

“I know of no pleasure deeper than that which comes from contemplating the natural world and trying to understand it.” – Sir David Attenborough

To Eino

In the hope that you will grow to embrace creativity and curiosity on your journey of discovery.

UNIVERSITY OF TURKU
Faculty of Medicine
Department of Clinical Medicine
Anaesthesiology, Intensive Care, Emergency Care and Pain Medicine
ALEKSI NUMMELA: Metabolic profiling in anaesthesiology and intensive care: Pharmacometabolic effects of anaesthetic agents and metabolomics after out-of-hospital-cardiac arrest
Doctoral Dissertation, 184 pp.
Doctoral Programme in Clinical Research
June 2025

ABSTRACT

In metabolomics a “snapshot” of the current metabolic state of an organism, a metabolic profile, is obtained from biofluid samples. Despite emerging metabolomics studies in the field of clinical anaesthesia and intensive care, the effects of routinely used anaesthetics/sedatives on the circulating human metabolome have remained largely unexplored. Recently, metabolic profiling upon hospital admission in out-of-hospital cardiac arrest (OHCA) enabled stratification of patient risk groups with respect to mortality. Identification of previously unrecognized metabolic routes associated with patient outcome after OHCA might contribute to the discovery of novel biomarkers.

This study examined two separate study populations. First, a randomised controlled phase IV clinical drug trial in which 160 healthy male subjects received equipotent doses (EC_{50} for verbal command) of dexmedetomidine, propofol, S-ketamine, sevoflurane, or placebo. Nuclear magnetic resonance (NMR) spectroscopy and liquid chromatography tandem mass spectrometry targeted metabolic profiling was conducted at baseline, at the end of anaesthetic/sedative administration (at 60 min), and at 70 min after anaesthetic/sedative cessation. Second, a randomised 2-group phase II clinical drug trial of 110 OHCA patients receiving targeted temperature management at 33 °C alone or in combination with inhaled xenon. The NMR metabolic profile was analysed upon hospital admission and at 24 and 72 h.

In healthy male subject statistically significant changes *vs.* placebo were observed in 21.5%, 35.4%, 3.6% and 1.5% of the analysed 195 metabolites in dexmedetomidine, propofol, S-ketamine and sevoflurane groups, respectively. Dexmedetomidine caused e.g. a wide-ranging decrease in bile acids and oxylipins, S-ketamine decreased branched chain amino acids (BCAA), and propofol altered the lipid profile while 9,10- and 12,13-dihydroxyoctadecenoic acid were markedly increased. In contrast, sevoflurane demonstrated relative inertness. In OHCA patients at 24 h, increased levels of lactate and decreased amounts of BCAAs leucine and valine associated with 6-month mortality. At 72 h, increases in the levels of lactate and alanine, and a decreased small HDL cholesteryl ester content (S-HDL-CE) associated with mortality.

In conclusion, exposure to routinely used anaesthetics/sedatives triggered unique alterations in the metabolic profiles. Furthermore, in OHCA patients at 24 and 72 h the concentrations of lactate, alanine, leucine, valine, and S-HDL-CE associated with 6-month mortality. Xenon did not alter the NMR metabolic profile.

KEYWORDS: Metabolomics, oxylipin, dexmedetomidine, propofol, S-ketamine, sevoflurane, xenon, out-of-hospital cardiac arrest

TURUN YLIOPISTO
Lääketieteellinen tiedekunta
Kliininen laitos
Anestesiologia, tehohoito, ensihoito ja kivunhoito
ALEKSI NUMMELA: Metabolinen profilointi anestesiassa ja tehohoidossa: Anesteettien farmakometaboliset ominaisuudet ja sairaalan ulkopuolisen sydämenpysähdyksen metabolinen profiili.
Väitöskirja, 184 s.
Turun Kliininen Tohtoriohjelma
Kesäkuu 2025

TIIVISTELMÄ

Metabolinen profiili kuvaa elimistön aineenvaihduntareittien heijastumista esimerkiksi verenkierrossa tietyssä ajanhetkessä. Vaikka metabolomiikan tutkimus anestesian ja tehohoidon aloilla lisääntyy alati, anesteettien/sedatiivien aiheuttamista suorista vaikutuksista ihmisen metabolomiin on hyvin vähän tutkimustietoa. Sairaalaan saapuessa määritetyn metabolisen profiilin keinoin on pystytty erottelemaan potilaskuolleisuuden riskiryhmiä sairaalan ulkopuolisessa sydänpysähdyksessä (OHCA). Uusien OHCA-potilaan kuolleisuuteen vaikuttavien metabolisten reittien tunnistaminen saattaisi edesauttaa käyttökelpoisten merkkiaineiden löytämistä tulevaisuudessa.

Data on kerätty kahdessa eri tutkimusasetelmassa. Ensimmäinen on satunnaistettu kontrolloitu faasin IV kliininen lääketutkimus, jossa 160 terveelle mieskoehenkilöille annosteltiin (EC_{50} sanalliselle komennolle) deksmedetomidiinia, propofolia, S-ketamiinia, sevofluraania tai plaseboa. Verinäytteet kerättiin ennen lääkkeen annostelua, 60 minuutin kohdalla annostelun lopettamisen yhteydessä ja 70 minuuttia annostelun lopettamisen jälkeen. Kohdennettu metabolinen profilointi toteutettiin käyttäen magneettiresonanssispektroskopiaa (NMR) ja nestekromatografia-tandemmassaspektrometriaa. Toinen tutkimusasetelma on satunnaistettu kontrolloitu faasin II kliininen lääketutkimus, jossa 110 elvytettyä OHCA-potilasta hoidettiin tavoitteellisella lämpötilan hallinnalla (TTM) 33 °C asteessa tai TTM-hoitoon yhdistettiin hengitettävä ksenon. Verinäytteet NMR:lla toteutettuun metaboliseen profilointiin kerättiin sairaalaan saapuessa sekä 24 tunnin ja 72 tunnin kohdalla.

Terveillä koehenkilöillä 195 metaboliitista tilastollisesti merkittäviä muutoksia plaseboon verrattuna havaittiin 21.5% deksmedetomidiinilla, 35.4% propofolilla, 3.6% S-ketamiinilla ja 1.5% sevofluraanilla. Esimerkiksi dexmedetomidiini laski laaja-alaisesti sappihappo- ja oksilipiinipitoisuuksia, S-ketamiini laski haaraketjuisten aminohappojen pitoisuutta ja propofoli vaikutti rasva-aineenvaihduntaan sekä nosti huomattavasti 9,10- ja 12,13-dihydroksioktadekeenihappo-pitoisuuksia. Sevofluraanin vaikutukset olivat vähäisiä. OHCA-potilaiden 6 kuukauden kuolleisuuteen assosioitui 24 tunnin kohdalla laktaatti, leusiini ja valiini sekä 72 tunnin kohdalla laktaatti, alaniini ja pienten HDL-partikkelien kolesteryyliesteripitoisuus (S-HDL-CE).

Tutkimuksessa todettiin, että altistus edellä mainituille anesteeteille/sedatiiveille aiheutti kullekin lääkkeelle ominaisia muutoksia metabolisessa profiilissa. Lisäksi OHCA-potilailla havaittiin laktaatin, alaniinin, leusiinin, valiinin ja S-HDL-CE assosioituvan 6 kuukauden kuolleisuuteen. Ksenon ei aiheuttanut muutoksia määritettyyn metaboliseen profiiliin.

AVAINSANAT: Metabolomiikka, oksilipiini, deksmedetomidiini, propofoli, S-ketamiini, sevofluraani, ksenon, sairaalan ulkopuolinen sydänpysähdys

Table of Contents

Abbreviations

95% CI	95% confidence interval
AA	Arachidonic acid
AAA	Aromatic amino acid
Acetyl-CoA	Acetyl-coenzyme A
ACh	Acetyl choline
ALAT	Alanine aminotransferase
ANOVA	Analysis of variance
ARDS	Acute respiratory distress syndrome
ASA I	American Society of Anaesthesiologists class I
ASBT	Apical sodium-dependent bile acid transporter
ATP	Adenosine triphosphate
BAT	Brown adipose tissue
BBB	Blood-brain barrier
BCAA	Branched chain amino acids
BCAT	Branched chain aminotransferase
BCKA	Branched chain α-ketoacids
BCKDH	Branched chain α-ketoacid dehydrogenase complex
CAP	The cholinergic anti-inflammatory pathway
CNS	Central nervous system
COX	Cyclooxygenase
CPR	Cardiopulmonary resuscitation
CPT	Carnitine palmitoyltransferase
CYP	Cytochrome P450 mixed function oxidase enzymes
DGLA	Dihomo-γ-linoleic acid
DHET	Dihydroxyeicosatrienoic acid
EC_{50} for verbal command	Effective consentration at which 50% of subjects would be expected to be unresponsive to a verbal command
EET	Epoxyeicosatrienoic acids
EM	Electromagnetic
EMS	Emergency medical services

EPA	Eicosapentaenoic acid
EpOME	Epoxyoctadecenoic acid
EudraCT	European Union Drug Regulating Authorities Clinical Trials
DiHETE	Dihydroxyeicosatetraenoic acid
DiHOME	Dihydroxyoctadecenoic acid
DHA	Docosahexaenoic acid
$FADH_2$	Flavin adenine dinucleotide (reduced)
FAO	Fatty-acid β-oxidation
FXR	Farnesoid X receptor
GABA	γ-aminobutyric acid
GlycA	Inflammatory marker glycoprotein acetylation
HCO	7α-Hydroxy-4-cholesten-3-one
HDL	High-density lipoprotein particle
HETE	Hydroxyeicosatetraenoic acid
HODE	Hydroxyoctadecadienoic acid
HOTrE	Hydroxyoctadecatrienoic acid
HR	Hazard ratio
ICU	Intensive care unit
IDL	Intermediate-density lipoprotein particle
IRI	Ischaemia-reperfusion injury
KODE	Keto-octadecadienoic (i.e. oxo-octadecadienoic) acid
LA	Linoleic acid
LCAT	Lecithin:cholesterol acyltransferase
LC-MS/MS	Liquid chromatography tandem mass spectrometry
LDL	Low-density lipoprotein particle
LLOQ	Lower limit of quantification
LNAA	Large neutral amino acids
LOX	Lipoxygenase
LPL	Lipoprotein lipase
LPS	Lipopolysaccharide
MAPK	Mitogen-activated protein kinase
MRI	Magnetic resonance imaging
MRM	Multiple reaction monitoring
MyD88	Myeloid differentiation primary response gene 88
m/z ratio	Mass-to-charge ratio
NAD^+	Nicotinamide adenine dinucleotide (oxidised)
NADH	Nicotinamide adenine dinucleotide (reduced)
Na^+/K^+-ATPase	Sodium-potassium adenosine triphosphatase
NF-κB	Nuclear factor κB

NMDA	N-methyl-D-aspartate
NMR	Nuclear magnetic resonance spectroscopy
OHCA	Out-of-hospital cardiac arrest
PCAS	Post-cardiac arrest syndrome
PCI	Percutaneous coronary angiography interventions
PET	Positron emission tomography
PLA_2	Phospholipase A_2
PRIS	Propofol infusion syndrome
PUFA	Polyunsaturated fatty acids
RASS scale	Richmond agitation-sedation scale
RCT	Reverse cholesterol transport
RF	Radiofrequency
ROS	Reactive oxygen species
ROSC	Return of the spontaneous circulation
SD	Standard deviation
SDS	Standard deviation score
sEH	Soluble epoxide hydrolase
SFA/FA	Saturated fatty acids to total fatty acids ratio
S-HDL-CE	Small high-density lipoprotein cholesteryl ester content
S/N ratio	Signal-to-noise ratio
STEMI	ST elevation myocardial infarction
TBI	Traumatic brain injury
TCA cycle	Tricarboxylic acid cycle
TLR	Toll-like receptor
TNF	Tumour necrosis factor
TTM	Targeted temperature management
TUDCA	Tauroursodeoxycholic acid
VF	Ventricular fibrillation
VLDL	Very-low-density lipoprotein particle
VT	Ventricular tachycardia
XXL-M VLDL	Chylomicrons and extremely large to medium VLDL particles
α7nAChR	The α7 subunit of the nicotinic acetyl choline receptor

List of Original Publications

This dissertation is based on the following original publications, which are referred to in the text by their Roman numerals:

I Nummela A., Laaksonen L., Laitio T., Kallionpää R., Långsjö J., Scheinin J., Vahlberg T., Koskela H., Aittomäki V., Valli K., Revonsuo A., Niemi M., Perola M., Scheinin H. Effects of dexmedetomidine, propofol, sevoflurane and S-ketamine on the human metabolome: A randomised trial using nuclear magnetic resonance spectroscopy. *European Journal of Anaesthesiology*, 2022; 39: 521-532.
https://doi.org/10.1097/EJA.0000000000001591

II Nummela A., Laaksonen L., Scheinin A., Kaisti K., Vahlberg T., Neuvonen M., Valli K., Revonsuo A., Perola M., Niemi M., Scheinin H., Laitio T. Circulating oxylipin and bile acid profiles of dexmedetomidine, propofol, sevoflurane and S-ketamine: A randomised controlled trial using tandem mass spectrometry. *British Journal of Anaesthesia Open,* 2022; 4: 100114.
https://doi.org/10.1016/j.bjao.2022.100114

III Nummela A., Scheinin H., Perola M., Joensuu A., Laitio R., Arola O., Grönlund J., Roine R., Bäcklund M., Vahlberg T., Laitio T. for the Xe Hypotheca Collaboration Group. A metabolic profile of xenon and metabolite associations with 6-month mortality after out-of-hospital cardiac arrest: A post-hoc study of the randomised Xe-Hypotheca trial. *PLoS One,* 2024; 19: e0304966.
https://doi.org/10.1371/journal.pone.0304966

1 Introduction

After the ground-breaking work of Watson, Crick and other esteemed scientists on discovering the double-stranded nature of DNA[1], the scientific community placed their hopes on whole exome sequencing to reveal the mysteries of life, sickness and health. However, unravelling the genome was only the first step in understanding the complexities of biological systems. A plethora of processes modify gene transcription into messenger RNA and translation of messenger RNA into proteins. Epigenetic modelling, gene enhancer regions and alternative RNA splicing are just a few exemplars of intracellular editing processes in the route from genes to active proteins, affecting the current state of a cell at any given time. These processes give rise to increasing levels of complexity by which the current state of cells can be assessed. The transcriptome is a manifestation of genomic transcription while the proteome is the outcome after messenger RNA translation into proteins. The complexity increases substantially, when cell-to-cell interactions of differentiated cell lines within the organism form an intricate weave of interconnected metabolic pathways. These pathways aim to maintain homeostasis against an everchanging internal and external environment of the organism in order to facilitate survival. Often, the pathways are further connected to the metabolism of other organisms, be it with the symbiotic microbes in the

Figure 1. The metabolome – A schematic representation

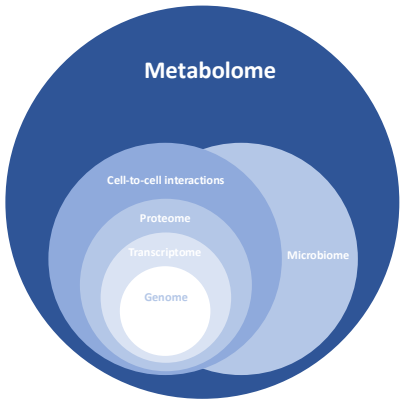

The metabolome is a snapshot of the organism's active metabolic state arising from gene expression, protein synthesis, the intricate weave of interconnected metabolic pathways and cell-to-cell interactions and, to some extent, the interactions between the microbiome and the host.

microbiome of the gastrointestinal tract of a human or a pathogenic microbe invading a host (Fig. 1). This striving towards the maintenance of homeostasis may be reflected in the bloodstream, or other biological fluids, via the circulating metabolites.

Metabolomics has shown promising results in multiple facets of medical science, including early diagnostics[2–12], biomarker discovery[13–15], stratification of disease risk-groups[14,16–21] and pharmacotherapy[22–34]. Despite emerging metabolomics studies in the field of clinical anaesthesia and intensive care, the isolated effects of routinely used anaesthetics/sedatives on the human metabolome have remained largely unexplored. From the perspective of biomarker discovery and risk-group stratification, out-of-hospital cardiac arrest (OHCA) is an area of intense research.

OHCA is one of the leading causes of premature mortality in the developed countries, claiming annually 3.7 million lives worldwide[35]. OHCA carries a relatively poor prognosis, leading to death or permamanent neurological damage despite prompt resuscitation and advanced life support. In the intensive care unit (ICU), prediction of outcome in post-resuscitation OHCA is a challenge. It has been shown that a reliable prognostic estimation requires the adoption of multimodal approaches combining electroencephalography, magnetic resonance imaging (MRI) and circulating biomarkers of hypoxic ischaemic cerebral damage[36]. Nonetheless, the optimal multimodal model remains to be established and thus the search for viable biomarkers is ongoing. Previously, metabolic profiling upon hospital admission has enabled a stratification of patient risk groups with respect to mortality[37]. Furthermore, changes in a targeted metabolic profile have been observed in response to targeted temperature management (TTM) at 33 °C vs. 36 °C, with several of the metabolites affected associating with patient mortality at 6 months[38]. It can be argued that replicating previous findings or identifying previously unrecognized metabolic routes associated with patient outcome in post-resuscitation OHCA might contribute to future biomarker discovery.

By analysing metabolomics data from two distinct and rigorously planned experimental protocols, this thesis aims to characterise the metabolic effects of certain widely used anaesthetics and sedatives (Studies I and II) and xenon (Study III), and to identify previously unrecognised metabolic routes associated with patient mortality in postresuscitation OHCA (Study III). In studies I and II, the effects of dexmedetomidine, propofol, S-ketamine and sevoflurane were investigated with targeted nuclear magnetic resonance spectroscopy (NMR) spectroscopy and liquid chromatography tandem mass spectrometry (LC-MS/MS) metabolic profiles to discover, characterise and compare the way these anaesthetic agents and sedatives interact with the metabolic pathways in healthy human volunteers. Metabolite subgroups of apolipoproteins and lipoproteins, cholesterol, glycerides and phospholipids, fatty acids, glycolysis, amino acids, ketone bodies, creatinine and

albumin, and the inflammatory marker glycoprotein acetylation (GlycA) were analysed with NMR. Oxylipin and bile acid profiles were quantified using LC-MS/MS. In study III, the same NMR methodology was implemented in OHCA patients randomised to receive TTM at 33 °C with or without inhaled xenon to search for previously unrecognised metabolic routes associating with 6-month mortality, the effects of inhaled xenon on the circulating metabolic profile were also investigated.

2 Review of the Literature

2.1 Targeted metabolic profiles

Metabolomics is an application of systems biology, utlising large scale data-capturing methods to reveal a metabolic profile; i.e. creating a "snapshot" from biofluid samples of the current metabolic state of an organism. Metabolomics relies on robust and large-scale data-capturing methods, most often utilising sophisticated technologies such as LC-MS/MS and NMR. In the field of metabolomics, data acquisition tends to follow one of two distinct approaches: Targeted versus non-targeted metabolomics. Targeted metabolomics focuses on a specific set of predetermined metabolites, chosen based on their role in the metabolic pathways of interest taking account of the technological limitations, feasibility and effectiveness of the quantification. In a non-targeted approach, all detectable metabolite signals are extracted from a sample for later identification without *a priori* knowledge of specific metabolites of interest. In the field of medicine, metabolomics has provided promising results in early diagnostics[2–12], stratification of disease risk groups[14,16–21], biomarker discovery[13–15] and pharmacotherapy[22–34].

Pharmacometabolomics examines the pharmacotherapy-induced shifts in the metabolic profile. These changes in the biochemical pathways may eventually enable the identification of baseline predictors of patient response via biomarker acquisition, offer an opportunity to enhance early prediction of treatment outcomes, reveal novel mechanisms of drug action and identify the metabolic pathways contributing to drug response phenotypes[24,26,31,33,39]. In the future, pharmacometabolomics may eventually provide novel tools for clinical decision-making and the optimisation of personalised medical therapy. Previous research on pharmacometabolomics has focused on long-term treatments such as statins, proprotein convertase subtilisin/kexin 9 inhibitors, metformin, sertraline and hormonal contraception, with an aim to characterise drug-related changes in the metabolome and/or predict the response to pharmacotherapy[24,26,30,31,40], or adverse events related to pharmacotherapy[25,27,41].

In contrast, the acute effects of intravenous or inhalational anaesthetics/sedatives dexmedetomidine, propofol, S-ketamine, sevoflurane and especially inhaled xenon on the circulating metabolic profile in humans have remained largely unexplored. Prior to the current study, it was unsure whether or not there would be an observable acute metabolic response to anaesthetics/sedatives after 1-hour anaesthetic/sedative administration at moderate dosing. Additionally, at the time of metabolite analysis, the literature on metabolomics of OHCA and TTM was relatively scarce, and the metabolite coverage of the targeted NMR methodology was considered relevant in this context. Thus, the targeted NMR and LC-MS/MS methodologies were chosen based on metabolite coverage in several metabolic routes of interest, cost-effectiveness, feasibility and availability.

2.2 Metabolic pathways

2.2.1 Cholesterol, lipoproteins, apolipoproteins

The metabolism of cholesterol, lipoproteins and apolipoproteins are connected to several processes of interest in the context of the current study. First, propofol is administered in a lipid emulsion and propofol-induced hypetriglyceridaemia is a known complication of prolonged propofol infusion in the ICU setting[42]. Moreover, propofol-induced changes in cellular bioenergetics via fatty-acid β-oxidation (FAO) have been reported[43,44]. Second, adrenergic receptors are connected to lipid metabolism[45–47]. The adrenergic response to acute critical illness in the context of OHCA might alter the lipid profile. Furthermore, adrenergic receptors are of interest due to the dexmedetomidine-induced α_2-adrenoceptors agonism as well as the effect of S-ketamine on catecholamines[48,49]. Third, it is possible that lipoproteins might be affected in OHCA patients with a high incidence of ischaemic heart disease and acute myocardial ischaemia[50]. All of the quantified metabolites under the subcategory of cholesterol, lipoproteins and apolipoproteins have been summarised in Table 1.

Table 1. Cholesterol, lipoprotein and apolipoprotein metabolites in the current study

Metabolites analysed	**Subgroups**	**Modality of quantification**
Cholesterol	Serum total cholesterol. Total cholesterol in VLDL, LDL, HDL, HDL_2 and HDL_3. Remnant cholesterol, esterified cholesterol, free cholesterol.	NMR
Apolipoproteins (apo)	ApoA1, apoB and apoB/apoA1 ratio.	NMR
Lipoproteins		
Very-low-density lipoprotein particle (VLDL)	Chylomicron and VLDL particle concentrations. Particle total lipid, phospholipid, total cholesterol, cholesteryl ester, free cholesterol and triglyceride content. Particle diameter.	NMR
Intermediate-density lipoprotein particle (IDL)	IDL particle concentration. Particle total lipid, phospholipid, total cholesterol, cholesteryl ester, free cholesterol and triglyceride content.	NMR
Low-density lipoprotein particle (LDL)	LDL particle concentration. Particle total lipid, phospholipid, total cholesterol, cholesteryl ester, free cholesterol and triglyceride content. Particle diameter.	NMR
High-denisty lipoprotein particle (HDL)	HDL particle concentration. Particle total lipid, phospholipid, total cholesterol, cholesteryl ester, free cholesterol and triglyceride content. Particle diameter.	NMR

Cholesterol can be biosynthesized by all mammalian cells. Nonetheless, in humans 50% of total cholesterol synthesis occurs in the liver. In the cell, the majority of cholesterol resides in the cell membranes where it regulates the rigidity, fluidity and permeability of the lipid bilayer. Furthermore, it serves as a precursor for the synthesis of steroid hormones and bile acids. The dynamic balance of biosynthesis, uptake, export and esterification is reflected in cellular cholesterol levels. The regulatory steps of this process have been reviewed by Luo and colleagues[51].

Briefly, cholesterol *de novo* biosynthesis begins from acetyl-coenzyme A (acetyl-CoA) and is carried out by numerous enzymatic processes, most of which are located in the endoplasmic reticulum with 3-hydroxy-3-methyl-glutaryl-coenzyme

A reductase and squalene monooxygenase being the rate limiting steps[51]. From dietary sources, the presence of Nieman-Pick type C1-like 1 protein at the apical surface of enterocytes is a central effector in facilitating cholesterol absorption[52,53].

Lipoprotein transportation of lipids and cholesterol can be simplified into 3 categories: Exogenous, endogenous and reverse cholesterol transport (RCT) pathways[54]. The liver serves as a central hub for endogenously synthesized and exogenously acquired cholesterol redistribution. Lipoprotein particles consist of a lipid core of mainly cholesteryl esters and triglycerides enclosed in a phospholipid monolayer as well as certain apolipoproteins. They are divided into subcategories based on their size, lipid composition and apolipoproteins: Chylomicrons, chylomicron remnants, very-low-density lipoprotein particle (VLDL), intermediate-density lipoprotein particle (IDL), low-density lipoprotein particle (LDL), high-density lipoprotein particle (HDL) and lipoprotein (a)[51,53]. Apolipoproteins perform several functions e.g. guiding lipoprotein formation, contributing to lipoprotein structure, acting as ligands for lipoprotein receptors and modifying lipoprotein metabolism by activating or inhibiting specific enzymes[53].

Lipoprotein transport via the exogenous pathway is facilitated by chylomicrons transferring dietary-acquired fatty acids and cholesterol (e.g. as triglycerides and cholesteryl esters, respectively) from enterocytes to the peripheral tissues and eventually to the liver. Chylomicron constituent apolipoproteins include a truncated form of hepatic apoB-100, apoB-48. In enterocytes, apo-IV is added to nascent chylomicrons, resulting in the formation of lipoprotein-rich chylomicrons which are secreted in the lymph eventually entering the venous circulation. Lipoprotein lipase (LPL) catalyses the hydrolysis of chylomicron triglycerides forming chylomicron remnants. The recognition of these remnants by hepatic receptors for elimination is facilitated by apoE[53].

The endogenous pathway of lipoprotein mediated lipid transport to peripheral tissues begins with the synthesis of apoB100 in the hepatocyte. Initially, in conditions of lipid abundance, apoB100 is transferred to the rough endoplasmic reticulum, triglycerides are added to apoB100 by microsomal triglyceride transfer protein forming pre-VLDL. In the smooth endoplasmic reticulum, TG-rich nascent VLDL are formed containing small proportions of free cholesterol, cholesteryl esters and phospholipids. Both endo- and exogenously acquired cholesterol and lipids are transferred to peripheral tissues via VLDL transport. Eventually, LPL mediated hydrolysis of the VLDL's triglyceride core forms IDL consisting of nearly equal proportions of triglycerides and cholesteryl esters. Further metabolism of IDL triglycerides may form apoB100 containing remnant lipoproteins absorbed by the liver, or TG-depleted cholesteryl-ester-rich apoB100 containing LDL. LDL can be taken up by peripheral tissues by receptor mediated endocytosis via the LDL receptor[53,55]. Interactions between the lipoprotein particle and LPL are governed by

several apolipoproteins such as apoB100, apoCII, apoCIII and apoE[53]. In peripheral tissues, surplus cholesterol is stored as cholesteryl esters, a conversion which is carried out by acyl coenzyme A:cholesterol acyltransferase. In most cell types, cholesteryl esters are present only at low levels stored in cytosolic lipid droplets. In steroidogenic organs, cholesteryl esters are utilised as cholesterol reservoirs for steroid synthesis[56]. In the circulation, cholesteryl esters are present as a major constituent of VLDLs, IDLs, LDLs, and via cholesteryl ester transfer protein also in HDLs[53].

HDL is a central effector in RCT, which ensures cholesterol efflux from peripheral cells lacking ways to catabolise cholesterol (including foam cells in atherosclerotic plaques) to the liver and eventually excretion via bile either directly or after transformation to bile-acids/salts[57,58]. Apoliprotein A-I is the major structural component of HDL, which is secreted as pre-apoA-I from hepatic and intestinal endoplasmic reticulum, the conversion to apoA-I occurs in plasma. Lipid free apoA-I forms nascent HDL via the transfer of free cholesterol and phospholipids in a process involving, among others, adenosine triphosphate (ATP) binding cassette transporter A1 in the liver, intestine or foam cells[53]. Nascent HDL is converted to HDL upon free cholesterol esterification by lecithin:cholesterol acyltransferase (LCAT) forming cholesteryl esters. HDL consists of a core of cholesteryl esters and triglycerides stabilised by a phospholipid layer and apolipoproteins, mainly apoA-I[57]. Furthermore, LCAT modifies the structure of HDL by transferring fatty acyl chains to free cholesterol, relocating these new cholesteryl esters to the core of the growing HDL, forming spherical cholesteryl ester -rich HDL_3 and eventually HDL_2[53]. Cholesterol efflux to HDL from foam cells in atherosclerotic plaques is mediated by the ATP binding cassette transporter G1 and G4, as well as the scavenger receptor B1. In addition to the direct transfer of HDL cholesteryl esters from the periphery to the liver for elimination via the hepatic scavenger receptor B1, an alternative pathway exists. In this indirect RCT pathway, triglycerides and cholesteryl esters are exchanged between apoB100 containing lipoproteins (namely VLDL, VLDL remnants, IDLs and LDLs) and HDL by the action of cholesteryl ester transfer protein, the net overall effect is a transfer of cholesteryl esters from HDL to the other aforementioned lipoproteins, and triglycerides to HDL from those lipoproteins. Eventually, LDL cholesteryl ester uptake in the liver is facilitated via the LDL receptor[53,59].

2.2.2 Fatty acids

Fatty acid metabolism shares many interesting connections to the anaesthetics/sedatives and OHCA as described earlier in the context of cholesterol,

lipoproteins and apolipoproteins. Concerning fatty acid metabolism, the metabolic response to propofol infusion is of special interest due to the lipid emulsion of propofol and the bioenergetic properties of propofol emulsion on FAO[43,44]. Moreover, polyunsaturated fatty acids (PUFA) act as precursors compounds e.g. for oxylipin synthesis which will be discussed in more detail later. In the context of OHCA, the level of linoleic acid (LA) was decreased upon hospital admission in non-survivors[37]. All of the quantified metabolites under the subcategory of fatty acids have been summarised in Table 2.

Table 2. Fatty acid metabolites in the current study

Metabolites analysed	**Modality of quantification**
Arachidonic acid (n-6)	LC-MS/MS
22:6 docosahexaenoic acid (n-3)	NMR
Eicosapentaenoic acid (n-3)	LC-MS/MS
Estimated degree of unsaturation	NMR
18:2 linoleic acid (n-6)	NMR
Monounsaturated fatty acids	NMR
Omega-3 fatty acids (n-3)	NMR
Omega-6 fatty acids (n-6)	NMR
Polyunsaturated fatty acids	NMR
Ratio of docosahexaenoic acid to total fatty acids	NMR
Ratio of linoleic acid to total fatty acids	NMR
Ratio of monounsaturated fatty acids to total fatty acids	NMR
Ratio of omega-3 fatty acids to total fatty acids	NMR
Ratio of omega-6 fatty acids to total fatty acid	NMR
Ratio of polyunsaturated fatty acids to total fatty acids	NMR
Ratio of saturated fatty acids to total fatty acids	NMR
Saturated fatty acids	NMR
Total fatty acids	NMR

Omega-3 and -6 fatty acids are denoted as n-3 and n-6, respectively.

Fatty acids obtained from dietary or endogenous sources, serve numerous crucial roles in human biology. They play a central role in energy metabolism and storage, and act as metabolic precursors for the production of a vast array of bioactive lipids. Fatty acids consist of a carboxylic group and a saturated or unsaturated aliphatic hydrocarbon chain, glyceride-bound fatty acids forming triglycerides, serving as neutral storage form of fatty acids. The division of saturated and unsaturated fatty acids is determined by the presence of one or more double bonds in the hydrocarbon

chains of the unsaturated fatty acids. The nomenclature "omega" in the context of fatty acids refers to the methyl end of the hydrocarbon chain i.e. omega-6 fatty acid signifies that the carbon-carbon double bond is at the sixth carbon counting from the methyl end, i.e. n-6. PUFA contain two or more double bonds in their hydrocarbon chains. An extensive review of hepatic fatty acid and triglyceride metabolism has been published by Alves-Bezerra and Cohen[60].

In brief, three major sources of fatty acids for hepatic fatty acid metabolism exist: Dietary, *de novo* synthesized fatty acids and adipose tissue derived fatty acids. After hydrolysis of dietary triglycerides primarily by pancreatic lipase, bile acid facilitated absorption of free fatty acids occurs from intestinal lumen and subsequently the resynthesis of triglycerides in enterocytes. This is followed by chylomicron-mediated transport via the lymphatic system eventually to the circulation where much of the triglycerides are taken up by muscle and adipose tissue in an LPL mediated process as discussed earlier. In situations where carbohydrates are abundant, *de novo* lipogenesis occurs in the liver, a process activated by plasma insulin. When plasma insulin levels are low e.g. in the fasting state, lipolysis from adipose tissue refreshes the plasma fatty acid pool that is available for uptake by the liver.

In the circulation, fatty acids are largely albumin-bound. Upon entry to the hepatocytes, fatty acids are esterified to glycerol-3-phosphate and to cholesterol, forming triglycerides and cholesteryl esters respectively, which are then stored in cytoplasmic lipid droplets or secreted into the bloodstream within VLDL. During fasting, stored fatty acids serve as an energy supply via FAO and a substrate for ketone body production[53,60]. Mitochondrial FAO generates acetyl-CoA and reducing equivalents i.e. reduced nicotinamide adenine dinucleotide (NADH, while the oxidised form is abbreviated NAD^+) and flavin adenine dinucleotide ($FADH_2$) which are linked to the tricarboxylic acid (TCA) cycle and oxidative phosphorylation to yield ATP. During fasting, FAO provides up to 80-90% of cellular energy requirements, with acetyl-CoA derived ketone bodies being especially important in the central nervous system (CNS). FAO occurs in the mitochondria and the transportation of fatty acids depends on the chain length. Short- and medium-chain fatty acids (C_4-C_6, C_8-C_{12} carbon atom lengths, respectively) diffuse freely across plasma and mitochondrial membranes. The cellular uptake of long-chain fatty acids (C_{14}-C_{20}) occurs via both passive diffusion and active carrier-mediated mechanisms. Faty acids are converted to their respective fatty acyl-coenzyme A esters by fatty acyl-coenzyme A synthetases e.g. long-chain acyl-coenzyme A synthetase for long chain fatty acids. Long-chain fatty acyl-coenzyme A esters require transport via the carnitine shuttle mechanism to traverse the mitochondrial membrane and access FAO. There are several enzymes involved in the carnitine shuttle e.g. carnitine palmitoyltransferase (CPT) I, CPT II, and carnitine acylcarnitine translocase[61]. In

addition to their central role in energy metabolism, fatty acids are important precursors in the synthesis of phospholipids and for example oxylipins.

2.2.3 Ketone bodies

Ketone bodies, i.e. acetone, acetoacetate and 3-hydroxybutyrate, function as oxidative fuels especially in situations when carbohydrates are in short supply. In addition to their role in energy metabolism, ketone bodies serve as metabolic and signalling regulators and lipogenic precursors. The way in which ketone body metabolism is interwoven into many crucial metabolic pathways such as FAO, the TCA cycle, gluconeogenesis, *de novo* lipogenesis and sterol biosynthesis, underscores the importance of ketone bodies in maintaining homeostasis. As discussed in the context of cholesterol, lipoproteins, apolipoproteins and fatty acids, the studied anaesthetics/sedatives have several properties of potential interest which might be connected to ketone body metabolism. In the context of OHCA, the catabolic state induced by an acute critical illness is likely to affect ketone metabolism. All of the quantified metabolites under the subcategory of ketone bodies have been summarised in Table 3.

Table 3. Ketone body metabolites in the current study

Metabolites analysed	Modality of quantification
Acetate	NMR
Acetoacetate	NMR
3-hydroxybutyrate	NMR

Plasma acetate is generated mainly via three routes, exogenous acetogenesis e.g. via the breakdown of dietary fibers by the microbial flora in the intestines, endogenous acetogenesis from acetyl-CoA hydrolysis in the liver or exogenous acetate, and from the diet (e.g. dairy products, vinegar, ethanol). The central metabolic fate of acetate is the acetyl-CoA-synthetase mediated formation of acetyl-CoA, which serves as a nexus between glycolysis and the TCA cycle and it is thus an important substrate for many metabolic pathways e.g in the synthesis of cholesterogenesis and *de novo* lipogenesis[62,63].

In humans, ketone bodies are predominantly of hepatic origin and are synthesised from FAO derived acetyl-CoA with a rate proportional to total fat oxidation. Moreover, during fasting, the catabolism of amino acids (especially leucine) accounts for approximately 4% of the ketone body pool via acetyl-CoA

formation. After acetyl-CoA is metabolised into acetoacetyl-coenzyme A, the fate-committing step via the hepatic mitochondrial isoform of 3-hydroxymethylglutaryl-coenzyme A synthase occurs forming hydroxymethylglutaryl-coenzyme A which is then cleaved to produce acetyl-CoA and acetoacetate. The latter compound is then reduced to 3-hydroxybutyrate by phosphatidylcholine-dependent mitochondrial 3-hydroxybutyrate dehydrogenase in a reaction favoring 3-hydroxybutyrate production, and furthermore the ratio of acetoacetate/3-hydroxybutyrate is directly proportional to the mitochondrial NAD^+/NADH ratio[63]. Lipolysis (formation of fatty acids from triglycerides), transport to and from the hepatocyte's plasma membrane, transport to mitochondria via CTP1, FAO, the activity of the TCA cycle and the concentrations of its intermediate metabolites, hormonal regulators (primarily glucagon and insulin) are the major regulators of ketogenesis[63]. The metabolic fate of hepatic ketone bodies is mainly to be catabolized in the mitochondria of extrahepatic tissues to acetyl-CoA to feed the TCA cycle yielding energy via terminal oxidation, although to some extent they are diverted to lipogenesis or sterol synthesis or excreted in the urine. Furthermore, ketone bodies contribute to anti- and proinflammatory responses, oxidative-stress-mitigation and even epigenetics, as extensively reviewed by Puchalska and Crawford[63].

2.2.4 Glycerides and phospholipids

The triglycerides are the most relevant members of the glyceride group in the context of the current study and the potential mechanisms that might link the currently studied anaesthetics/sedatives to triglyceride metabolism have been discussed in detail in the previous chapters. Moreover, it is known that cell membrane phospholipids act as a reservoir for oxylipin precursors as will be discussed[64]. All of the quantified metabolites under the subcategory of glycerides and phospholipids have been summarised in Table 4.

Table 4. Glyceride and phospholipid metabolites in the current study

Metabolites analysed	Modality of quantification
Phosphatidyl choline and other cholines	NMR
Ratio of triglycerides to phosphoglycerides	NMR
Serum total triglycerides	NMR
Sphingomyelins	NMR
Total cholines	NMR
Total phosphoglycerides	NMR
Triglycerides in very-low-density lipoprotein particles	NMR
Triglycerides in low-denisty lipoprotein particles	NMR
Triglycerides in high-denisty lipoprotein particles	NMR

Glycerides are esters of glycerol and fatty acids, with the most relevant for the current study being triglycerides that have been discussed earlier. In phospholipids, a hydrophilic phosphate group is attached to two hydrophobic fatty acids via an alcohol residue; in the context of glycerol, the resulting molecule is called a glycerophospholipid. The groups attached to the alcohol residue are denoted by “sn1” and “sn2” binding fatty acids and “sn3” binding the polar headgroup. The amphipathic nature of phospholipids enables the formation of lipid bilayers in aqueous solutions e.g. forming cellular membrane structures. Phospholipids are subdivided based on the polar headgroup into phosphatidyl choline, phosphatidyl ethanolamine, phosphatidyl glycerol, phosphatidyl inositol and phosphatidyl serine. A further division into molecular species depends on the fatty acid composition at the sn1 and sn2 positions in the glycerol backbone. The synthesis and remodelling of phospholipids occurs via several interconnected pathways, including Kennedy pathway (phosphatidyl choline, phosphatidyl ethanolamine synthesis), the cytidine diphosphate diacylglycerol pathway (synthesis of phosphatidyl serine and

phosphatidyl inositol), and the Lands cycle (fatty acid removal and reattachment to phospholipids), further discussion of this is outwith the scope of the current study[65].

In addition to their central role in cell membrane structures, phospholipids have an important role in the context of immunity, vascular inflammation, cell-to-cell communication, the regulation of hemostasis and thrombosis. This is exemplified by the observations that the oxylipin precursor PUFAs, for example arachidonic acid (AA), LA, docosahexaenoic acid (DHA) and eicosapentaenoic acid (EPA) are strongly represented in the phospholipids of blood cells. Furthermore, in immune cells, AA, the precursor for many immunomodulative and vasoactive oxylipins, is present at sn2 in at least a 10-fold higher concentration than other PUFAs. Upon immune cell activation, phospholipase A_2 (PLA_2) mediated hydrolysis increases substrate availability e.g. for oxylipin synthesis by releasing lysophospholipids and the oxylipin precursor fatty acids from membrane phospholipids. The role of phospholipids in the context of immune cells has been reviewed by O'Donnel and Rossjohn et al[65].

Sphingolipids are a complex group of lipids defined by their sphingoid base backbone binding various fatty acid chains. This group includes sphingosine, ceramides and sphingomyelins. These complex lipids are essential building blocks in the composition of plasma membranes of various cell types and are especially abundant in the cells of the nervous system[66]. In the context of the current study, spingomyelins will not be further discussed, as there were no significant findings. An extensive review on the properties of sphingolipids in health and disease has been published by Hannun and Obeid[67].

2.2.5 Oxylipins

Oxylipins are PUFA-derived oxygenated unsaturated fatty acids with diverse biological functionalities found throughout the body. In brief, they possess immunomodulatory, anti- and proinflammatory and vasoactive properties, and can contribute to cellular bioenergetics. Considering the reported effects of anaesthetics/sedatives e.g. on ischaemia-reperfusion injury (IRI), organoprotection and immunity, the possible interactions between anaesthetics/sedatives and oxylipins are worth investigating[43,44,68–78]. All of the quantified metabolites under the subcategory of oxylipins have been summarised in Table 5.

Table 5. Oxylipins and related metabolites in the current study

Metabolites analysed	Modality of quantification
Oxylipin precursors	
Arachidonic acid	LC-MS/MS
Docosahexaenoic acid	NMR
Eicosapentaeonic acid	LC-MS/MS
Linoleic acid	NMR
Polyunsaturated fatty acids	NMR
COX oxylipins from AA	
12-HHT (12-hydroxy-5,8,10-heptadecatrienoic acid)	LC-MS/MS
TXB2 (thromboxane B2)	LC-MS/MS
CYP oxylipins from AA	
20-COOH-AA (20-carboxy-arachidonic acid)	LC-MS/MS
5,6-DHET (5,6-dihydroxy-8,11,14-eicosatrienoic acid)	LC-MS/MS
11,12-DHET (11,12-dihydroxy-5,8,14-eicosatrienoic acid)	LC-MS/MS
14,15-DHET (14,15-dihydroxy-5,8,11-eicosatrienoic acid)	LC-MS/MS
16-HETE (16-hydroxy-5,8,11,14-eicosatetraenoic acid)	LC-MS/MS
18-HETE (18-hydroxy-5,8,11,14-eicosatetraenoic acid)	LC-MS/MS
CYP oxylipins from EPA	
17,18-DiHETE (17,18-dihydroxy-5,8,11,14-eicosatetraenoic acid)	LC-MS/MS
CYP oxylipins from LA	
9,10- DiHOME (9,10-dihydroxy-12-octadecenoic acid)	LC-MS/MS
12,13-DiHOME (12,13-dihydroxyoctadec-9-enoic acid)	LC-MS/MS
9,10-EpOME (9,10-epoxy-12-octadecenoic acid)	LC-MS/MS
12,13-EpOME (12,13-epoxy-9-octadecenoic acid)	LC-MS/MS
LOX oxylipin from α-LA	
9-HOTrE (9-hydroxy-10,12,15-octadecatrienoic acid)	LC-MS/MS
LOX oxylipin from AA	
5-HETE (5-hydroxy-6,8,11,14-eicosatetraenoic acid)	LC-MS/MS
11-HETE (11-hydroxy-5,8,11,14-eicosatetraenoic acid)	LC-MS/MS
12-HETE (12-hydroxy-5,8,10,14-eicosatetraenoic acid)	LC-MS/MS
15-HETE (15-hydroxy-5,8,11,13-eicosatetraenoic acid)	LC-MS/MS
LOX oxylipin from EPA	
12-HEPE (12-hydroxy-5,8,10,14,17-eicosapentaenoic acid)	LC-MS/MS
LOX oxylipin from DHA	
14-HDoHE (14-hydroxydocosa-4,7,10,12,16,19-hexaenoic acid)	LC-MS/MS
LOX oxylipin from LA	
9-HODE (9-hydroxy-10,12-octadecadienoic acid)	LC-MS/MS
13-KODE (13-oxo-9,11-octadecadienoic acid)	LC-MS/MS

The most relevant precursors for oxylipin synthesis in the context of the current study are LA, α-LA, AA and EPA. Other oxylipin precursors include DHA, dihomo-γ-linoleic acid (DGLA) and adrenic acid[79]. Oxylipins can be classified based on the length of their respective parent fatty acid carbon chain e.g. docosanoids (C22, e.g. adrenic acid, DGLA), eicosanoids (C20, e.g. AA, DGLA and EPA), octadecenoids (C18, e.g. LA and α-LA). The subclasses of eicosanoids include prostaglandins, thromboxanes, and leukotrienes[64].

Oxylipin biosynthesis is a multistep process requiring several pathways (Fig. 2). The initiation of synthesis occurs upon release of PUFA from membrane phospholipids at the sn2-position, a process catalysed by enzymes in the PLA_2 superfamily as briefly mentioned earlier. The PLA_2 superfamily contains more than 50 enzymes in mammals, these enzymes have varying substrate preferences and their effects are mediated e.g. via increasing oxylipin precursor availability[65,80]. Thus, even though a diet high in n-3 PUFA has been associated with elevated levels of n-3 PUFA-derived oxylipins, the circulating oxylipin profile does not directly mimic dietary PUFA intake per se. Rather, it is affected by the current physiological state

Figure 2. Oxylipin pathways focusing on currently analysed oxylipins

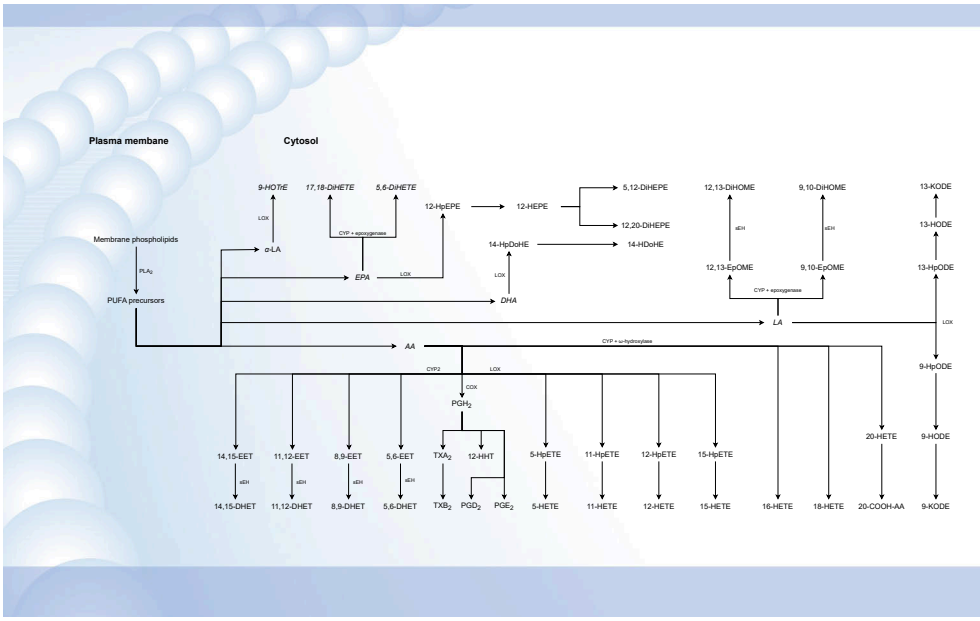

The summary of oxylipin synthesis with a focus on currently analysed oxylipins. Pathways as modified from Gabbs et al.[79] and the Kyoto encyclopedia of Genes and Genomes (KEGG)[191].

e.g. inflammation, immune cell regulation and the abundance of precursor molecules including those released from cell membrane phospholipids by PLA_2[64,65,79,80].

The three main pathways of enzymatic oxylipin synthesis are cyclooxygenase (COX), lipoxygenase (LOX) and the cytochrome P450 mixed function oxidase enzymes (CYP) pathways. The initial oxygenation of non-esterified fatty acids is catalysed by COX, producing prostaglandin H, a precursor molecule for many prostanoids e.g. prostaglandins D, E and F, prostacyclins, thromboxanes, and hydroxy fatty acids. COX are heme-containing enzymes with both oxygenase and peroxidase activities with two principal isoforms COX-1 and COX-2. COX-1 is constitutively active, particularly in blood vessels, smooth muscle cells, interstitial cells, platelets and mesothelial cells. COX-2 is an inducible enzyme; it is activated in response to inflammatory stimuli. However, some constitutive expression of COX-2 has been observed in blood vessels, brain, GI-tract, kidney, lung and thymus. LOX are a family of dioxygenases encoded by six functional LOX-genes in the human genome which are expressed in a wide range of tissues. LOX catalyses the formation of hydroxyperoxyl fatty acids and their metabolites e.g. leukotrienes, lipoxins, specialised pro-resolving-mediators including resolvins, protectins and maresins. Lastly, CYP enzymes possess monooxygenase activity and an ability to catalyse epoxidation, hydroxylation or allylic oxidation reactions, enabling metabolism of PUFAs to oxylipins such as epoxyeicosatrienoic acids (EETs), hydroxyeicosatetraenoic acids (HETEs), among others. EPA, DHA and AA are the preferred substrates for the majority of CYP isoforms[64].

Reviews of oxylipins and their complex role in human biology have been published earlier[64,65,79,81,82]. An in-depth review of each oxylipin and its biological function is outwith the scope of this introduction. The oxylipins most relevant for the current study will be discussed in more detail in the discussionsection.

2.2.6 Aerobic and anaerobic glycolysis

Aerobic and anaerobic glycolysis are central bioenergetic pathways. The glucose concentration is of interest in the current study e.g. due to dexmedetomidine-induced effects on insulin secretion[83]. Understandably, lactate as a hallmark of tissue hypoxia/hypoperfusion, is an extremely relevant metabolite in the context of OHCA due to its known association with mortality in OHCA patients[37,38,84,85]. Citrate is the only TCA cycle intermediate which was quantified by the current methodology. It has been previously demonstrated that upon admission after OHCA, TCA intermediates associate with patient outcome. The level of citric acid (citrate is the anion of citric acid under physiological pH) upon admission and at 48 hours post-admission associated with patient mortality[37,38]. All of the quantified metabolites under the subcategory of aerobic and anaerobic glycolysis have been summarised in Table 6.

Table 6. Glycolysis related metabolites in the current study

Metabolites analysed	Modality of quantification
Citrate	NMR
Glucose	NMR
Lactate	NMR

In brief, glycolysis is a 10-step anaerobic process during which glucose is metabolised into pyruvate. In this process, each glucose molecule provides a net energy of two molecules of ATP and two molecules of NADH. Importantly, glycolysis produces two molecules of pyruvate for each molecule of glucose. Moreover, many other essential molecules for cell sustenance are produced e.g. glucose-6-phosphate, thus linking glycolysis to cholesterol, fatty acid and glycogen synthesis via the pentose phosphate pathway, and the glycerol precursor glucose-3-phosphate essential for triglyceride and phospholipid synthesis. Glycolysis is also linked with the biosynthesis of many amino acids[86,87]. The schematic of the pathways relevant to the current study is illustrated in Figure 3.

Pyruvate is the main carbon fuel input supporting the TCA cycle carbon flux. The entry of pyruvate into the mitochondrial matrix via the mitochondrial pyruvate carrier is followed by the formation of acetyl-CoA by the action of pyruvate dehydrogenase. The subsequent entry of pyruvate carbons into the TCA cycle occurs either via citrate or oxaloacetate, with TCA cycle produced NADH and $FADH_2$ eventually fueling oxidative phosphorylation in the mitochondrial electron transport chain providing energy for the cell in the form of ATP. As the electron transport

chain requires oxygen as the final electron acceptor, abundant amounts of O_2 are required[87]. This process has a net gain of about 34 ATP from each molecule of glucose (2 ATP from the TCA cycle, 32 from oxidative phosphorylation)[88].

Under conditions where the demand for energy exceeds the mitochondrial production capacity of ATP, glycolysis is hindered by the diminishing amounts of NAD^+ and the accumulation of NADH. This can be counteracted by the conversion of pyruvate into lactate via lactate dehydrogenase. Importantly, the production of lactate replenishes the stores of NAD^+, allowing continued ATP production via glycolysis to maintain work rates exceeding those that could be supported by oxidative phosphorylation alone. In the Cori cycle, the lactate produced by peripheral tissues e.g. skeletal muscle, is transported to the liver, where lactate dehydrogenase converts lactate back into pyruvate thus supporting gluconeogenesis, while the resulting glucose supports peripheral glycolysis. A less efficient but often co-existing alanine cycle depends on the activity of alanine aminotransferase (ALAT), which catalyses the reversible transamination of pyruvate and glutamate to alanine and α-ketoglutarate. In brief, skeletal muscle pyruvate is transaminated to alanine, which enters the circulation and eventually is deaminated to pyruvate by ALAT in the liver. The relative lower efficiency is due to the requirement to deaminate

Figure 3. The TCA cycle and a summary of metabolic connections

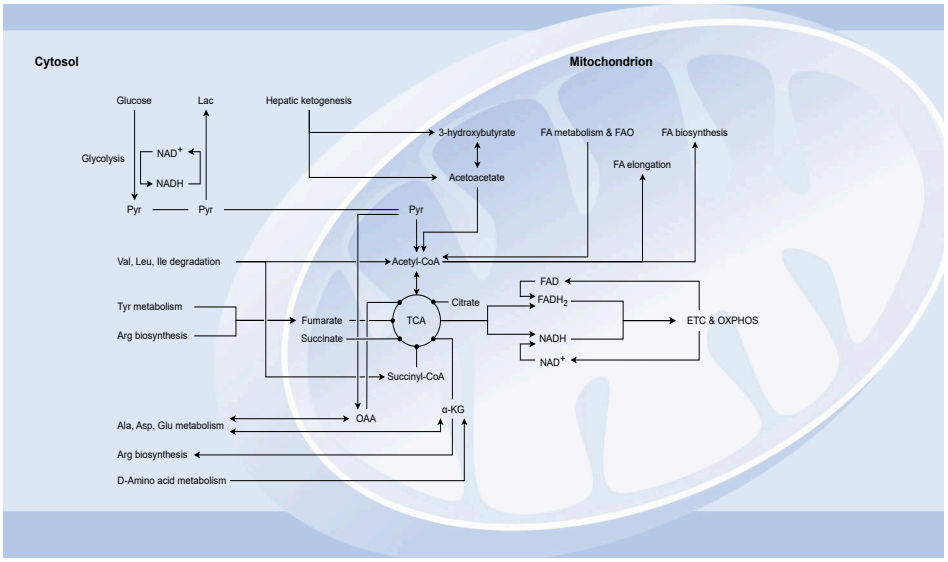

A schematic representation of the tricarboxylic acid (TCA) cycle and the metabolic connections to glucose, lactate, ketone body, amino acid and fatty acid metabolism. Pathways as modified from Gabbs et al.[79] and the Kyoto encyclopedia of Genes and Genomes (KEGG)[191].

glutamate via glutamate dehydrogenase, producing ammonia which needs to be detoxified in the urea cycle[87].

2.2.7 Amino acids

Relatively little is known about the effects of anaesthetics/sedatives on amino acids. While well known for their role as the molecular building blocks of proteins, they also participate in several processes including cellular bioenergetics as described previously as well as in the synthesis of several neurotransmitters. In the psychiatric framework, there have been studies reporting that specific amino acids associate with the treatment response to S-ketamine in major depressive disorder[89]. Furthermore, in the context of OHCA, the levels of certain amino acids (e.g. alanine, leucine, isoleucine, tyrosine, phenylalanine) have been associated with patient outcome upon admission, and the branched chain amino acids (BCAA) valine, leucine at 48 hours[37,38]. All of the quantified metabolites under the subcategory of amino acids have been summarised in Table 7.

Table 7. Amino acid metabolites in the current study

Metabolites analysed	Modality of quantification
Alanine	NMR
Glutamine	NMR
Histidine	NMR
Isoleucine	NMR
Leucine	NMR
Phenylalanine	NMR
Tyrosine	NMR
Valine	NMR

Amino acids are organic molecules consisting of functional amino and carboxylic groups and a side chain affecting the properties of each amino acid. Of the 8 amino acids identified by the current NMR metabolic profile, alanine, tyrosine and the three BCAA valine, leucine, isoleucine showed most relevance in the current study and will be discussed here in more detail. A detailed overview on the pharmacological attributes of BCAAs has been published previously[90].

Alanine is a non-essential amino acid with a non-polar methyl group sidechain. As a non-essential amino acid, it can be synthesized e.g. from pyruvate via the alanine cycle. Moreover, BCAAs leucine, valine and isoleucine are major sources of

nitrogen in the synthesis of alanine (and glutamine) in muscle cells. Alanine is closely involved in several metabolic pathways such as gluconeogenesis and the TCA cycle via the alanine cycle as discussed earlier[91].

Tyrosine is an aromatic amino acid (AAA) with a polar phenol sidechain. It is present in the proteins involved in signal transduction as a receiver of phosphate groups being transferred by protein kinases. Tyrosine is considered the primary substrate for the synthesis of the neurotransmitter dopamine, which can be further metabolised into noradrenaline and adrenaline[92].

The three BCAAs leucine, valine and isoleucine are essential amino acids with nonpolar sidechains accounting for ~35% of the essential amino acids and ~21% of the total amino acids in muscle protein. Due to their hydrophobicity and small size, BCAAs make an important contribution to the structural properties of proteins[93].

The initial steps of BCAA metabolism are shared: All three undergo transamination by branched chain aminotransferases (BCAT) producing branched chain α-ketoacids (BCKA) followed by irreversible oxidative decarboxylation by mitochondrial branched chain α-ketoacid dehydrogenase complex (BCKDH). Simultaneously, as a flux-controlling step, BCKDH traps all of the metabolites generated (except 3-hydroxyisobutyrate) inside the mitochondria by adding a hydrophilic co-enzyme A adduct. The function of BCKDH is an important point of regulation as exercise, nutrition and hormones can affect BCKDH's function via its inhibition by BCKD kinase. The inhibition occurs via phosphorylation of E1α subunit of BCKDH. Conversely, protein phosphatase 2Cm can promote BCKDH activity by removing the phosphorylated moiety. From this stage onwards, the metabolism of each BCAA differs. Ultimately the carbons from BCAAs enter the TCA cycle as acetyl-CoA and succinyl-coenzyme A. At a whole-body level, Neinast et al. demonstrated in mice that the highest BCAA oxidation flux per gram of tissue occurred in heart and brown adipose tissue (BAT), followed by pancreas and kidneys. The three organs with the most prominent isoleucine oxidation were skeletal muscle (59% of whole body oxidation), BAT (19%) and liver (8%), whereas incorporation into protein occurred most predominantly in the liver (27%), pancreas (24%), skeletal muscle (24%)[93].

In animal models, under physiological circumstances, BCAA utilisation in the brain is relatively modest. Of the three aforementioned BCAAs, the oxidative flux of valine was most prominent[93]. Evidently, BCAAs play an indirect, yet important role in neurotransmitter metabolism. The synthesis of the AAA derived neurotransmitters, i.e, the two catecholamines dopamine and noradrenaline (from tyrosine), and serotonin (from tryptophan) in the CNS is tied to the shared competitive transport mechanism of all large neutral amino acids (LNAA) across the blood-brain barrier (BBB). As a whole, the LNAAs include BCAAs (valine, isoleucine, leucine) and AAA (phenylalanine, tyrosine, tryptophan). Since the

transport mechanism is almost fully saturated at normal plasma LNAA concentrations, the uptake of each LNAA into the brain will be affected not only by its own concentration in plasma but also by that of its competitors. For example, if plasma levels of BCAAs decrease, more AAA cross the BBB, increasing the tyrosine/tryptophan concentration in the brain. As the rate limiting enzyme (AAA hydroxylase) is not saturated with substrate at normal brain concentrations, changes in tyrosine/tryptophan concentrations will lead rapidly to alterations in their respective neurotransmitters[94]. BCAAs are also directly involved in the synthesis and compartmentalisation and regulation of excitatory neurotransmitter glutamate[95–97].

2.2.8 Other metabolites: Albumin, creatinine and GlycA

In the context of the current study, albumin and creatinine are of interest as they both have been reported to associate with the outcome after OHCA[98,99]. Furthermore, as an inflammatory marker, GlycA might be of interest considering the inflammatory state that is set in motion after OHCA[100]. All of the quantified metabolites under the subcategory other metabolites have been summarised in Table 8.

Table 8. Other metabolites and markers in the current study

Metabolites analysed	Modality of quantification
Albumin	NMR
Creatinine	NMR
Glycoprotein acetylation	NMR

Albumin, the most abundant protein in human plasma, is synthetised in the liver. It has several important functions including the maintenance of oncotic pressure, transportation of e.g. hormones, fatty acids and drugs.

Creatinine is a breakdown product arising from the creatine derived high-energy compound called phosphorylcreatine via the action of creatine kinase. Creatinine is produced at a relatively stable rate, roughly proportional to muscle mass. The elimination of creatinine occurs mainly via glomerular filtration, thus making it a viable and widely utilised marker for glomerular filtration and renal function[101].

GlycA is a composite NMR marker reflecting inflammation. The major contributors to the GlycA signal arise from inflammatory markers α_1-acid glycoprotein, haptoglobin, α_1-antitrypsin, α_1-antichymotrypsin and transferrin. The NMR quantification of these molecules relies on their post-translational glycan chain attachments, which produce an NMR signal proportional to the glycan N-acetylglucosamine concentrations[102]. GlycA has several biomarker properties, e.g. it

has been associated with the risk of cardiovascular disease, chronic inflammation and its levels predict the long term risk for severe infection, and α_1-acid glycoprotein has been associated to all-cause mortality[3,7,14,103].

2.2.9 Bile acids

Bile acids are cholesterol-derived nutritional detergents synthesised by the liver, facilitating the absorption of dietary lipids and fat-soluble nutrients by acting as emulsifiers in the small intestine. For example, previous research has demonstrated that dexmedetomidine induces changes in intestinal motility and modulates vagal nerve activity[104,105]. These properties might alter circulating bile acid profiles. All of the quantified metabolites under the subcategory bile acids have been summarised in Table 9.

Table 9. Bile acid and related metabolites in the current study

Metabolites analysed	**Modality of quantification**
Precursor for bile acid synthesis	
7α-Hydroxy-4-cholesten-3-one	LC-MS/MS
Total cholesterol	NMR
Primary bile acids	
Chenodeoxycholic acid	LC-MS/MS
Cholic acid	LC-MS/MS
Secondary bile acids	
Deoxycholic acid	LC-MS/MS
Lithocholic acid	LC-MS/MS
Tertiary bile acids	
Ursodexoycholic acid	LC-MS/MS
Bile acid conjugates	
Glycochenodeoxycholic acid	LC-MS/MS
Glycocholic acid	LC-MS/MS
Glycodeoxycholic acid	LC-MS/MS
Glycolithocholic acid	LC-MS/MS
Glycoursodeoxycholic acid	LC-MS/MS
Hyodeoxycholic acid	LC-MS/MS
Taurochenodeoxycholic acid	LC-MS/MS
Taurocholic acid	LC-MS/MS
Taurodeoxycholic acid	LC-MS/MS
Tauroursodeoxycholic acid	LC-MS/MS

It has been estimated that approximately 500 mg of cholesterol is converted into bile acids daily, accounting for 90% of the cholesterol that has been actively metabolised in the human body, the remainder is accounted for by the biosynthesis of steroid hormones. Approximately 95% of bile acids secreted to the small intestine are recovered in each cycle of the enterohepatic circulation with the 5% loss being replenished by hepatic synthesis. In humans, cholic acid and chenodeoxycholic acid are the predominant primary bile acids. The diversity of the bile acid pool is expanded by the action of microbial flora in the intestine as bile acids are metabolised into secondary (e.g. deoxycholic- and lithocholic acid) and tertiary bile acids (e.g. ursodeoxycholic acid)[106,107]. Primary and secondary bile acids comprise 95% of the 3-5 g bile acid pool in adult humans[108].

As discussed, the synthesis and excretion of bile acids represent a central pathway of cholesterol elimination in mammals. The pathway involves 17 different enzymes that are predominantly expressed in the liver. The synthesis is initiated by the conversion of cholesterol into 7α-hydroxycholesterol by cholesterol 7α-hydroxylase, followed by modifications of the ring structures, oxidation and a shortening of the side chain and eventually conjugation with amino acids (usually glycine or taurine). The enzymes, as well as the regulation of synthesis and genetics of bile acid synthesis have been reviewed extensively[106].

After excretion to the small intestine from hepatocytes, bile acids take part in the enterohepatic circulation. Bile acids are transported into hepatocytes by the Na^+-taurocholate cotransporting polypeptide and organic anion transport polypeptide. The initial excretion of bile acids from hepatocytes occurs via the bile salt export pump and multidrug resistance proteins. For example, the transcellular transport of bile acids in bile duct epithelium is facilitated by apical sodium-dependent bile acid transporter (ASBT) and organic solute transporters α and β on apical and basolateral membranes, respectively. In the small intestine, bile acid absorption by enterocytes via ASBT in apical membranes, is followed by transportation across the cells by ileal bile acid binding protein and released into the portal circulation via organic solute transporters α and β. Under physiological states, only a small fraction of the bile acids end up in systemic circulation[108].

In addition to their role as nutritional detergents, the discovery of an interaction between bile acids with G-protein coupled and nuclear receptors throughout the body has sparked interest in their role as signalling molecules[107–110]. In the cardiovascular system, direct interactions of bile acids with endothelial cells and vascular smooth muscle cells via the nuclear receptor farnesoid X receptor (FXR) have been demonstrated. Moreover, G-protein coupled receptor mediated interactions have been demonstrated in hepatic sinusoidal endothelial cells, cardiomyocytes and endothelial cells. Furthermore, potassium-channel mediated interactions in vascular smooth muscle cells have been described. In animal models and laboratory studies,

associated effects of bile acids on cardiovascular tissues have included vasodilation, ino- and chronotropic effects, angiogenesis, as well as changes in the nitric oxide pathway[108]. G-protein and nuclear receptor interactions have been demonstrated also in the immune system, e.g. via G-protein bile acid receptor 1 and FXR. These receptors are present at the interface of the host's immune system and intestinal microbiota e.g. in intestinal and liver macrophages, dendritic cells and natural killer T cells and contribute to the maintenance of a tolerogenic phenotype in entero-hepatic tissues. In macrophages, bile acid mediated effects via both G-protein bile acid receptor 1 and FXR inhibit nuclear factor κB (NF-κB)[107]. In the BBB and the CNS, several bile acid transporters and bile acid receptors have been described e.g. ASBT and FXR[110]. Bile acid metabolism has been implicated in neurodegenerative diseases and there are even reports of bile acid -associated neuroprotection[111].

2.3 Anaesthetics/sedatives

Disconnectedness, analgesia, amnesia and immobility, are the classical hallmarks of general anaesthesia[112,113]. In clinical practise, many anaesthetic agents have demonstrated their ability to aid in reaching these goals via diverse pharmacologic mechanisms of action. However, the biologic functionality of anaesthetics and sedatives seems to extend beyond their primary pharmacologic effects in terms of modulating conscious perception. Anaesthetic/sedative induced effects on IRI, organoprotection and immunity have sparked interest in the field of anaesthesia research[68–77,114–116]. An exploration of anaesthethic/sedative induced alterations in the metabolic profile might offer novel insights into the mechanisms underlying organoprotection.

In pharmacometabolic profiling, large scale data capturing methods are harnessed to uncover pharmacotherapy-induced shifts in the metabolic profile. A further analysis of these changes and identification of baseline predictors of patient response via biomarker acquisition, may eventually offer an opportunity to enhance the early prediction of treatment outcomes, to reveal novel mechanisms of drug action and to identify the metabolic pathways contributing to drug response phenotypes[33].

2.3.1 Dexmedetomidine

Dexmedetomidine is a highly selective α_2-adrenoceptor agonist, producing sedation resembling natural sleep, anxiolysis, analgesia, sympatholysis and it also has an anaesthetic sparing effect with minimal respiratory depression. Sedative and hypnotic effects of dexmedetomidine are thought to originate from activation of

central pre- and postsynaptic α_2-receptors in locus coeruleus, while hyperpolarisation of interneurons and suppression of pronociceptive transmitters via central and spinal cord α_2-receptors is thought to underlie the analgesic effects of the drug. Unlike many other anaesthetics/sedatives, dexmedetomidine does not exert its effects via γ-aminobutyric acid (GABA) receptors. Dexmedetomidine is eliminated mainly via glucuronidation and hydroxylation to inactive metabolites in the liver and has a hepatic extraction ratio of 0.7[49].

2.3.2 Propofol

Propofol has been widely used in anaesthetic induction, maintenance of anaesthesia and sedative-hypnotic agent in the ICU. Compared to other intravenous anaesthetics that can be administered in aqueous salts, the structure of propofol makes it extremely lipophilic. Thus, in current clinical practise, propofol is administered in a lipid emulsion formulation[117]. The mechanism of action involves the potentiation of the inhibitory GABA neurotransmitter via $GABA_A$ receptors. As with other anaesthetics, the effects on other potential targets for the hypnotic effects of propofol have been described, including glycine, neuronal nicotinic acetylcholine, N-methyl-D-aspartate (NMDA) receptors and voltage-gated sodium channels[118]. Propofol is metabolised in the liver and has a hepatic extraction ratio of approximately 0.9. Approximately 70% of propofol is metabolised into propofol glucuronide and 29% to 4-hydroxypropofol. The major metabolites possess no hypnotic activity[119,120].

2.3.3 S-Ketamine

S-ketamine is the S(+)-enantiomer of racemic ketamine, a phencyclidine derivative; it functions as a dissociative anaesthetic at high doses and as an analgesic at low doses. Noncompetitive antagonism of the NMDA receptor in the CNS is thought to underlie the anaesthetic and analgesic effects; this interaction is stronger with the S(+) enantiomer than with racemic ketamine. As with other anaesthetics, the mechanism of action is complex, for example ketamine is believed to interact with non-NMDA glutamate receptors such as alpha-amino-3-hydroxy-5-methyl-4-isoxazole-propionic acid (known as AMPA) and kainate receptors. Furthermore, interactions with voltage-dependent ion channels, nicotinic and muscarinic cholinergic receptors, as well as monoaminergic and opioid receptors have been demonstrated. S-ketamine inhibits both the neuronal and extra-neuronal uptake of catecholamines, e.g. increasing circulating noradrenaline concentrations. Similarly, inhibition of dopamine and 5-HT uptake occurs in response to S-ketamine. In

contrast to many other anaesthetics/sedatives, the affinity of S-ketamine to CNS $GABA_A$ receptors is relatively low. Thus, the role of GABA is of minor importance concerning the pharmacologic effects of S-ketamine[48,121–123]. Racemic ketamine undergoes extensive metabolism to several active metabolites[124].

2.3.4 Sevoflurane

Sevoflurane is a fluorinated methyl isopropyl ether widely used as a volatile anaesthetic. The precise molecular mechanisms of action of sevoflurane remain incompletely characterised. However, interactions with GABA, NMDA, acetyl choline (ACh), voltage-gated sodium channels, hyperpolarisation-activated cyclic nucleotide-gated channels and two-pore domain potassium channels have been described. *In vivo* studies have suggested that $GABA_A$ and ACh receptors, and hyperpolarisation-activated cyclic nucleotide-gated channels play a role as potential targets for the hyponotic effects of sevoflurane[125]. The primary metabolites of the biotransformation of sevoflurane are fluoride and hexafluoroisopropanol. The latter was rapidly glucuronidated and eliminated in the urine. The overall extent of sevoflurane metabolism approximated to 5%[126].

2.3.5 Xenon

Xenon is the only noble gas with anaesthetic properties at normobaric and normothermic conditions. Despite possessing desirable attributes of an ideal anaesthetic, its clinical utility has been hindered by its rarity in the atmosphere (no more than 0.0875 ppm), resulting in high manufacturing costs. As a noble gas, it is characterised by a fully occupied octet of electrons on the outer atomic orbital; this means that, under biologic conditions it is incapable of covalent bonding and forming adducts. From a biochemical perspective this would suggest relative inertness. However, xenon has a relatively high polarizability value of 4 (in comparison to helium with 0.2), allowing its shell to be polarized by surrounding molecules forming dipoles. This enables biochemical functionality via an affinity to amino acid residues in preformed hydrophobic cavities in proteins. As such, xenon is not biotransformed nor metabolised; in the context of anaesthesia, this signifies that there will be an absence of toxic metabolites, and allows closed-loop anaesthetic administration[127].

Initially, the anaesthetic properties of xenon were deduced by Behnke in 1939 after observing progressive narcosis in deep-sea divers exposed to xenon, argon or krypton in 20% oxygen under hyperbaric conditions[128]. The first surgical application of the anaesthetic occurred in 1951[129]. The favourable pharmacokinetic profile of

xenon, with a rapid induction and emergence after anaesthesia, is largely owing to its low blood-gas partition coefficient of 0.115, lower than those of other inhalational anaesthetics (e.g. nitrous oxide and sevoflurane)[127]. The anaesthetic effects of xenon are thought to be mediated via inhibitory effects on the NMDA receptors. These receptors play a key role in the context of neuronal damage. In excitotoxicity, a bioenergetic malfunction in the CNS (e.g. from stroke or cardiac arrest) triggers a destructive cascade of events leading to neuronal cell death involving overactivation of NMDA receptor and excessive release of the neurotransmitter glutamate i.e. glutaminergic excitotoxicity. Therefore, the discovery of non-competitive antagonism of the NMDA subtype of glutamate receptors sparked numerous preclinical studies in several different species and in various models of neuronal injury to assess the neuroprotective potential of xenon.

A central mechanism for xenon-induced neuroprotection is the potent non-competitive inhibition of the excitatory NMDA receptor at the binding site for the co-agonist glycine[130,131]. Xenon induced inhibition of kainate and α-amino-3-hydroxy-5-methyl-4-isoxazolepropionic acid receptors (known as AMPA receptors) is thought to contribute to the gas's neuroprotective effects[132]. Moreover, xenon-mediated modulation of potassium channels such as TREK, and ATP-sensitive potassium channels has been claimed to confer neuroprotection[133,134]. Indeed, xenon protected neuronal cell cultures against NMDA, glutamate or oxygen deprivation-induced injury. Moreover, the same study demonstrated the neuroprotective effects of xenon in an *in vivo* rat model in the context of NMDA-induced neuronal injury[135]. Apart from these anti-excitotoxicity effects, some antiapoptotic properties of xenon have been described as demonstrated by decreased expression of Bax and enhancement of Bcl-x_L expression in neonatal rat models of hypoxic ischaemic injury[136]. Indeed, in mice models of transient cerebral ischaemia, a reduced infarct size and improved functional neurologic outcome have been observed after xenon anaesthesia when the ischaemic injury occurred during anaesthesia[137]. Moreover, in a similar setting, the neuroprotective effects have been described in animal models when xenon was administered post-injury[138–140]. Furthermore, in porcine models of experimental cardiac arrest, reductions in surrogate markers of brain damage, histological and functional neuroprotection have been exhibited[141–143]. Preclinical evidence has consistently demonstrated the additive, or possibly, synergistic neuroprotective effect when combined with TTM with hypothermic target[136,144–147]. As previously reported by Laitio et al., inhaled xenon has neuroprotective properties after OHCA in human patients: Inhaled xenon in combination with TTM at 33 °C preserved white matter tracts better than TTM alone, as assessed by global fractional anisotropy[115]. In the same study, its cardioprotective properties were demonstrated as xenon treatment resulted in a less severe myocardial injury as determined by a reduced release of troponin-T[114].

The cardioprotective properties of xenon have been described previously in animal models. Previous experiments in rats demonstrated a decreased infarct size in response to xenon with TTM at 34 °C *vs.* control (the reductions in TTM or xenon alone did not reach significance)[148]. Similar findings were observed by Roehl et al. on reduced initial infarct size in rat models. Furthermore, decreases in the remodelling index (a ratio between left ventricular mass and end-diastolic volume) and reduced impairment in cardiac function (e.g. in ejection fraction and end-diastolic volume) were noted in response to xenon *vs.* control at 28 days[149]. In elective non-cardiac surgery patients with coronary artery disease, xenon anaesthesia maintained arterial blood pressures, with no signs of cardiovascular compromise and furthermore the ultrasonographic indices were better in comparison with propofol anaesthesia[150]. Similarly, in elective surgery patients randomized to propofol induction with xenon maintenance *vs.* propofol anaesthesia, systolic arterial pressures returned to baseline values after propofol induction in the xenon group, the propofol group in comparison had lower systolic arterial pressures. Xenon decreased heart rate more in the xenon *vs.* propofol comparison, but there was no difference in the incidence of bradycardia between the groups. As discussed by Arola et al., many underlying molecular mechanisms of xenon pre- and postconditioning effects have been identified, such as effects on protein kinase cε, protein kinase B and glycogen synthase kinase 3β which are enzymes reported to inhibit mitochondrial permeability transition pore opening thus preserving mitochondrial function and preventing ischaemic reperfusion injury and cell death. Other survival promoting kinases associated with the cardioprotective properties of xenon include p38 mitogen-activated protein kinase (MAPK), MAPK-activated kinase-2, heat-shock protein 27 and extracellular signal regulated kinases 1/2[114].

2.3.6 Metabolomics and anaesthetics/sedatives

Anaesthetics/sedatives possess several pharmacologic attributes that might cause alterations in the circulating metabolic profile. This is exemplified by dexmedetomidine-induced sympatholysis, organoprotective effects and modulation of insulin secretion[70,74,83,151–154], as well as the ability of S-ketamine to evoke increases in the levels of circulating catecholamines[48]. Furthermore, propofol (and the accompanying lipid emulsion) influences lipoprotein and triglyceride metabolism and exerts possible effects on bioenergetics[42–44,155–157].

Nonetheless, the literature on the effects of dexmedetomidine on the circulating metabolome in human subjects remains sparse.

The plasma metabolomics of propofol vs. etomidate were briefly mentioned by Ghini et al., however while their focus was on the metabolomics of non-metastatic colorectal cancer and colorectal cancer with liver metastasis, the combined effects

of anaesthesia (and other concomitant medications) on metabolome were also assessed. While the decrease in the levels of isoleucine, leucine and valine was less evident in the propofol group *vs.* etomidate, the change was non-significant[28].

Of the anaesthetics and sedatives relevant to the current study, racemic ketamine has been most widely studied in the context of metabolomics, mostly in the psychiatric framework due to its antidepressant properties[32,34,89,158]. However, only one of these studies reported results due to S-ketamine[89]. S-ketamine exposure has been associated with decreases in the levels of tyrosine, alanine and tryptophan[89].

Sevoflurane-induced changes in serum metabolites have been studied in neonatal primates, brain and cerebrospinal fluid samples were also assessed. A significant reduction was observed in serum levels of free carnitines and concomitantly acylcarnitines and ketone bodies regardless of the fact that glucose levels were actively maintained. According to the authors, this reflected reduced FAO at 2 h after exposure. In support of this hypothesis, the serum triglyceride content was elevated *vs.* control at 9 h and the triglycerides contained more long-chain fatty acid side chains (16:0 and 18:1). Though the amounts of long-chain acylcarnitines were not affected by sevoflurane in brain tissue samples, those of short-chain acylcarnitines (3:0, 4:0 and 4:0-OH) were lower, as were acetyl carnitines in the cerebrospinal fluid. According to the authors, this was indicative of reduced amino acid utilization in the brain's energy metabolism in response to sevoflurane, without affecting FAO. Moreover, since the amounts of poly-unsaturated fatty acids (PUFA, especially DHA, docosapentaenoic acid and adrenic acid) were decreased in response to sevoflurane, the authors suggested this may have been due to the increased utilisation of n-3 and n-6 fatty-acids in the synthesis of anti- and proinflammatory mediators. [25] Prenatal exposure to sevoflurane has been studied in rat models to assess possible biomarkers for anaesthetic induced neurotoxicity; in that experiment, untargeted mass-spectrometry metabolomics identified 29 altered metabolites including metabolites from arginine/proline, porphyrin, cysteine/methionine, glycerophospholipid and tryptophan metabolism, as well as alterations in the metabolites involved in the biosynthesis of unsaturated fatty acids and primary bile acids and aminoacyl-transfer RNA. The specific change most relevant to the current study was a reduction in the cholic acid concentration.[29] There have been no prior analyses on circulatory metabolomics in response to inhaled xenon in human subjects.

2.4 Out-of-hospital cardiac arrest

OHCA is a common public health problem and a significant cause of premature mortality claiming annually 3.7 million lives worldwide[35]. OHCA is defined as loss

of functional cardiac mechanical activity in association with absence of a systemic circulation occurring outside of the hospital setting[159]. Ventricular tachycardia (VT) degenerating into ventricular fibrillation (VF) and eventually to asystole or pulseless electrical activity appears to be the most common cascade of events involved in fatal arrhythmias[160]. In Europe, it has been estimated that 275 000 individuals per year experience all-rhythm cardiac arrest treated by the emergency medical services (EMS), with only 29 000 of those surviving to hospital discharge[161]. In Finland, the incidence of OHCA has been estimated to be 46–80/100 000 inhabitants annually, the survival rate to hospital discharge was between 13-27%. In the FinnResusci trial covering nearly half the population of Finland, the incidence of OHCA with attempted resuscitation was 51/100 000 inhabitants annually and the overall survival to hospital discharge was 19.9%, 1-year survival after OHCA was 13.4%[162].

The etiology of OHCA can be broadly divided into two categories, cardiac and non-cardiac. Cardiac etiologies predominate in those who are reached by the EMS crew and in whom resuscitation is considered possible[163]. Of 84 consecutive survivors of OHCA, immediate angiography showed evidence of clinically significant coronary artery disease in 71% of patients, while coronary artery occlusion was evident in 48%[164]. The annual incidence rate of specific non-cardiac etiologies in OHCA between 2005-2011 in a Japanese population were external causes (including trauma, hanging, drowning, asphyxia, drug overdose) 12.3-13.3, for respiratory diseases 1.3-2.2, malignancy 1.3-1.8 and stroke 1.2-2.0 per 100 000 persons[165].

In patients with ischaemic heart disease, acute myocardial ischaemia or pre-existing myocardial scarring are common initiators for malignant tachyarrhythmias. Other non-ischaemic causes include structural defects as in Wolf-Parkinson-White syndrome, genetically determined ion-channel abnormalities (e.g. Long QT syndrome, Brugada syndrome), cardiomyopathy (dilated cardiomyopathy, left ventricular non-compaction cardiomyopathy, hypertrophic cardiomyopathy, arrhythmogenic right ventricular cardiomyopathy), catecholaminergic polymorphic VT, other infiltrative or inflammatory myocardial diseases, myocarditis, valvular heart disease and congenital heart disease. There are many extracardial causes e.g. malignancy, trauma, non-traumatic bleeding, asphyxia/hypoxia, drug overdose, hypoglycemia, hypothermia, epilepsy, septic shock[159,160,165].

In VT/VF generated OHCA, it is paramount to achieve a rapid restoration of organized electrical activity and contractile function of cardiac muscle and thus a return of the spontaneous circulation (ROSC). Cardiopulmonary resuscitation (CPR) followed by early defibrillation to minimize the no-flow time (the absence of perfusion if CPR is not provided) and thus minimizing hypoxic-ischaemic brain damage is essential for patient survival. Unfortunately, the destructive events set in motion by OHCA are far from over even after achieving ROSC.

2.4.1 Ischaemia-reperfusion injury

The cascade of events leading to IRI is set in motion upon the initial perfusion standstill ("no-flow") induced by OHCA. During "no-flow", oxygen and metabolic substrate delivery and the removal of metabolic waste products abrubtly ceases, yet the continuous consumption of ATP and glucose does not. The circulation standstill leads to depletion of O_2 within 20 seconds and ATP within 4-6 minutes. Eventually, this results in plasma membrane depolarization, a fall of mitochondrial membrane potential and an increase in the intracytoplasmic calcium concentration leading to cell and tissue damage[100]. This imbalance between metabolic supply and demand sets the scene for IRI.

Upon initial restoration of perfusion during the "low-flow"-phase (created by CPR) and after ROSC, IRI ensues leading to an exacerbation of the injury. Reperfusion and reoxygenation of ischaemic areas trigger the formation of reactive oxygen species (ROS) e.g. superoxide anion (O_2^-), hydrogen peroxide (H_2O_2) and the hydroxyl radical (OH^-). In mice, IRI-induced ROS production has been demonstrated to be a biphasic process occurring at 3 and 72 h following reperfusion. Under physiological conditions, the mitochondrial electron transport chain accounts for approximately 95% of ROS production. Under these conditions, the produced O_2^- undergoes neutralisation by superoxide dismutase to H_2O_2 and eventually into O_2 and H_2O by catalase or glutathione peroxidase[166]. In IRI, free radical production via the electron transport chain occurs via reverse electron transfer and the oxidation of accumulated succinate[166,167]. Eventually, endogenous antioxidant defences become depleted resulting in the unmatched generation of ROS allowing O_2^- to form other ROS such as H_2O_2, HO_2^- and OH^-, or NO_3^- leading to an exacerbation of the cellular injury[100,166,168].

The aforemention processes including disseminated vascular endothelial injury evolves IRI towards systemic inflammation via the production of interleukins IL-1, IL-6, IL-8, tumour necrosis factor (TNF) α, complement activation, AA metabolism and the subsequent recruitment of inflammatory cells[100]. This IRI-associated profound inflammatory response is facilitated by a wide range of pathological mechanisms, e.g. the activation of NF-κB[168].

IRI activates innate immunological mechanisms resembling the host immune response to invading micro-organisms. Yet, with a few exceptions such as bacterial translocation after intestinal injury, the inflammation in IRI is non-microbial in its origin. For example, instead of pathogen-associated molecular patterns, endogenously derived damage associated molecular patterns can act as ligands, binding to toll-like receptors (TLR) and activating several signalling pathways e.g. NF-κB, MAPK and type I interferon pathways, inducing proinflammatory cytokines and chemokines. In IRI, damage associated molecular patterns can both activate an immune response or restrain harmful immune responses and promote tissue

integrity. Particularly during the early stages of IRI, the sterile inflammation is characterised by the accumulation of inflammatory cells. It is unclear whether they contribute to the activation of pathological inflammatory mechanisms or aid in the resolution of injury. IRI also elicits a robust adaptive immune response. Both antigen specific and independent mechanisms lead to an activation of T-lymphocytes. T_{reg} cells appear to have a protective role. Complement-mediated recognition of damaged cells and anaphylatoxin release may fuel inflammation and lead to further recruitment of immune cells[168].

Excessive platelet aggregation and the release of plateled-derived mediators exacerbate IRI. Several mechanisms have been postulated to be involved such as those involving integrins, FERM domain containing protein and the inorganic polyphosphates produced by platelets[168]. The inflammatory response triggered by IRI generates secondary endothelial damage increasing thrombosis and affecting capillary permeability[100].

The brain is especially vulnerable to ischaemic damage due to its high metabolic demand and limited energy reserves. Even though ROSC is achieved, regional perfusion deficits may persist, this is known as the “no reflow” phenomenon. Ischaemia disrupts normal endothelial nitric oxide production exacerbating the vascular dysfunction. Cardiac arrest and IRI lead to BBB breakdown and a loss of integrity in the endothelial glycocalyx. In the brain, a hypoperfusion-induced bioenergetic failure results in the cessation of sodium-potassium adenosine triphosphatase (Na^+/K^+-ATPase) activity leads to dysregulation in the ionic homeostasis. Eventually, the cytosolic Ca^{2+} concentration which drives the release of excitatory amino acid neurotransmitter glutamate causes glutaminergic excitotoxicity. Astrocytic glutamate uptake and recycling are impaired under the bioenergetic strain and glutamate transport may be reversed. These processes lead to a vicous circle of aberrant glutamate release and elevations in the intracellular Ca^{2+} concentration. Activation of Ca^{2+}-dependent enzymes further aggravates neuronal cell death via ROS formation, edema and inflammation[166,169].

2.4.2 Post-cardiac arrest syndrome

The pathophysiology of post-cardiac arrest syndrome (PCAS) is complex and remains incompletely characterised. The OHCA-induced global IRI and the resulting nonspecific systemic inflammatory response are thought to underlie PCAS. The cardiocirculatory failure usually dominates the clinical presentation with varying degrees of severity of multiple organ failure[100]. PCAS consists of four key components: Post-cardiac arrest cardiac dysfunction, post-cardiac arrest brain injury, systemic IRI, and the precipitating pathology that caused the initial OHCA[170].

Post-cardiac arrest shock is a combination of cardiogenic and vasodilatory components. Reversible left ventricular dysfunction with systolic and diastolic components starts within minutes after ROSC, reaching its peak in approximately 8 hours and resolving within 48-72 h, occurring even in the absence of coronary causes. The inflammatory syndrome due to IRI leads to severe vasodilation. The shock state may be exacerbated by relative adrenal insufficiency[100,170].

Anoxic-ischaemic brain damage remains the greatest cause for mortality after OHCA[171]. The neurological damage is initiated during the circulatory standstill in OHCA and is accentuated during IRI as discussed earlier. Excitotoxicity, disrupted calcium homeostasis, free radical formation, pathological protease cascades, and the activation of cell-death signaling pathways occur in a time frame from hours to days after OHCA. Cerebral oxygen delivery is further compromised by hypotension, hypoxemia, impaired cerebrovascular autoregulation and oedema[170].

Other IRI complications include acute renal or respiratory dysfunction, which occur in 40-50% of patients after resuscitation from cardiac arrest. PCAS patients are at a high risk of infectious complications. The vulnerability to infectious complications has multiple possible explanations: Loss of airway protection, coma, pulmonary contusion, emergency airway and vascular access, mechanical ventilation and IRI. Gastrointestinal tract IRI is often underestimated and may lead to organ dysfunction via bacterial translocation and a resulting endotoxemia[100].

2.4.3 Metabolomics and out-of-hospital cardiac arrest

The complex pathophysiological state in the context of OHCA, IRI and PCAS is met with a range of compensatory metabolic responses striving to restore and maintain homeostasis. Whether this goal is met or not is likely to be reflected in the circulating metabolic profile.

In 281 OHCA patients examined in the single center COMMUNICATE trial, a targeted mass spectrometry metabolic profile was acquired upon ICU admission to quantify 39 acyl carnitines. The results suggested that high levels of serum short chain acyl carnitines (C2, C3, C5) as well as the sum of all acyl carnitines associated with higher 30-day mortality and poor neurological outcome. Other metabolic determinants of worse patient outcome were lower pH as well as higher levels of lactate, creatinine and urea. However, there was no mention that a multiple correction procedure had been implemented[15]. Several articles have been published from the same dataset in which e.g. elevated concentration of procalcitonin, lactate and taurine were associated with higher mortality[172,173].

In a Danish TTM trial, a targeted mass spectrometry metabolic profile of 61 prespecified metabolites was analysed from blood samples upon patient admission.

Adrenaline and noradrenaline levels were quantified. The findings were corrected for multiple comparisons using the false-discovery-rate method. Most of the variation between survivors and nonsurvivors was explained by metabolites associated with the TCA cycle, i.e. malic acid, fumaric acid, succinic acid. In non-survivors compared to survivors LA, DGLA and oxylipins 12,13-dihydroxyoctadecenoic acid (DiHOME), 13-oxo-octadecadienoic acid i.e. 13-keto-octadecadienoic acid (KODE) were significantly downregulated while among others acylcarnitines (C3, C4, C5, C14, C16), TCA cycle intermediate and associated metabolites (fumaric acid, malic acid, succinic acid, lactic acid) amino acids (alanine, asparagine, aspartic acid, glycine, methionine, ornithine, phenylalanine, proline, tryptophan, tyrosine) and other metabolites (e.g. pyroglutamic acid and kynurenine, trimethylamine N-oxide) were significantly increased. The authors were able to distinguish certain metabolic clusters, the two groups associated with the worst prognosis showed increases in TCA cycle, amino acid and acyl carnitine markers when compared with the other two clusters. BCAA valine, leucine and isoleucine were higher in nonsurvivors with a significant P-value for leucine and isoleucine[37].

Importantly, these studies focused on metabolic profiling upon hospital admission, thus assessing the initial state of OHCA induced metabolic alterations. As discussed, OHCA sets in motion IRI and PCAS, processes which are thought to substantially affect patient outcome in the days following OHCA[170]. A single study has described the changes in a targeted metabolic profile during the first 48 hours after OHCA. In this study, Beske et al. assessed the effects of TTM at 33 °C *vs.* 36 °C on a targeted metabolic profile of 60 metabolites. A total of 9 metabolites were significantly altered between the groups after correction for multiple comparisons; these were TCA cycle metabolites (fumaric acid, malic acid, 2-oxoglutaric acid i.e. α-ketoglutarate), amino acids (isoleucine, leucine, valine), prostaglandin E2, pyruvic and lactic acid. The levels of these TCA cycle metabolites as well as pyruvic and lactic acid decreased less in response to TTM at 33 °C *vs.* 36 °C, while those of isoleucine, leucine and valine decreased more in response to the lower TTM target. In the same study, the associations of these 9 metabolites with 6-month mortality were assessed at 48 hours. While higher concentrations of leucine and valine associated with survival, higher levels of TCA metabolites and lactic acid associated with mortality. In a multivariable model (age, gender, creatinine, bilirubin at day 2 and TTM group), higher valine level associated with survival while elevated α-ketoglutarate levels were associated with mortality[38].

3 Aims

The aims of the present study were as follows:

1. To examine the acute effects of anaesthetic/sedative exposure in a targeted human metabolome in healthy male volunteers in the absence of the confounding factors often present in clinical anaesthesia and the perioperative period.
2. To characterise and compare the pharmacometabolic profiles of anaesthetic exposure between anaesthetics/sedatives.
3. To observe the changes occurring in the targeted metabolic profile within the first 72 hours of ICU treatment after OHCA and to determine the association of metabolite change and 6-month mortality.
4. To explore whether the use of inhaled xenon affects the metabolic profile in OHCA patients.

4 Materials and Methods

4.1 Pharmacometabolic profiles

4.1.1 Ethics

In studies I and II ("The Neural Mechanisms of Anaesthesia and Human Consciousness", European Union Drug Regulating Authorities Clinical Trials (EudraCT) identifier 2015-004982-10, National Clinical Trial number NCT02624401) the ethical approval was provided by the Ethics Committee of Hospital District of Southwest Finland, Turku, Finland.

4.1.2 Trial design and participants

"The Neural Mechanisms of Anaesthesia and Human Consciousness"-trial was an open label, randomised, controlled, parallel group, phase IV clinical drug trial conducted in the Turku positron emission tomography (PET) Centre, University of Turku, Finland. A detailed description of study protocol has been published earlier[174]. The flow of participants through the trial is represented in Figure 4.

Figure 4. CONSORT flow diagram of studies I-II

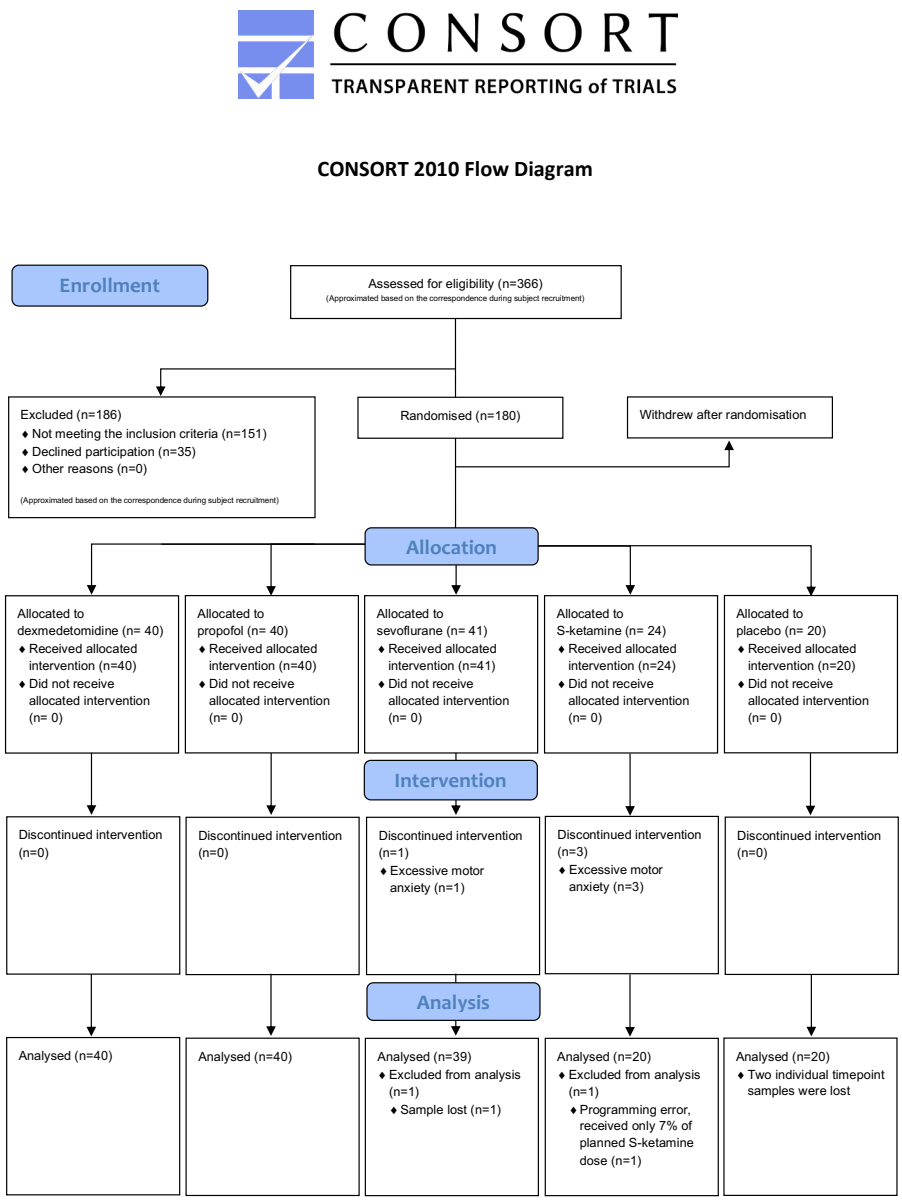

A diagram representing the flow of participants through the trial, from original studies I-II.

A total of 180 subjects were recruited with the goal of having 160 subjects to be evaluated, the goal was reached as planned as discussed earlier[174]. Healthy, American Society of Anaesthesiologists class I (ASA I) male subjects were randomised to receive anaesthetics/sedatives at targeted concentrations that would render 50% of subjects unresponsive to a verbal command (EC_{50} for verbal command). The inclusion of male subjects only was due to the radiation exposure related to the subsequent PET study of human consciousness. Studied anaesthetics/sedatives included dexmedetomidine (Dexdor 100 μg ml^{-1}, Orion Pharma; n=40), propofol (Propolipid 10 mg ml^{-1}; Fresenius Kabi; n=40), sevoflurane (Sevoflurane 100%, Abbvie; n=40), S-ketamine (Ketanest-S 25 mg ml^{-1}, Pfizer; n=20). Ringer's acetate placebo was used (n=20). A formal power analysis was not considered applicable due to the exploratory nature of the study. Randomisation was carried out using balanced permuted block sizes of 16.[174]

The subjects had to meet the following inclusion criteria:

1. Male, due to the subsequent PET study
2. Age 18–30 years
3. Good general health i.e. ASA I physical status.
4. Fluent in Finnish language
5. Right handedness
6. Written informed consent
7. Good sleep quality

The subject was excluded if any of the following criteria were met:

1. Chronic medication
2. History of alcohol and/or drug abuse
3. Strong susceptibility to suffer allergic reactions
4. Serious nausea in connection with previous anesthesia
5. Strong susceptibility to suffer nausea
6. Any use of drugs or alcohol during the 48 hours preceding anesthesia
7. Use of caffeine products 10–12 hours prior the study
8. Smoking

9. Clinically significant previous cardiac arrhythmia / cardiac conduction impairment
10. Clinically significant abnormality in prestudy laboratory tests
11. Positive result in the drug screening test
12. Blood donation within 90 days prior to the study
13. Participation in any medical study with an experimental drug or device during the preceding 60 days
14. The study subject had undergone a prior PET or SPECT study
15. Any contraindication to MRI
16. Hearing impairment
17. Detected unsuitability based on MRI scanning results if available before the PET scanning
18. Sleep disorder or severe sleep problem

4.1.3 Treatment protocol

Prior to the study treatments, all subjects fasted from midnight until study-drug administration. Details of the 60 minute anaesthetic/sedative administration protocol have been published earlier[174]. Target-controlled infusion with a Harvard 22 syringe pump (Harvard Apparatus, South Natick, MA, USA) and Stanpump software (www.opentci.org/code/stanpump) was utilised for intravenous anaesthetics/sedatives with the previously reported pharmacokinetic parameters (Domino-, Talke-, Marsh-models)[175–177]. The Primus anaesthesia workstation (Drägerwerk AG & Co KGaA, Lübeck, Germany) was used for administration and monitoring of sevoflurane[174].

For each anaesthetic, the previously established target concentrations (EC_{50} for verbal command) were used: 1.5 ng ml^{-1} for dexmedetomidine, 1.7 µg ml^{-1} for propofol, 0.75 µg ml^{-1} for S-ketamine, and end-tidal target of 0.9% for sevoflurane[178–180]. The target concentrations of intravenous anaesthetics were determined from arterial blood samples while end-tidal concentration of sevoflurane was monitored continuously during administration.

4.1.4 Blood sampling

In studies I and II, arterial blood samples were collected at three timepoints. The baseline sample was obtained before study-drug administration (timepoint 1), the second sample at the end of 60 min study-drug administration (timepoint 2) and the third approximately 70 min after the cessation of study-drug administration (timepoint 3). At each timepoint 9 ml whole blood ethylenediaminetetraacetic acid (known as EDTA) sample was collected. The obtained samples were immediately protected from light and placed on ice. Within 30 minutes, plasma separation was carried out by the means of cold centrifugation (+4ºC), followed by sample division into amber tubes (Matrix 1.0 mL 2D Screw tubes Amper PP, Thermo Scientific, USA). The amber tube samples were immediately frozen at -20ºC and within the same day transferred to -70ºC. During sample transfers, the temperature was kept under -70 ºC using dry ice. Sampling, storage and transfer of the samples were conducted according to the specifications of the collaborators responsible for metabolite quantification.

4.1.5 NMR metabolomics, analysis

In ^{1}H NMR, the behavior of the spins of covalently bound hydrogen atoms (^{1}H) under the effect of an external magnetic field are utilised to quantify metabolites of interest. The underlying principles of the ^{1}H NMR spectroscopy will be discussed here briefly based on the article by Bothwell and Griffin[181]. A detailed description of the physics underlying ^{1}H NMR spectroscopy is outwith the scope of this thesis.

The magnetic field of a nucleus is considered to arise from the spinning motion of its electrical charge. Under an external magnetic field, the ^{1}H nucleus has two possible spin states, + ½ and − ½. The proportion of the nuclei in the higher energy state (+ ½) and the lower energy state (− ½) depends on the energy difference between these spin states: The higher the energy difference, the more nuclei will be in the lower energy − ½ state.

Briefly and generally, the ^{1}H NMR spectroscopy procedure is as follows:

1. The prepared sample is placed under a strong external magnetic field (B0).
2. A second electromagnetic (EM) field (B1) excites the sample nuclei from lower energy spin states (− ½) to higher energy spin states (+ ½) via transient EM radiofrequency (RF) pulses, sometimes in a cluster i.e. a pulse sequence.

3. ^{1}H nuclei absorb RF EM radiation over a characteristic range of frequencies affected by the immediate chemical surroundings within the molecule. This phenomenon is the foundation for a parameter called a chemical shift (δ), which conveys information e.g. on different functional groups within the molecule. For example, ethanol ^{1}H containing chemical groups $-CH_3$, $-CH_2-$, -OH have different δ values.
4. Nuclei in excited spin states relax back to their equilibrium population in distinct half-lives of around 500-1000 ms emitting EM radiation in the RF frequency. Similiarly to δ, the immediate chemical environment within the molecule affects its half-life. The relaxation signal is measured as a decay of signal intensity over a few seconds i.e. the free induction decay.
5. The phase-information of the emitted RF waves enabled e.g. the development of fast Fourier Transformation, which is a mathematical procedure converting free induction decays in the time domain into the frequency domain to produce a spectrum representation of NMR data.
6. The intensity of the signal, e.g. the height of the peaks in the one dimentional representation of the NMR spectrum, enables the deduction of molecule concentrations.
7. Thus, the ^{1}H emitted RF radiation has four parameters: 1. intensity, 2. chemical shift (δ), 3. half-life and 4. phase. These parameters enable the differentiation and quantification of molecules within a sample.

In the current study, metabolite markers were quantified using targeted ^{1}H NMR method (Nightingale Health Ltd, Helsinki, Finland). The company uses proprietary data processing methods to overcome overlaps in individual molecular signals and metabolite quantification. This process enables simultaneous quantification of routine lipids, lipoprotein subclass profiling, fatty acid composition, and various low-molecular weight metabolites including amino acids, ketone bodies and glycolysis-related metabolites in molar concentration units. In the current study, 146 metabolite markers and 9 ratios were analysed. The analysed biomarkers included 101 lipoprotein measures, 37 lipid-related markers (including 16 fatty acid, 9 cholesterol, 9 glycerides and phospholipids and 3 apolipoprotein measures), concentrations of 8 amino-acids, 3 glycolysis related metabolites, 3 ketone bodies, creatinine and albumin and an inflammatory marker GlycA. As predetermined metabolites were quantified, the obtained profile was considered to represent a targeted metabolic profile. The current methodology has been described in more detail previously[182,183].

4.1.6 NMR metabolomics, *in vitro* analysis

In study I, extensive changes in lipoprotein and lipid metabolism occurred in response to propofol administration *in vivo*. As a quality control measure, *in vitro* analyses were carried out to assess whether propofol and the accompanying lipid emulsion had direct effects on NMR quantification of metabolites. The previously described NMR method was used (Nightingale Health, Helsinki, Finland). Propofol was incrementally added to pooled human serum samples previously prepared from whole blood samples, collected in lithium heparin tubes and stored at -80ºC, similar to the main analysis. A comparison of NMR metabolic profiles of *in vitro* samples with incremental propofol concentrations of 1.75 - 100 μg ml^{-1} and blank pooled samples (without added propofol) was conducted. Furthermore, the mean changes in VLDL markers in the propofol group *in vivo* were compared with the VLDL changes in the *in vitro* experiment to assess the possibility of propofol emulsion constituent accumulation during a continuous infusion in *in vivo* samples.

4.1.7 LC-MS/MS metabolomics analysis

A total of 45 oxylipin and bile-acid analytes (28 and 17, respectively) were quantified by the means of LC-MS/MS. The process begins with liquid chromatography. Here, a general review on the working principles of LC-MS/MS is provided based on previous articles[184–187].

Briefly, the principles of LC-MS/MS are as follows:

1. In liquid chromatography, the molecules of interest in the mobile phase pass through a column of stationary solid phase separating molecules of interest based on their physiochemical properties. The development of columns with sub-2 μm particles, numerous column chemistries and extending the pressure ranges of the instrumentation up to 600 to 1300 bar enabled ultra high-pressure liquid chromatography which conferred multiple advantages (i.e. reduction of matrix effects, improvement in sensitivity, higher throughput and better resolution).
2. The separated sample is introduced to the mass spectrometer and ionised. In electrospray ionisation, liquid phase from liquid chromatography containing the analytes of interest is directed to a perforated capillary. Upon applying a high voltage, there is a dispersion to charged droplets, followed by solvent evaporation and ion ejection, creating a mist of charged droplets.

3. The ionised sample is then accelerated with an electric field and introduced to the mass analyser, which separates the accelerated beam of ions based on the mass-to-charge (m/z) ratio and the interactions of charged ions under the effects of external magnetic and electric fields. In the current study, a Qtrap instrument was used, often referring to a configuration of mass analyser in which the third quadrupole of a triple quadrupole MS operates as a linear ion trap e.g. in which ions are trapped and sequentially ejected based on m/z ratio.
4. The ions are registered on the detector and the computer displays the signals graphically as a mass spectrum, a plot of relative intensity of observations on the y-axis and m/z ratio on the x-axis, eventually enabling the identification and quantification of molecules in the sample.
5. Tandem mass spectrometry refers to a method in which the first selection of precursor ions based on their m/z is followed by fragmentation of the precursor ions and measurement of resulting product ions based on their m/z ratio offering structural information of their precursors.

In the current study, analysis of plasma concentrations of bile acids and lipid mediators was conducted in the Department of Clinical Pharmacology, University of Helsinki, using a Nexera X2 ultra high-pressure liquid chromatography system (Shimadzu, Kyoto, Japan) coupled to a 5500 Qtrap mass spectrometer interfaced with an electrospray ion source (ABSciex, Toronto, ON). Stable isotope labaled internal standards, reference bile acids and lipid mediators were purchased from Cayman Chemical Company (Ann Arbor, MI) and Toronto Research Chemicals (North York, ON). Other chemicals and organic solvents were of commercially available analytical grade.

Quantification of 17 bile acids was conducted as previously described, with minor modifications[188]. For each bile acid, calibration standards (0.001-5 μmol/L) prepared in charcoal-stripped plasma, were processed along with the plasma samples. A total of 50 μL of 0.005% formic acid containing the internal standards was mixed with 150 μL plasma samples, followed by an incubation period of 10 minutes at +4 ˚C. Strata-X polymeric reversed-phase 96-well extraction plate (10 mg/well, Phenomenex, Torrance, CA) was used for bile acid extraction. Prior to sample loading, the plate was preconditioned according to the manufacturer's instructions. The wells were washed with 100 μL of 0.05% formic acid and 100 μL of 5% methanol, and the analytes were eluted with 100 μL of methanol followed by 100 μL of acetonitrile. Vacuum evaporator (GeneVac, Thermo Fisher Scientific) was used for drying the sample extracts which were reconstituted in 100 μL of 60% methanol. A 5 μL sample volume was injected into the LC-MS/MS system. The

chromatographic separation was carried out on Atlantis T3 analytical column, 2.1×100 mm, 3 µm particle size (Waters. Corp., Milford, MA) using a gradient elution of 5 mM ammonium acetate containing 0.005% formic acid in water (mobile phase A) and methanol (mobile phase B). The flow rate was set at 0.3 mL/min with the column temperature at 40 ˚C. Negative multiple reaction monitoring (MRM) mode was used for mass spectrometry, except for 7-OH-4-cholesten-3-one which was analysed in the positive mode (ion transition m/z 401-177). The within- and between-day accuracies (% of nominal concentration) of the method ranged from 87.9% to 113%, and precisions (coefficient of variation i.e. CV%) were ≤ 14.1%, except for lower limit of quantification (LLOQ) for which accuracies and precisions were ±20 and <20%.

Using authentic reference standards as calibrators, 158 target eicosanoids and related compounds were monitored in human plasma. The process has been described in detail previously[189]. The detection limit was set at a signal-to-noise (S/N) ratio larger than 3 and quantification limit was set at a S/N ratio larger than 7. In plasma samples, 28 lipids could be reliably quantified.

Aliquots of 100 µl plasma were precipitated with 400 µl of methanol containing 18 stably labeled internal standards. The sample mixtures were then centrifuged at 14 000 g for 10 min, supernatants were diluted with 0.003% formic acid (1:5 v/v) prior to loading into the pre-conditioned Strata-X extraction plate (10 mg/well, Phenomenex). The wells were serially washed with 100 µL of 0.03% formic acid and 100 µL of 10% methanol and eluted with 150 µL of methanol followed by 150 µl of ethanol. Vacuum evaporator (Thermo Fisher Scientific) was used for eluent evaporation to dryness. The reconstitution of lipids was carried out in 25 µL of methanol. In the chromatographic separation of lipids, a reversed-phase analytical column Kinetex C8 2.1×150 mm was used, with 2.6 µM particle size (Phenomenex) utilising 0.1% formic acid and acetonitrile as the mobile phase A and B. The flow rate of the mobile phase was 0.35 mL/min and the column temperature was set at 40 ˚C. The mass spectrometer was operated both in positive and in negative MRM modes, the scheduled MRM method was applied to minimize the number of ion transitions acquired simultaneously. Similarly to bile-acid quantification, a S/N -ratio larger than 3 was defined as the detection limit and the S/N -ratio larger than 7 was set as the quantification limit. 3-6 different concentration levels of quality control samples covering the relevant plasma concentration range for each oxylipin were used to determine the within- and between-day accuracy and precision of the method. The accuracies were within ±15% and the precisions below 15% at the QC concentration levels of at least three times of LLOQ, and <20% and ±20 at the level of LLOQ. All analytes were quantified using internal standard methods.

4.1.8 LC-MS/MS metabolomics, *in vitro* analysis

As discussed previously, propofol is administered in a lipid emulsion. To assess the role of accompanying lipid emulsion in propofol formulation (Propolipid 10 mg/mL) in the results of the current LC-MS/MS analysis, a dilution series of propofol emulsion was prepared in human plasma in ratios of 1:10, 1:100, 1:200, and 1:1000 (v/v). Blank human plasma was used as a control sample. Oxylipin levels in these samples were analyzed using the same method as for the study samples.

4.1.9 Statistical analysis

Zero values and values under the detection limit were omitted from the analyses (4 and 6.8%, studies I and II, respectively). A total of 155 NMR analytes and 40 LC-MS/MS oxylipin and bile acid related metabolites were evaluable and were included in the analyses in studies I and II, respectively. Five metabolites were omitted from the analysis due to the extensive number of values under the detection limit: taurolithocholic acid, prostaglandins E2 and D2, 5,6-dihydroxyeicosatetraenoic acid (DiHETE) and 8,9-dihydroxyeicosatrienoic acid (DHET). Logarithmic transformation was performed for metabolites with skewness >1 (42% in study I, 100% in study II). All metabolites were scaled to baseline standard deviation (SD), with the mean group difference in SD change units being referred to as the standard deviation score (SDS). In both studies, repeated measures analysis of variance (ANOVA) was performed with each metabolite marker as the outcome and time as a within factor and group as a between factor[190]. There was no assumption concerning dependency between metabolites as all metabolites were analysed using separate ANOVA models. The mean differences in SD changes [95% confidence interval (i.e. 95% CI)] between groups for all metabolites were estimated from a repeated measures model using a group by time interaction effect. The intergroup (drug *vs.* placebo and drug *vs.* drug) differences in SD changes were estimated between timepoints 1 *vs.* 2 and 1 *vs.* 3. The P-values were Bonferroni corrected for multiple testing by a factor of 3100 and 800, in studies I and II, respectively. An alpha threshold of 0.05 was used. In both studies, data were expressed as SDS [95% CI], P-value. Statistical analyses were carried out with SAS software (version 9.4; SAS Institute Inc., Cary, NC).

Forest plots and line graphs were created using R (Version 1.1.383, https://www.R-project.org/) gglpot2 function (Version 3.2.1, https://ggplot2.tidyverse.org). Illustrations of the metabolic routes were created with draw.io (https://www.drawio.com/) and Microsoft PowerPoint, as modified from

Kyoto Encyclopedia for Genes and Genomes i.e. KEGG human metabolic pathways[191]. Figure 1 was created with Microsoft PowerPoint.

4.2 Metabolomics after out-of-hospital cardiac arrest

4.2.1 Ethics

In study III ("Effect of Xenon and Therapeutic Hypothermia, on the Brain and on Neurological Outcome Following Brain Ischemia in Cardiac Arrest Patients", Xe-Hypotheca; EudraCT 2009-009505-25, National Clinical Trial number NCT00879892), the ethical approval was provided by the Ethics Committee of Hospital District of Southwest Finland, Turku, Finland and the institutional review boards of the Helsinki University Hospital and the Finnish Medicines Agency. The data was reviewed by an independent data and safety monitor committee after enrollment of every 4 patients and at 6-month intervals. Within 4 hours of hospital arrival, written informed assent was obtained from the next of kin or from a legal representative of the patient in accordance with the Declaration of Helsinki. The right to withdraw and the use of data collected prior to possible withdrawal, was informed to the patient's family, as predefined in the trial protocol. Upon regaining consciousness, patients were informed accordingly.

4.2.2 Trial design and participants

The Xe-Hypotheca -trial was a randomised, 2-group, single-blind, phase 2 clinical drug trial taking place at 2 multipurpose ICU in Finland. The flow of patients through the trial is represented in Figure 5. The complete trial protocol has been published previously[115].

Briefly, 224 comatose survivors of OHCA consecutively admitted to Turku and Helsinki University Hospitals were assessed for eligibility. A total of 110 patients (66 and 44 from Turku and Helsinki University hospital, respectively) were recruited between 5th of August 2009 and 9th of September 2014 and randomised to receive TTM at 33 3˚C alone, or in combination with inhaled xenon (LENOXe, Air Liquide Medical GmbH). The sample size of 110 was based on power analysis on the primary endpoint of Xe-Hypotheca trial, brain MRI functional anisotropy. Randomisation was carried out using permuted blocks with random block sizes 4, 6 and 8. Patients were allocated 1:1 to receive TTM with or without inhaled xenon.

As published previously[115], the inclusion criteria were:

1. VF or non-perfusive VT as initial presenting cardiac rhythm
2. The first attempt of resuscitation by EMS within 15 minutes after the collapse
3. The cause of collapse should be considered primarily as cardiogenic
4. ROSC within 45 minutes after the collapse
5. The patient should be still unresponsive in the emergency room
6. Age: 18–80 years
7. Consent from the next of kin or the legal representative and the initiation of inhaled xenon within 4 hours after hospital arrival

As published previously[115], the study exclusion criteria were:

1. Asystole as the primary rhythm
2. Admission hypothermia (< 30 °C core temperature)
3. Unconsciousness before cardiac arrest (cerebral trauma, spontaneous cerebral haemorrhage, intoxication etc.)
4. Response to verbal commands after ROSC and before randomisation
5. Pregnancy
6. Coagulopathy
7. Terminal phase of a chronic disease
8. Systolic arterial pressure < 80 mmHg or mean arterial pressure < 60 mmHg for over 30 min period after ROSC
9. Factors making participation in follow-up unlikely
10. Enrolment in another study

Figure 5. CONSORT flow diagram of study III

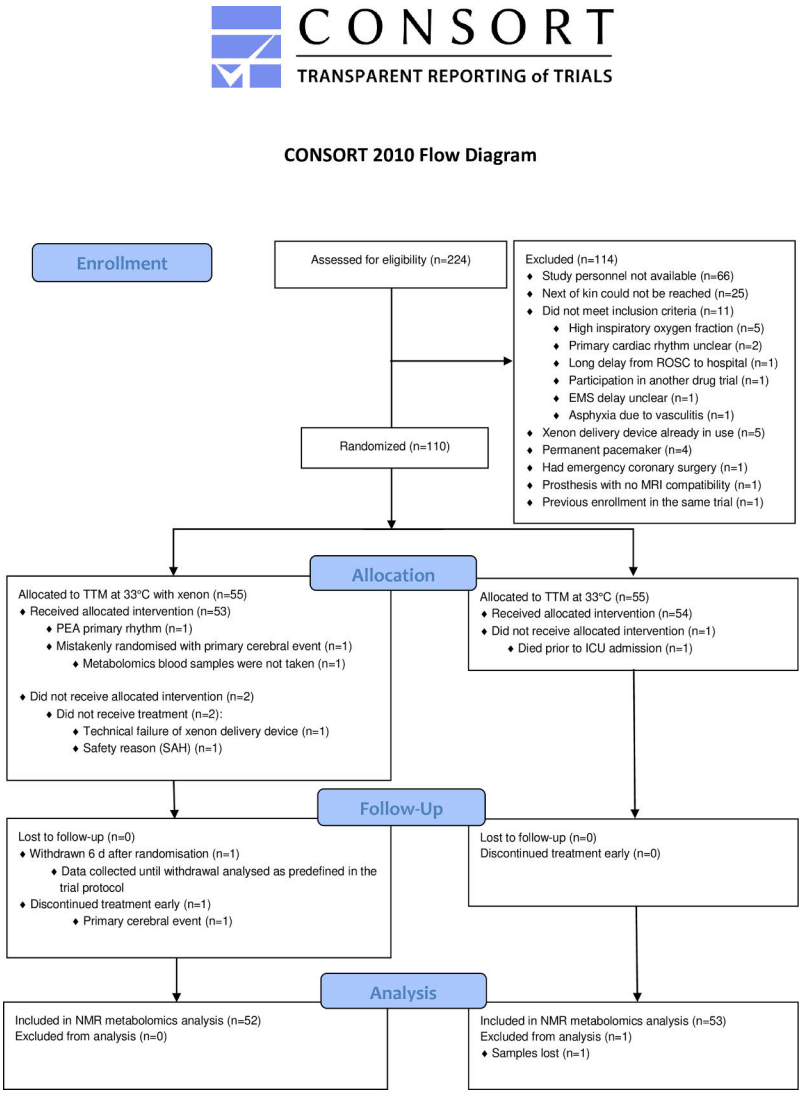

A diagram representing the flow of patients through the trial, from original study III.

4.2.3 Treatment protocol

Upon arriving at the emergency department, a routine initial assessment and treatment including mechanical ventilation and correction of cardiovascular instability were performed, a brain CT scan was acquired for all patients before initiation of the study treatments. When clinically indicated, invasive cardiac procedures e.g. percutaneous coronary angiography interventions (PCI) were performed prior to ICU admission and the initiation of active cooling or xenon treatment. Arterial and central venous catheters were inserted into all of the patients.

Upon arrival to the ICU, TTM was initiated with cooling of patients to a target core temperature of 33-34 °C. Immediately after the written informed consent was obtained, inhaled xenon was initiated in the ICU with a closed-system ventilator specifically designed for xenon administration (PhysioFlex, Dräger, Lübeck, Germany). Xenon concentration was continuously monitored by the thermoconductive device on the ventilator. Xenon treatment continued until the start of rewarming from TTM. End-tidal concentration target was 40% ± 10%, with the maximal allowed xenon concentration 65%.

TTM was induced by invasive intravascular temperature management device (Alcius CoolGuard 3000 thermal regulation system; Zoll Medical Corporation, Chelmsford, MA, USA) and the target core temperature was maintained at 33-34 °C for 24 hours. During TTM, sedation was maintained with propofol infusion (1-5 mg/kg/h) and additional boluses when indicated. Alternatively, midazolam infusion and boluses were used especially in hypotensive patients. Sedation was adjusted to a Richmond agitation-sedation scale (RASS scale) of -4 to -5, sedative doses were adjusted accordingly in patients receiving concomitant xenon treatment. Continuous fentanyl-infusion 50–100 μg/h, with additional 25–50 μg boluses when indicated, was administered to ensure analgesia. TTM induced shivering was terminated by deepening sedation and analgesia or with neuromuscular blocking agents (e.g. cisatracurium, rocuronium).

Rewarming was initiated at a maximum rate of 0.5 °C/h after 24 hours of TTM at the target temperature. At the start of rewarming, xenon treatment was discontinued and substituted to propofol or midazolam. To prevent reactive hyperthermia, the invasive endovascular balloon membrane-cooling catheter (Microtherm, Alsius Co) was preserved.

Predefined reasons for premature withdrawal by the decision of the investigator or attending physician:

1. A failure to maintain xenon concentration ≥ 20%

2. A failure in ventilation and/or oxygenation of the patient with xenon delivery device
3. TTM was terminated prematurely by the decision of the attending physician
4. Adverse event/serious adverse event
5. Protocol violation
6. If for any reason the investigator or the attending physician believed that continued participation in the study was not in the best interest of the patient

Predefined haemodynamic, chemical and arterial blood gas targets during intervention were as follows:

1. Mean arterial pressure 60-90 mmHg
2. Systolic arterial pressure >100 mmHg
3. Central venous pressure, positive end-expiratory pressure corrected 6-10 mmHg
4. Heart rate (during TTM) >30 beats/min
5. Heart rate (after TTM) >40 beats/min
6. Blood glucose 5.0-8.0 mmol/l
7. Blood haemoglobin >70 g/l
8. Blood haematocrit 0.3-0.45
9. Partial pressure of arterial oxygen 10-18 kPa
10. Partial pressure of arterial carbon dioxide 4.5-5.5 kPa

Vasoactive treatments (adrenaline, noradrenaline, dopamine, dobutamine, levosimendan, vasopressin, etc.) were used according to the decision of the attending physician to meet the haemodynamic targets. Similarly, bradycardia of <30 beats/min was treated with atropine boluses of 0.01 mg/kg and/or a rise in the body target temperature (0.5 °C/h). If a core temperature increase beyond 34 °C was needed for safety reasons, TTM and xenon exposure were discontinued. Used medication and fluids were recorded in case report forms.

4.2.4 Blood sampling

In study III, blood samples for metabolomic analysis were collected at baseline upon arriving at the ICU prior to initiation of TTM or xenon, after completing study treatment at 24 hours, and at 72 hours. A 10 ml blood sample was drawn and stored at -70 C. Sampling, storage and transfer of the metabolomics samples was carried out as specified by the company responsible for metabolite quantification (Nightingale Health, Helsinki, Finland).

4.2.5 NMR metabolomics

The NMR methodology has been discussed in detail previously (Study I).

4.2.6 Statistical analysis

Continuous characteristic variables between xenon and control groups were compared using two-sample t-test and Mann-Whitney U-test, categorical characteristic variables were compared with chi-square test or Fisher exact test.
Logarithmic transformation was performed for all metabolites with skewness >1 (46.5% of all metabolites in the 6-month mortality analysis). Metabolites were scaled to baseline SD.

Associations of metabolites with 6-month mortality were analysed utilising Cox regression after adjusting for age, sex, center and group. The age, sex and center adjusted mean differences in metabolites between the xenon and control groups were analyzed using a linear mixed model with a random intercept for each patient. The model included the main effects for group and time and group by time interaction effect. From this model, the group differences for a metabolite change from baseline to 24 hours and from baseline to 72 hours were estimated using contrasts. Due to the high correlation between several of the measured metabolite values, a principal component analysis was carried out for each time point, with over 95% of variation in metabolomic data being explained by 14 components for all three time points. Based on the principal component analysis, all reported p-values were adjusted by a factor of 14 to account for multiple testing with an alpha threshold of 0.05 being used[192]. The results are reported as adjusted hazard ratios (HR) [95% CI] and adjusted p-values. Statistical analyses were carried out with SAS software (version 9.4; SAS Institute Inc., Cary, NC).

5 Results

5.1 Pharmacometabolic profiles

The baseline characteristics of subjects in study I and II are summarised in Table 10. The study was completed as planned (Fig. 4). Anaesthetic concentrations were stable in all groups, however, dexmedetomidine and S-ketamine concentrations were slightly higher than targeted (Fig. 6). NMR and LC-MS/MS metabolomics data of 159 subjects were evaluable (all timepoint samples of one subject in the sevoflurane group and two individual timepoint samples in the placebo group were lost).

Statistically significant changes *vs.* placebo (timepoints 1 *vs.* 2 or 1 *vs.* 3) were observed in 21.5%, 35.4%, 3.6% and 1.5% of the analysed 195 metabolites in dexmedetomidine, propofol, S-ketamine and sevoflurane groups, respectively. Many of these changes remained significant in anaesthetic-anaesthetic comparisons (Study I appendix A and Study II, appendix B). All analysed metabolite changes *vs.* placebo are shown in forest plots (Figs. 7-14, 16-23). In the text, data is expressed as SDS [95% CI] between timepoints 1 *vs.* 2, if not otherwise stated.

Table 10. Demographic characteristics of study subjects, studies I-II

	n	Height (cm)	Weight (kg)	BMI	Age (years)
Dexmedetomidine	40	179.1 (6.5)	77.3 (10.8)	24.1 (2.9)	24.7 [20;30]
Propofol	40	180.5 (6.0)	77.6 (11.1)	23.8 (3.3)	23.4 [18;28]
Sevoflurane	39	179.7 (7.2)	79.5 (9.7)	24.6 (2.8)	24.4 [19;30]
S-ketamine	20	182.7 (5.4)	79.9 (10.6)	23.9 (3.0)	23.4 [20;30]
Placebo	20	182.4 (8.8)	82.9 (14.2)	24.8 (2.6)	23.1 [20;28]

Data as numbers or means with SD or range. From original publication I.

Figure 6. Measured anaethetic/sedative concentrations

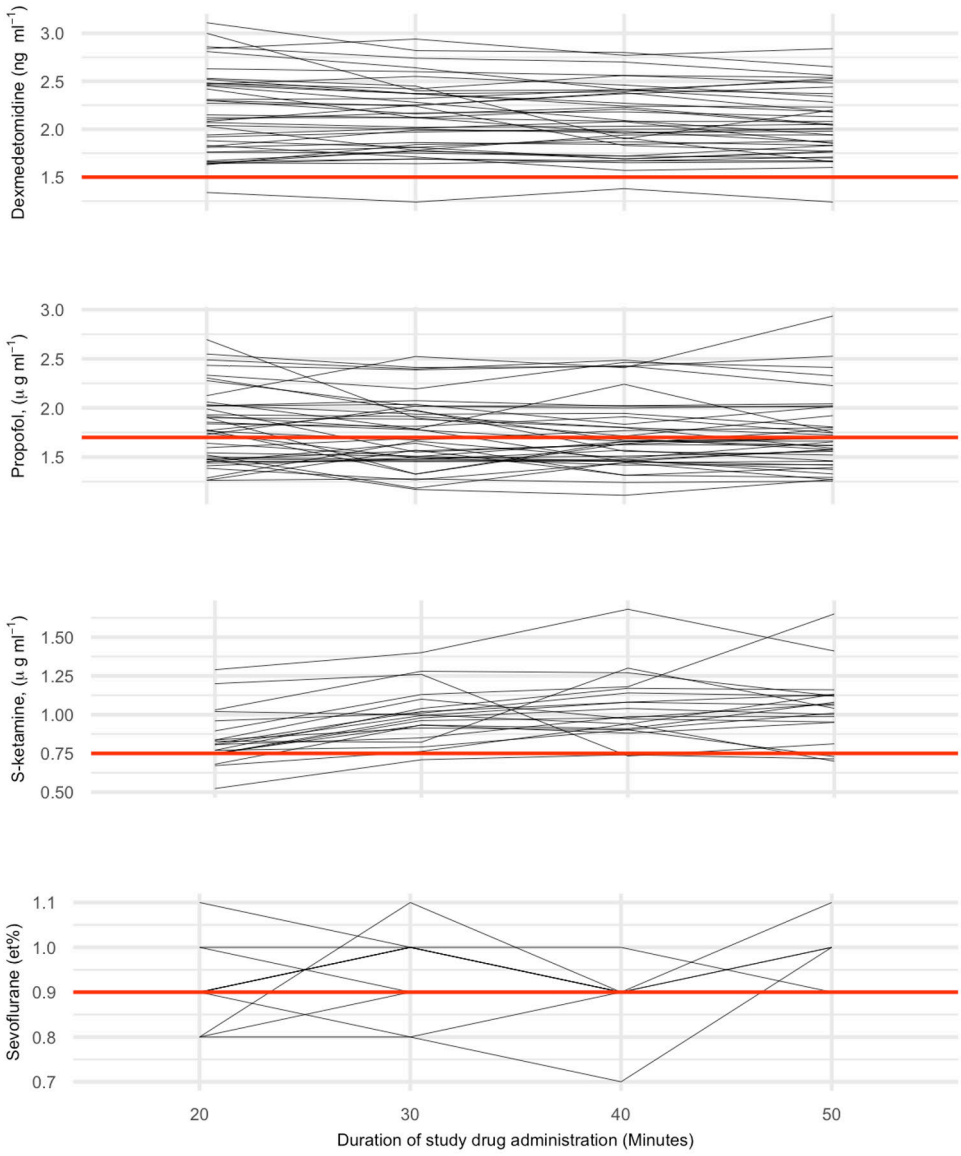

The target concentrations of intravenous anaesthetics/sedatives were determined from arterial blood samples while end-tidal concentration of sevoflurane was monitored continuously during administration. From original publication I.

5.1.1 Dexmedetomidine

In the dexmedetomidine group, the NMR metabolic profile showed a strong elevation of glucose levels 3.14 [2.56; 3.71], P <0.001 and a concomitant decrease in ketone bodies 3-hydroxybutyrate -1.60 [-1.97; -1.23], P<0.001 and at timepoints 1 *vs.* 3 acetoacetate -0.98 [-1.27; -0.69], P<0.001. Dexmedetomidine induced changes in the HDL composition and decreased the very large HDL concentration -0.29 [-0.42 to -0.17], *P*=0.024 (Figs. 7-9).

LC-MS/MS analysis revealed a widespread and significant decrease in both oxylipin and bile acid related metabolites (Fig. 10). For example, there were decreases in CYP-derived oxylipins 5,6-DHET -1.23 [-1.76; -0.69], P=0.011 (1 *vs.* 3), 11,12-DHET -1.35 [-1.86; -0.83], P<0.001, 14,15-DHET -1.31 [-1.82; -0.8], P<0.001, 9,10-DiHOME -1.19 [-1.6; -0.78], P<0.001 (1 *vs.* 3) and 12,13-DiHOME -1.22 [-1.66; -0.77], P<0.001. Many of the measured analytes decreased further when a 1 *vs.* 3 timepoint comparison was conducted, reaching statistical significance after the cessation of dexmedetomidine administration.

With respect to the NMR profile, the changes in the levels of glucose, 3-hydroxybutyrate and very large HDL phospholipid and free cholesterol content were significant in all intergroup comparisons. Of the significant changes in LC-MS/MS profile *vs.* placebo, 56% remained significant in all drug-drug-comparisons.

Figure 7. The dexmedetomidine-placebo comparison of the NMR profile, part 1

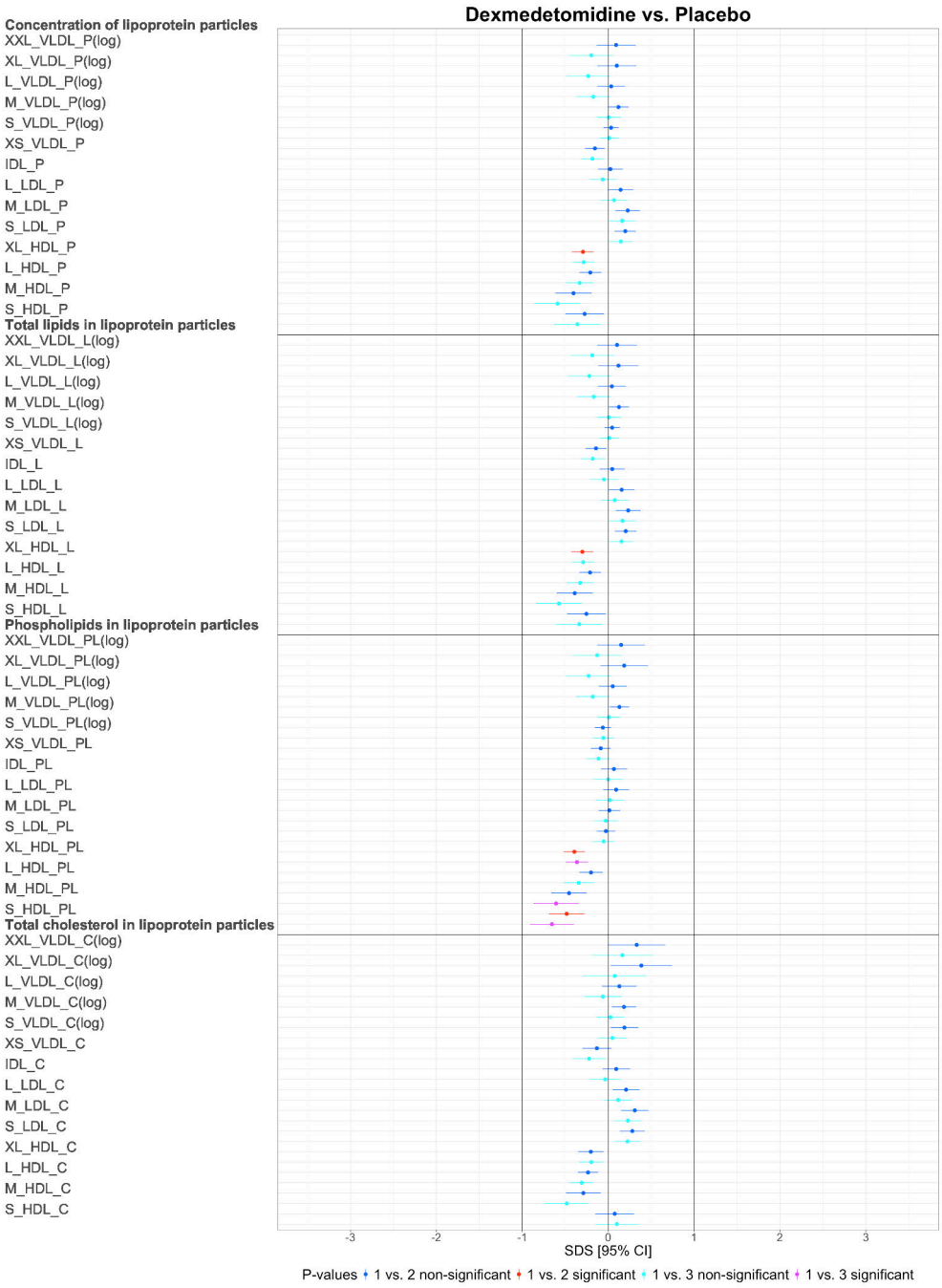

Figure 8. The dexmedetomidine-placebo comparison of the NMR profile, part 2

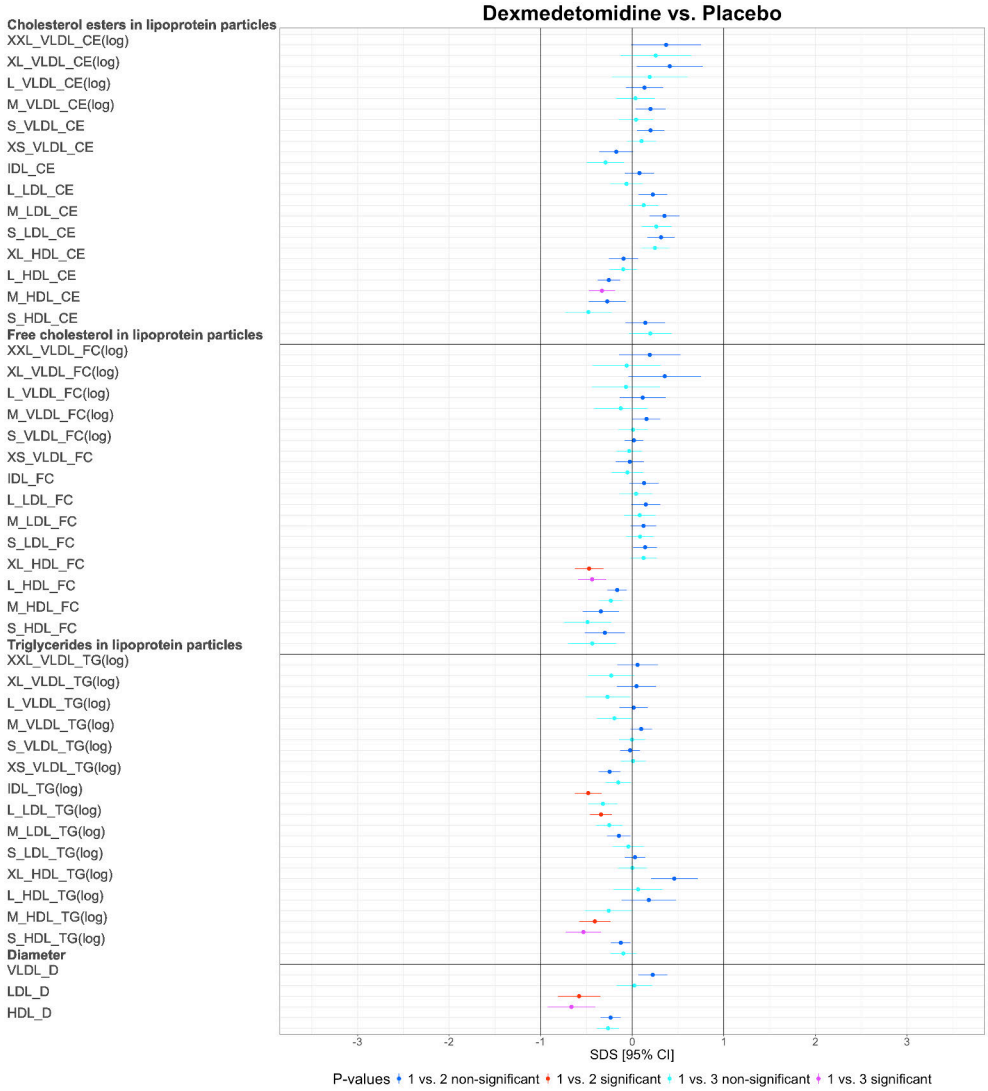

Figures 7-9: Forest plots of dexmedetomifine-placebo comparison of the NMR profile, as modified from study I. Data are reported as SDS and 95% CI. The vertical lines depict 0 and +/- 1 SDS thresholds. Positive values (to the right) depict an increase in metabolite concentration compared to placebo, while negative values (to the left) represent a decrease compared to placebo. The colour coding represents the changes during anaesthetic administration (in timepoints 1 vs. 2) and from baseline to 70 minutes after anaesthetic administration (in timepoints 1 vs. 3). Statistically significant changes are highlighted in red and pink (timepoints 1 vs. 2 and 1 vs. 3, respectively). Logarithmic transformation was carried out for skewed metabolites; these metabolites are marked with (log). All the metabolite abbreviations of the NMR metabolic profile can be found in study I, Appendix A.

Figure 9. The dexmedetomidine-placebo comparison of the NMR profile, part 3

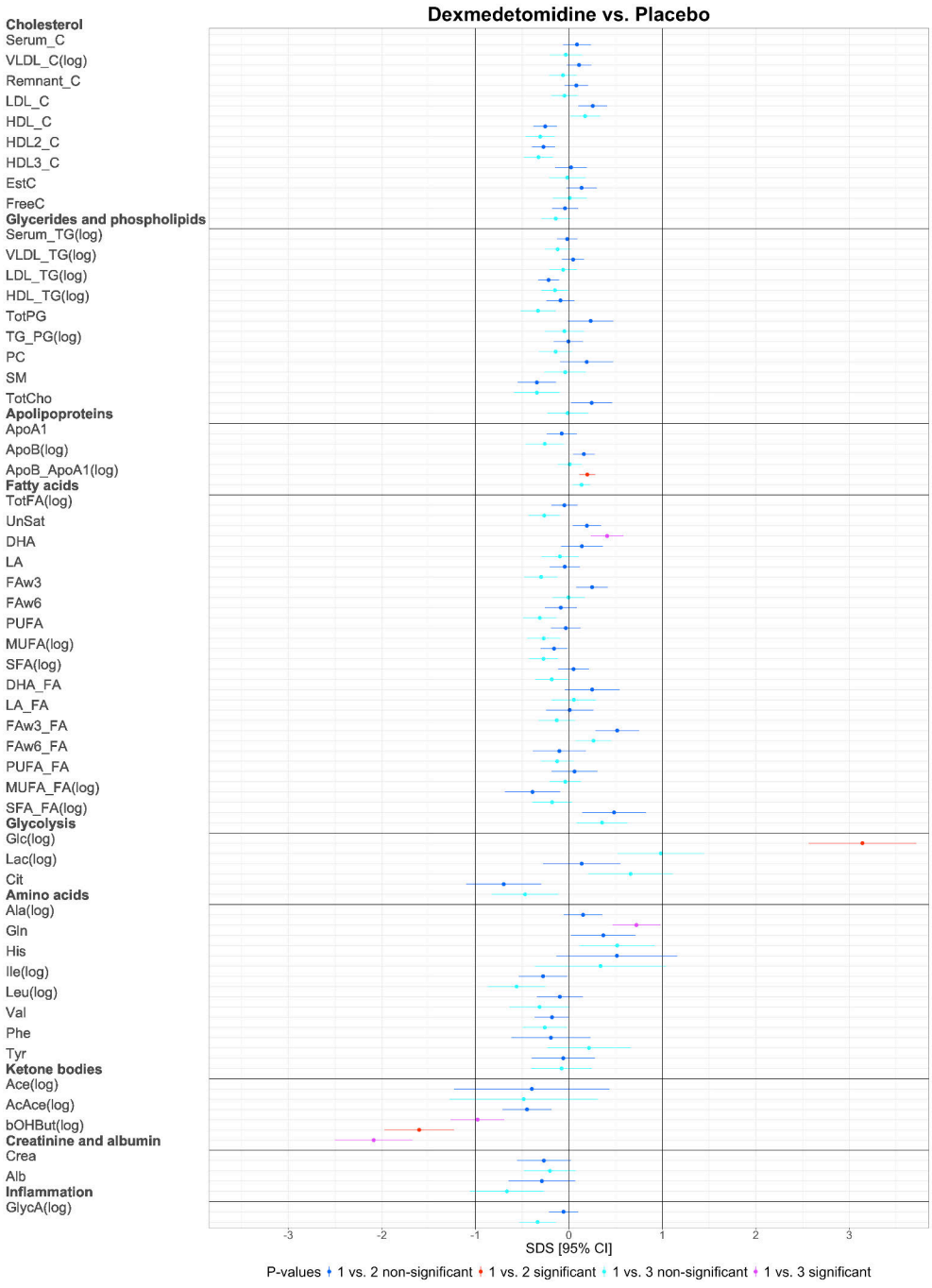

Figure 10. Forest plot of dexmedetomidine *vs.* placebo, LC-MS/MS

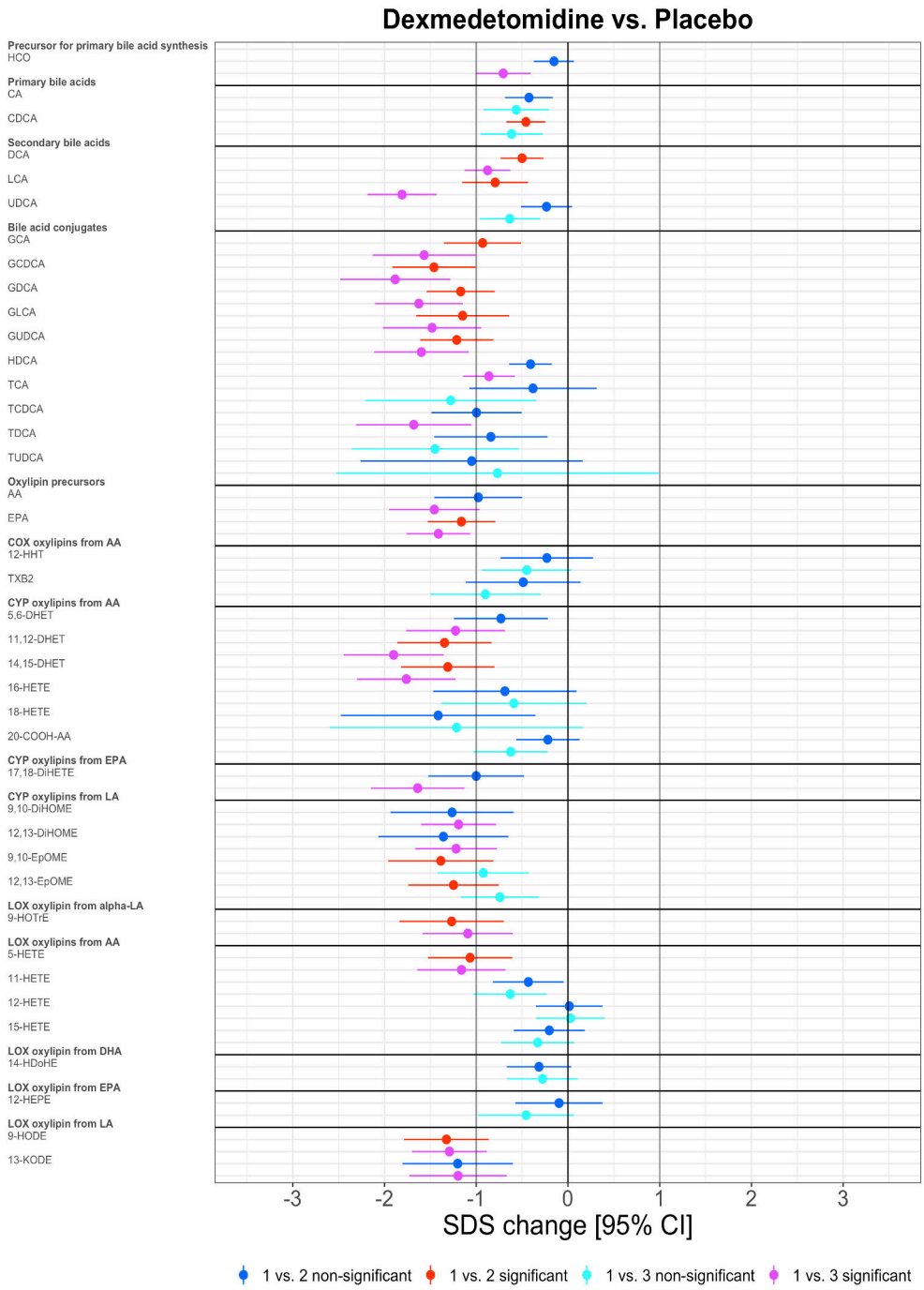

Figure 10: Forest plot of dexmedetomidine vs. placebo, all analysed metabolites in the LC-MS/MS profile, as modified from original publication II. Change is reported in SDS with 95% CI. The vertical lines depict 0 and +/- 1 SD thresholds. The colour coding represents the changes in time points 1 vs. 2 and 1 vs. 3, the significant changes are highlighted. HCO, 7α-Hydroxy-4-cholesten-3-one; CA, cholic acid; CDCA, chenodeoxycholic acid; DCA, deoxycholic acid; LCA, lithocholic acid; UDCA, ursodesoxycholic acid; GCA, glycocholic acid; GCDCA, glycochenodeoxycholic acid; GDCA, glycodeoxycholic acid; GLCA, glycolithocholic acid; GUDCA, glycoursodeoxycholic acid; HDCA, hyodeoxycholic acid; TCA, taurocholic acid; TCDCA, taurochenodeoxycholic acid acid; TDCA, taurodeoxycholic acid; TUDCA, tauroursodeoxycholic acid; AA, arachidonic acid; EPA, eicosapentaeonic acid; 12-HHT, 12-hydroxy-5,8,10-heptadecatrienoic acid; PGD2, prostaglandin D2; PGE2, prostaglandin E2; TXB2, thromboxane B2; 5,6-DHET, 5,6-dihydroxy-8,11,14-eicosatrienoic acid; 8,9-DHET, 8,9-dihydroxy-5,11,14-eicosatrienoic acid; 11,12-DHET, 11,12-dihydroxy-5,8,14-eicosatrienoic acid; 14,15-DHET, 14,15-dihydroxy-5,8,11-eicosatrienoic acid; 16-HETE, 16-hydroxy-5,8,11,14-eicosatetraenoic acid; 18-HETE, 18-hydroxy-5,8,11,14-eicosatetraenoic acid; 20-COOH-AA, 5,8,11,14-eicosatetraenedioic acid; 5,6-DiHETE, 5,6-dihydroxy-8,11,14,17-eicosatetraenoic acid; 17,18-DiHETE, 17,18-dihydroxy-5,8,11,14-eicosatetraenoic acid; 9,10-DiHOME, 9,10-dihydroxy-12-octadecenoic acid; 12,13-DiHOME, 12,13-dihydroxyoctadec-9-enoic acid; 9,10-EpOME, 9,10-epoxy-12-octadecenoic acid; 12,13-EpOME, 12,13-epoxy-9-octadecenoic acid; 9-HOTrE, 9-hydroxy-10,12,15-octadecatrienoic acid; 5-HETE, 5-hydroxy-6,8,11,14-eicosatetraenoic acid; 11-HETE, 11-hydroxy-5,8,12,14-eicosatetraenoic acid; 12-HETE, 12-hydroxy-5,8,10,14-eicosatetraenoic acid; 15-HETE, 15-hydroxy-5,8,11,13-eicosatetraenoic acid; 14-HDoHE, 14-hydroxy docosahexaenoic acid; 12-HEPE, 12-hydroxy-5,8,10,14,17-eicosapentaenoic acid; 9-HpODE, 9-hydroperoxyoctadeca-10,12-dienoic acid; 9-HODE, 9-hydroxy-10,12-octadecadienoic acid; 13-KODE, 13-keto-9,11,-octadecadienoic acid; LA, linoleic acid; alpha-LA, alpha-linoleic acid; DHA, docosahexaenoic acid.

5.1.2 Propofol

Lipid and lipoprotein metabolism were extensively affected by propofol administration (Figs. 11-13). In the NMR metabolic profile, the strongest changes were observed in saturated fatty acids to total fatty acids ratio (SFA/FA) 1.76 [1.42; 2.10], *P*<0.001, very large VLDL free cholesterol content 0.96 [0.55; 1.36], *P*=0.021 and very large HDL triglyceride content 0.93 [0.68; 1.18], *P*<0.001. A range of lipoprotein particle sizes were affected (Figs. 11-12). A decrease occurred in the levels of the unsaturated fatty acids -0.45 [-0.60; -0.30], *P*<0.001 whereas an increase was evident in those of the saturated fatty acids 0.54 [0.37; 0.70], *P*<0.001. A modest increase in total triglyceride level 0.32 [0.21; 0.42], *P*<0.001 was observed. Propofol increased the levels of the inflammatory marker GlycA 0.37 [0.21; 0.53], *P*=0.023. The ratios of oxylipin precursors PUFA and LA to total fatty acids decreased -0.66 [-0.91; -0.42], *P*=0.001 and -0.59 [-0.84; -0.33], *P*=0.035, respectively.

The LC-MS/MS profile showed strong increases in 4 specific oxylipins and a reduction in oxylipin precursor EPA. Bile acids remained unaffected by propofol administration (Fig. 14). Propofol infusion markedly increased CYP epoxygenase-derived oxylipins from LA 9,10-DiHOME 2.29 [1.62; 2.96], P<0.001 and 12,13-DiHOME 2.13 [1.42; 2.84], P<0.001. The levels of their less active precursor molecules 9,10- epoxyoctadecenoic acid (EpOME) and 12,13-EpOME remained unchanged. The amounts of LOX-derived oxylipins from LA 9-hydroxyoctadecadienoic acid (HODE) and α-LA 9-hydroxyoctadecatrienoic acid (HOTrE) increased, 1.35 [0.89; 1.82], P<0.001 and 1.98 [1.42; 2.53], P<0.001, respectively. A decrease in oxylipin precursor EPA was observed -0.81 [-1.18; -0.44], P=0.022.

When the NMR profile was inspected, 37 metabolites remained significant in all intergroup comparisons. Of the oxylipins quantified by LC-MS/MS, the increases in the concentrations of 9,10-DiHOME, 12,13-DiHOME, 9-HODE and 9-HOTrE were significant in all intergroup comparisons.

Figure 11. The propofol-placebo comparison of the NMR profile, part 1

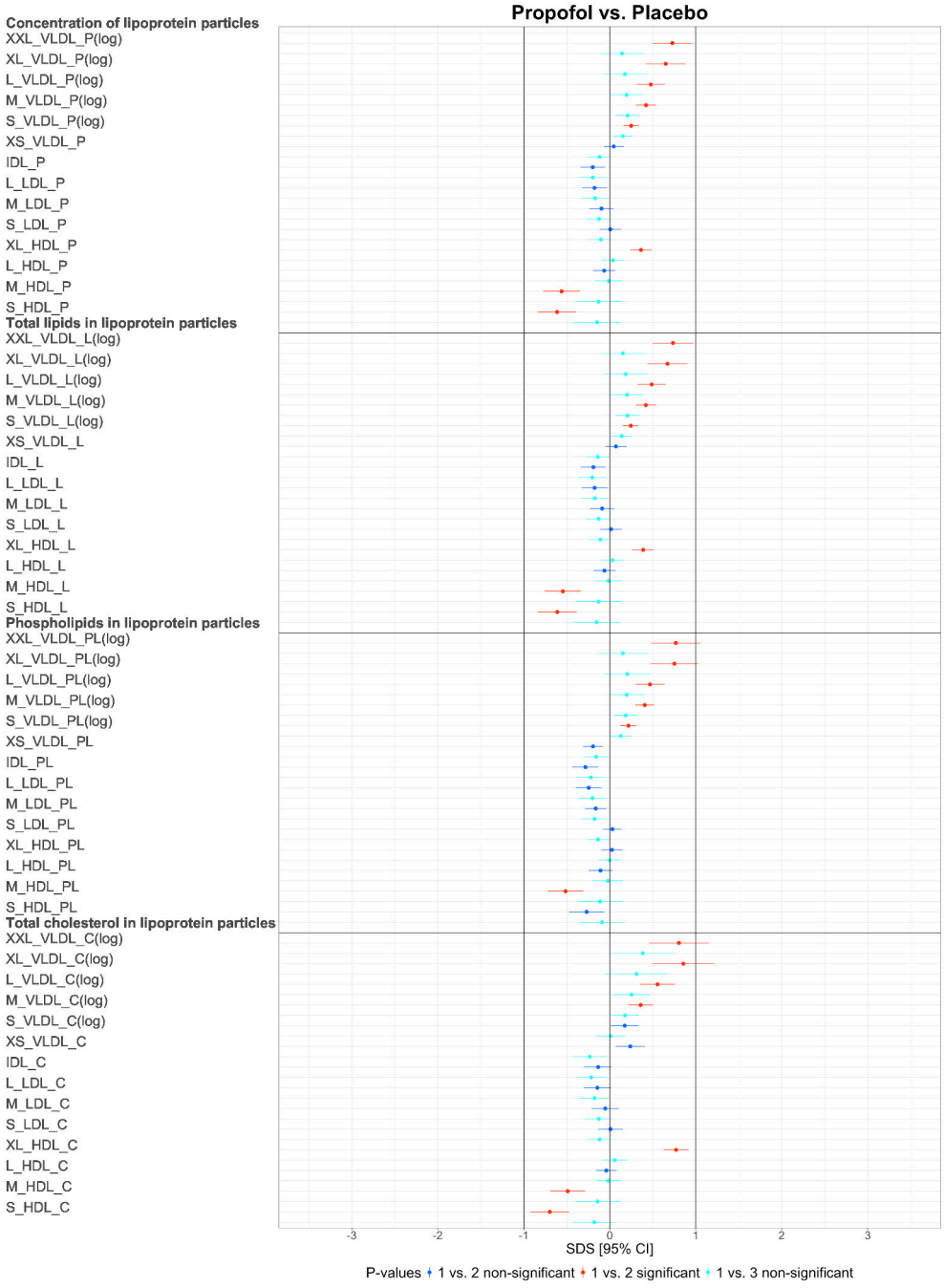

Figure 12. The propofol-placebo comparison of the NMR profile, part 2

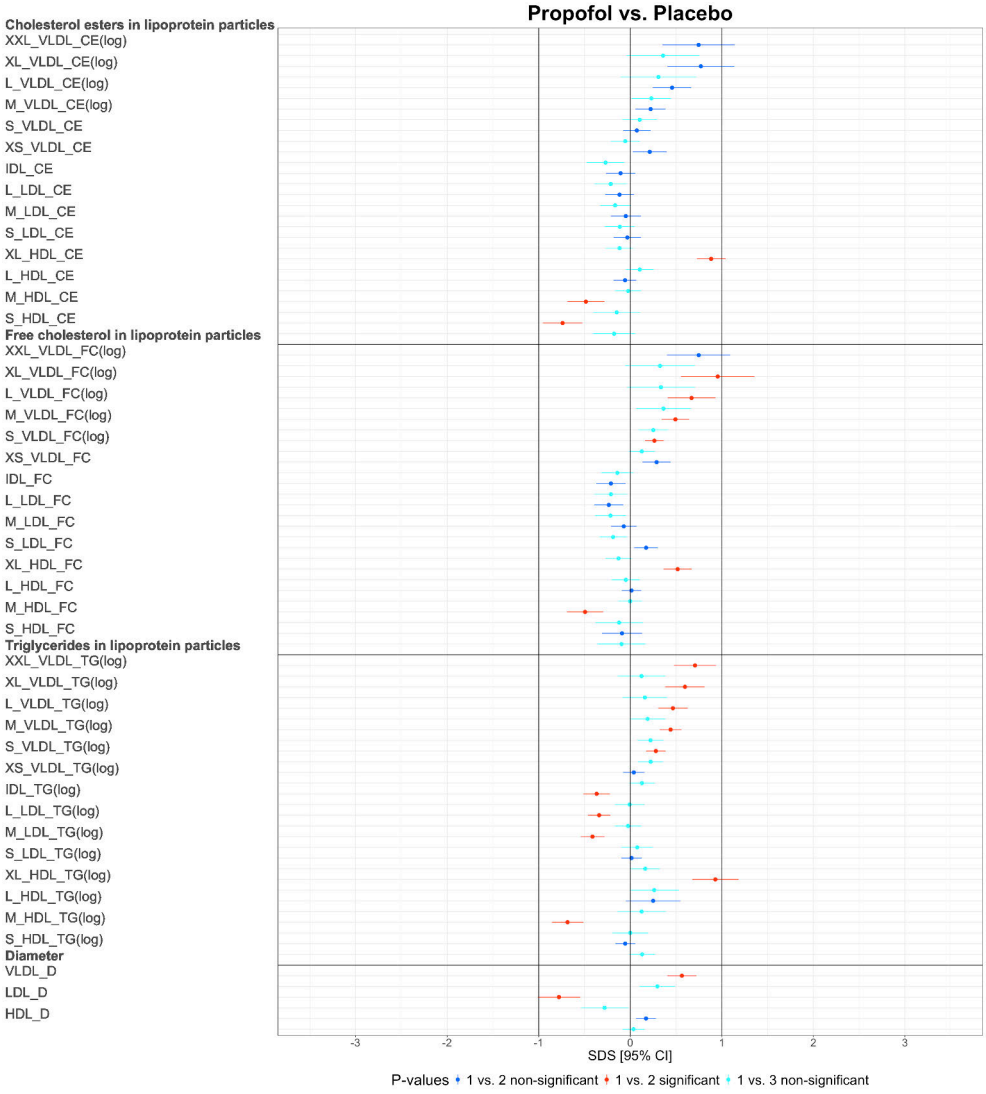

Figures 11-13: Forest plot of the propofol-placebo comparison of the NMR profile, as modified from study I. Data are reported as SDS and 95% CI. The vertical lines depict 0 and +/- 1 SDS thresholds. Positive values (to the right) depict an increase in metabolite concentration compared to placebo, while negative values (to the left) represent a decrease compared to placebo. The colour coding represents the changes during anaesthetic administration (in timepoints 1 vs. 2) and from baseline to 70 minutes after anaesthetic administration (in timepoints 1 vs. 3). Statistically significant changes are highlighted in red and pink (timepoints 1 vs. 2 and 1 vs. 3, respectively). Logarithmic transformation was carried out for skewed metabolites; these metabolites are marked with (log). All the metabolite abbreviations of the NMR metabolic profile can be found in study I, Appendix A.

Figure 13. The propofol-placebo comparison of the NMR profile, part 3

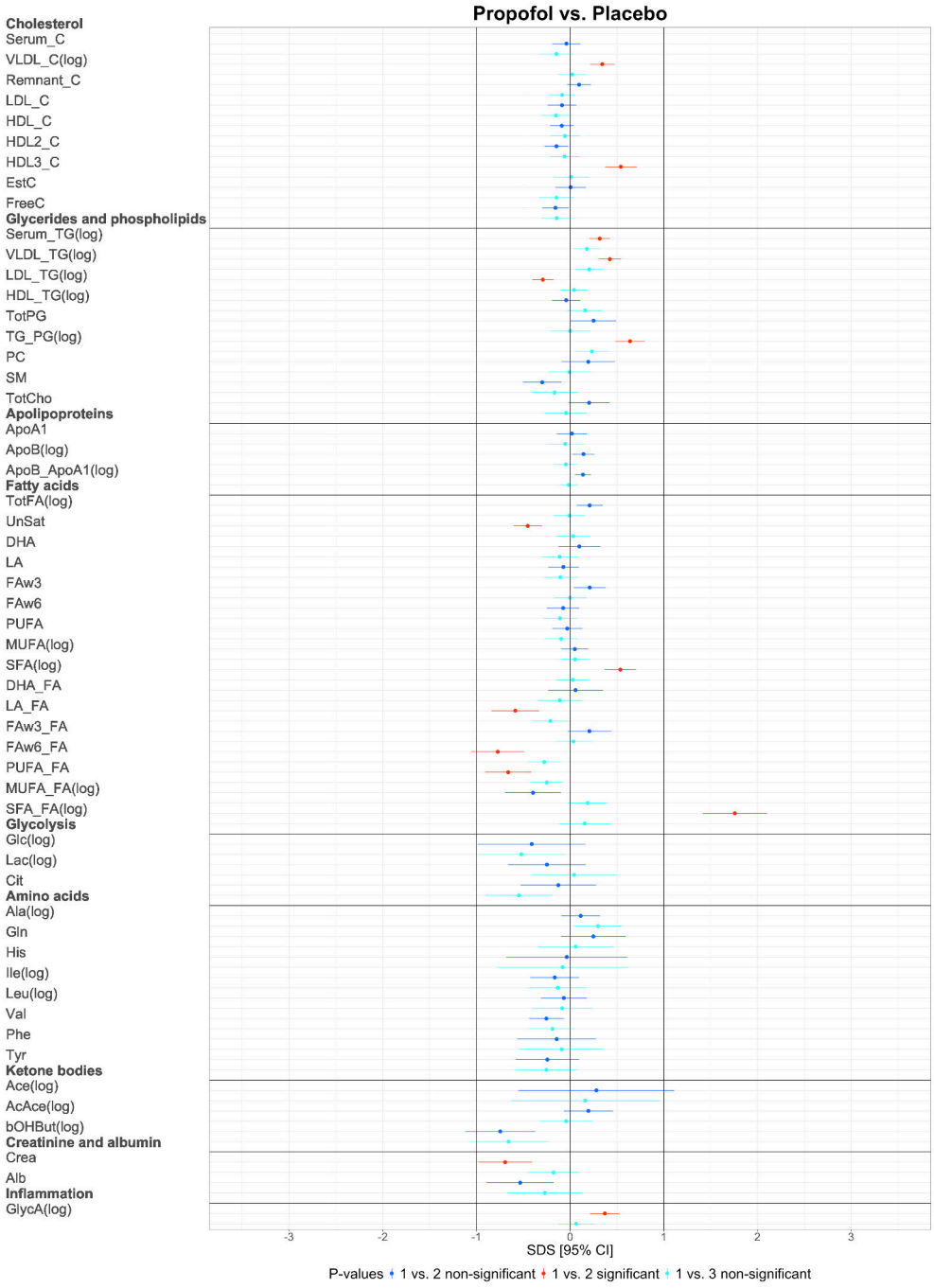

Figure 14. Forest plot of propofol *vs.* placebo, LC-MS/MS

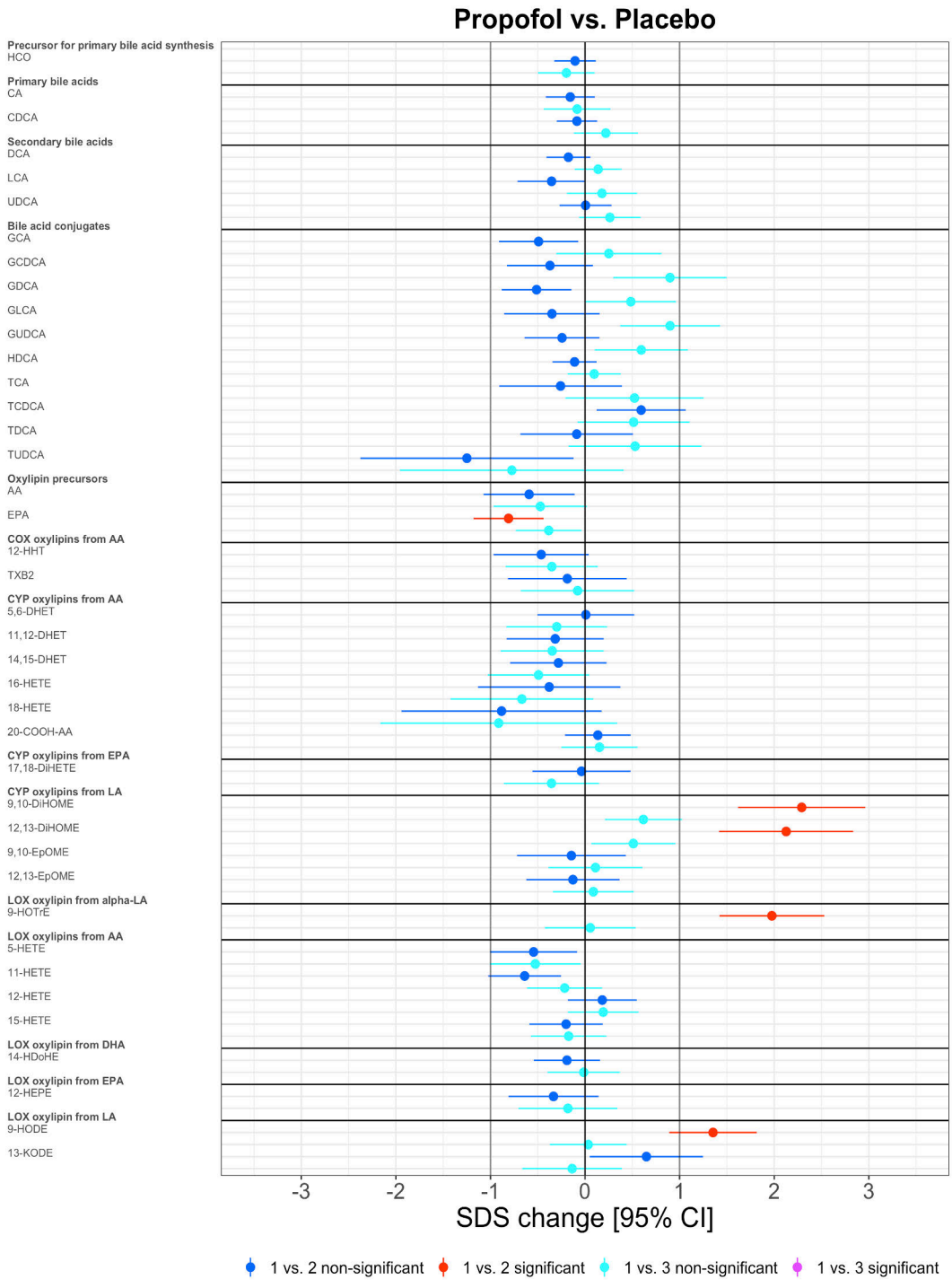

Figure 14: Forest plot of propofol vs. placebo, all analysed metabolites in the LC-MS/MS profile, as modified from original publication II. Change is reported in SDS with 95% CI. The vertical lines depict 0 and +/- 1 SD thresholds. The colour coding represents the changes in time points 1 vs. 2 and 1 vs. 3, the significant changes are highlighted. HCO, 7α-Hydroxy-4-cholesten-3-one; CA, cholic acid; CDCA, chenodeoxycholic acid; DCA, deoxycholic acid; LCA, lithocholic acid; UDCA, ursodesoxycholic acid; GCA, glycocholic acid; GCDCA, glycochenodeoxycholic acid; GDCA, glycodeoxycholic acid; GLCA, glycolithocholic acid; GUDCA, glycoursodeoxycholic acid; HDCA, hyodeoxycholic acid; TCA, taurocholic acid; TCDCA, taurochenodeoxycholic acid acid; TDCA, taurodeoxycholic acid; TUDCA, tauroursodeoxycholic acid; AA, arachidonic acid; EPA, eicosapentaeonic acid; 12-HHT, 12-hydroxy-5,8,10-heptadecatrienoic acid; PGD2, prostaglandin D2; PGE2, prostaglandin E2; TXB2, thromboxane B2; 5,6-DHET, 5,6-dihydroxy-8,11,14-eicosatrienoic acid; 8,9-DHET, 8,9-dihydroxy-5,11,14-eicosatrienoic acid; 11,12-DHET, 11,12-dihydroxy-5,8,14-eicosatrienoic acid; 14,15-DHET, 14,15-dihydroxy-5,8,11-eicosatrienoic acid; 16-HETE, 16-hydroxy-5,8,11,14-eicosatetraenoic acid; 18-HETE, 18-hydroxy-5,8,11,14-eicosatetraenoic acid; 20-COOH-AA, 5,8,11,14-eicosatetraenedioic acid; 5,6-DiHETE, 5,6-dihydroxy-8,11,14,17-eicosatetraenoic acid; 17,18-DiHETE, 17,18-dihydroxy-5,8,11,14-eicosatetraenoic acid; 9,10-DiHOME, 9,10-dihydroxy-12-octadecenoic acid; 12,13-DiHOME, 12,13-dihydroxyoctadec-9-enoic acid; 9,10-EpOME, 9,10-epoxy-12-octadecenoic acid; 12,13-EpOME, 12,13-epoxy-9-octadecenoic acid; 9-HOTrE, 9-hydroxy-10,12,15-octadecatrienoic acid; 5-HETE, 5-hydroxy-6,8,11,14-eicosatetraenoic acid; 11-HETE, 11-hydroxy-5,8,12,14-eicosatetraenoic acid; 12-HETE, 12-hydroxy-5,8,10,14-eicosatetraenoic acid; 15-HETE, 15-hydroxy-5,8,11,13-eicosatetraenoic acid; 14-HDoHE, 14-hydroxy docosahexaenoic acid; 12-HEPE, 12-hydroxy-5,8,10,14,17-eicosapentaenoic acid; 9-HpODE, 9-hydroperoxyoctadeca-10,12-dienoic acid; 9-HODE, 9-hydroxy-10,12-octadecadienoic acid; 13-KODE, 13-keto-9,11,-octadecadienoic acid; LA, linoleic acid; alpha-LA, alpha-linoleic acid; DHA, docosahexaenoic acid.

5.1.2.1 NMR *in vitro* analysis

When propofol was directly added to baseline samples at 1.75 µg ml^{-1} concentration (corresponding to the target concentration of propofol emulsion *in vivo* 1.7 µg ml^{-1}), only minor changes were seen in the NMR profile. However, increasing the propofol concentration *in vitro* (1.75-100 µg ml^{-1}) resulted in a dose-response relationship from chylomicrons and extremely large to medium VLDL (i.e. XXL-M VLDL) markers (Fig. 15).

The concentration of VLDL markers in the propofol group where the target was 1.7 µg ml^{-1} (Fig. 6), corresponded to the concentrations observed at an *in vitro* propofol concentration of 17.5 µg ml^{-1}. This 10-fold difference and the comparison of the NMR spectra between *in vivo* and *in vitro* samples suggested that there could have been an accumulation of the propofol emulsion constituents e.g. soybean oil, during continuous propofol infusion *in vivo*. This resulted in an accumulation of glycerol and triglycerides, and the glyceride component of triglycerides interfered with the NMR quantification of creatinine. At the corresponding propofol concentration of 17.5 µg ml^{-1}, other metabolites were largely unaffected. (Study I, Appendix B)

Figure 15. Propofol *in vitro* analysis

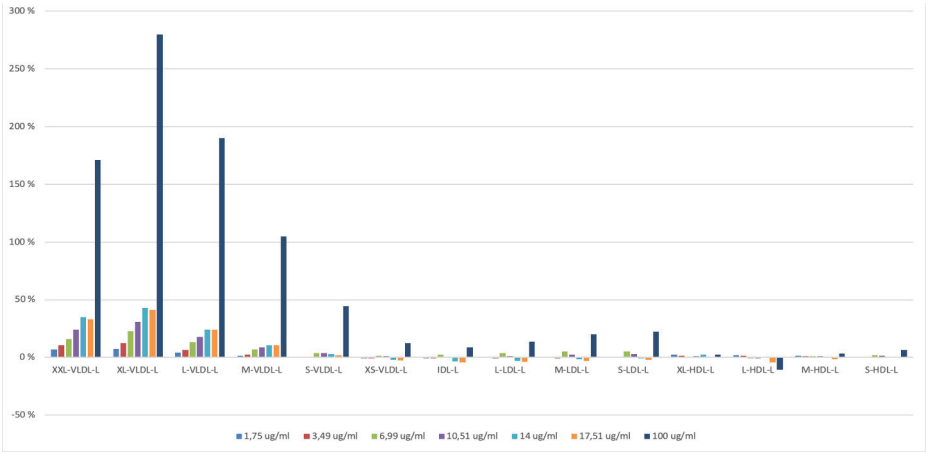

Propofol in vitro analysis from original publication I. Percentage change of total lipid subclasses compared to the blank serum sample. The dosage is presented with respect to propofol concentration. The changes caused by the soybean oil interference are more pronounced on the M-XXL VLDL groups, whereas other groups are mostly unaffected.

5.1.2.2 LC-MS/MS *in vitro* analysis

A similar analysis was carried out for the LC-MS/MS oxylipin profile. A dilution series of propofol emulsion was prepared in human plasma in ratios of 1:10, 1:100, 1:200, and 1:1000 (v/v) with a blank human plasma serving as control. Oxylipin levels in these samples were analyzed using the same method as utilized for the study samples.

The analysis of propofol emulsion dilution series *in vitro* demonstrated that the concentrations of several oxylipins were strongly and dose-dependently increased in the propofol emulsion containing plasma. The oxylipins most affected were those that showed a significant increased in the propofol group *in vivo*. *In vitro* 9,10-DiHOME and 12,13-DiHOME concentrations were 2.5-fold and 1.4-fold higher in 1:1000 v/v propofol emulsion dilution (mimicking relevant propofol dosing) *vs.* control. However, 9-HODE and 9-HOTrE remained unchanged *in vitro*, regardless of their significant increase *in vivo*.

5.1.3 S-ketamine

The NMR profile revealed increased lactate levels 1.13 [0.65; 1.6], *P*= 0.019 and also the concentration of glucose was elevated 1.21 [0.68; 1.75] *P*=0.042 (1 *vs.* 3). Decreases in the concentrations of several amino acids were observed i.e. isoleucine -0.89 (-1.25 to -0.54), *P*=0.006, tyrosine -0.89 [-1.27 to -0.52], *P*=0.017 (both 1 *vs*. 3) and leucine -0.64 [-0.92; -0.36], *P*=0.047 and -0.89 [-1.27; -0.52], *P*=0.013 (1 *vs*. 2 and 1 *vs.* 3, respectively) (Figs. 16-18).

In the LC-MS/MS profile, only a modest decrease was detected in the levels of the primary bile acid precursor 7α-Hydroxy-4-cholesten-3-one (HCO) -0.76 [-1.11; -0.42], p=0.019 (1 *vs.* 3) (Fig. 19).

In comparison to the other anaesthetics, the decrease in the levels of leucine was significant in all intergroup comparisons.

Figure 16. The S-ketamine-placebo comparison of the NMR profile, part 1

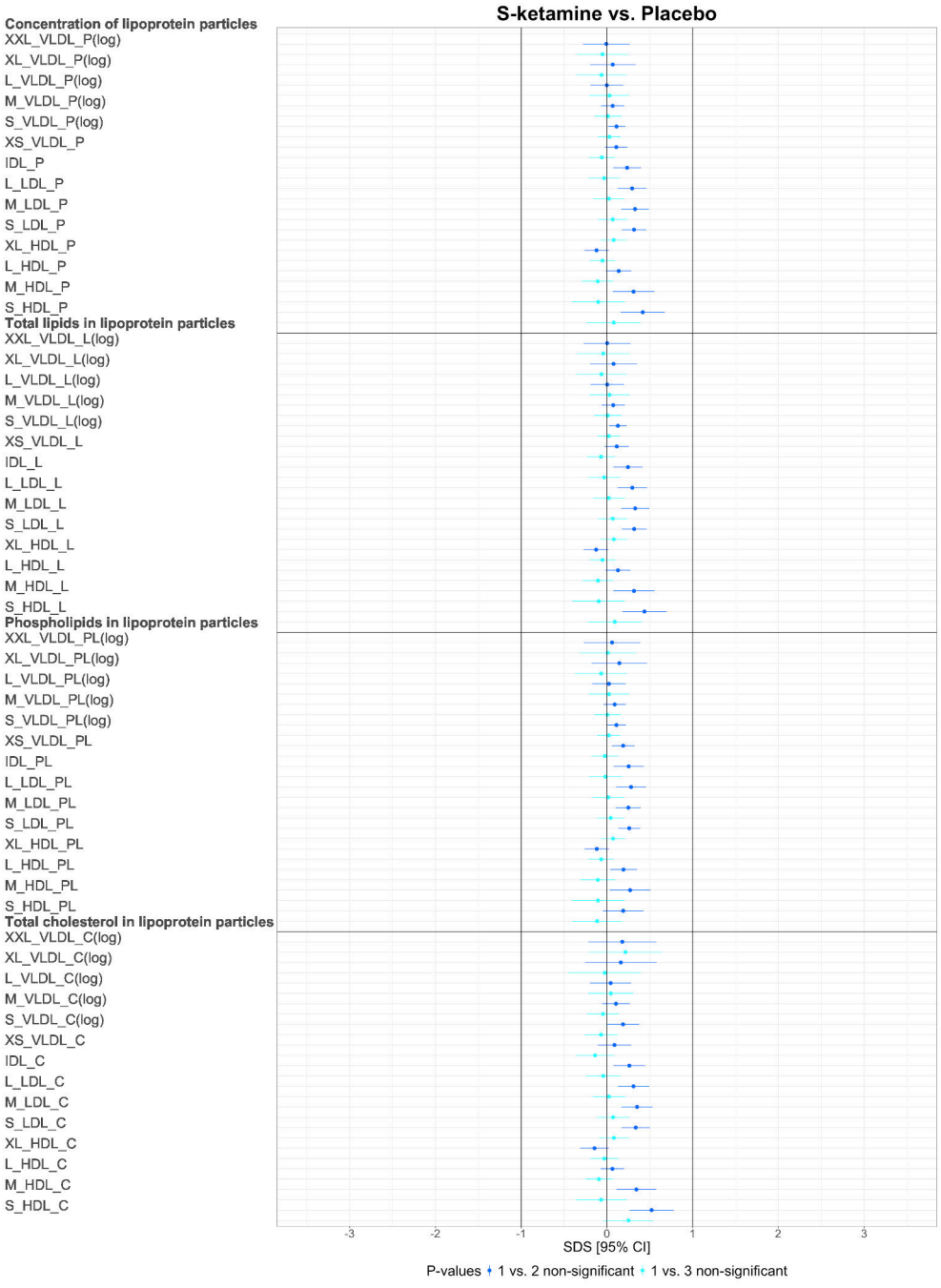

Figure 17. The S-ketamine-placebo comparison of the NMR profile, part 2

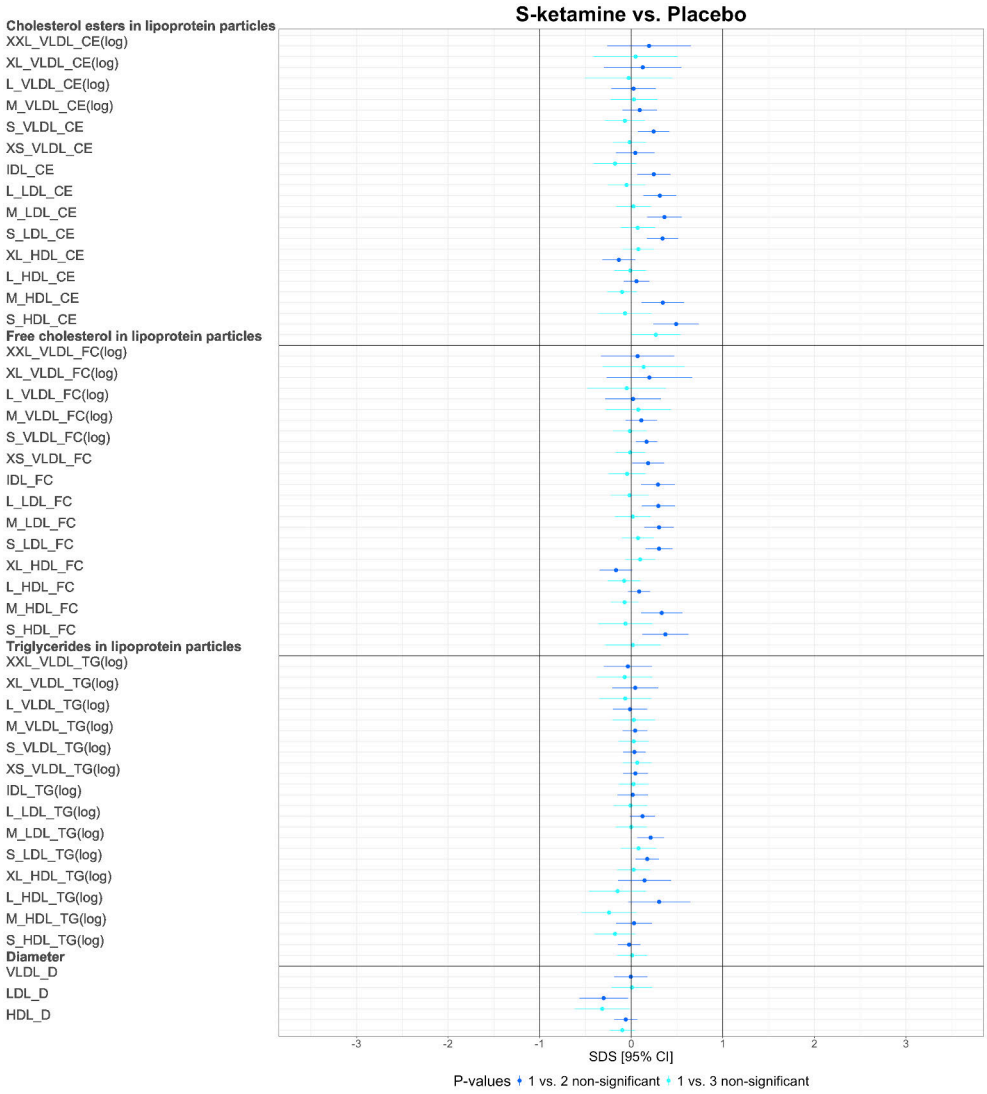

Figures 16-18: Forest plots of the S-ketamine-placebo comparison of the NMR profile, as modified from study I. Data are reported as SDS and 95% CI. The vertical lines depict 0 and +/- 1 SDS thresholds. Positive values (to the right) depict an increase in metabolite concentration compared to placebo, while negative values (to the left) represent a decrease compared to placebo. The colour coding represents the changes during anaesthetic administration (in timepoints 1 vs. 2) and from baseline to 70 minutes after anaesthetic administration (in timepoints 1 vs. 3). Statistically significant changes are highlighted in red and pink (timepoints 1 vs. 2 and 1 vs. 3, respectively). Logarithmic transformation was carried out for skewed metabolites; these metabolites are marked with (log). All the metabolite abbreviations of the NMR metabolic profile can be found in study I, Appendix A.

Figure 18. The S-ketamine-placebo comparison of the NMR profile, part 3

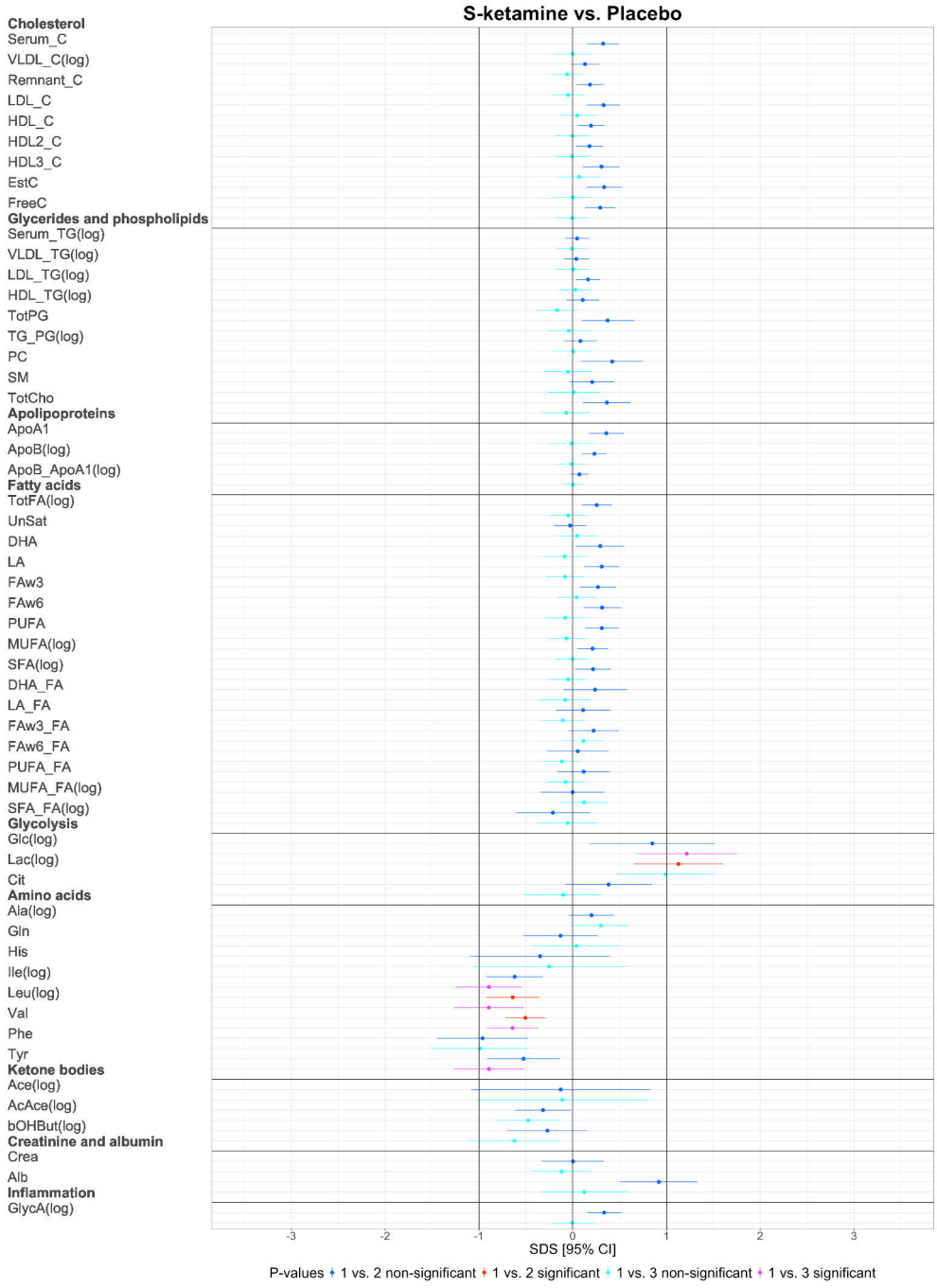

Figure 19. Forest plot of S-ketamine *vs.* placebo, LC-MS/MS

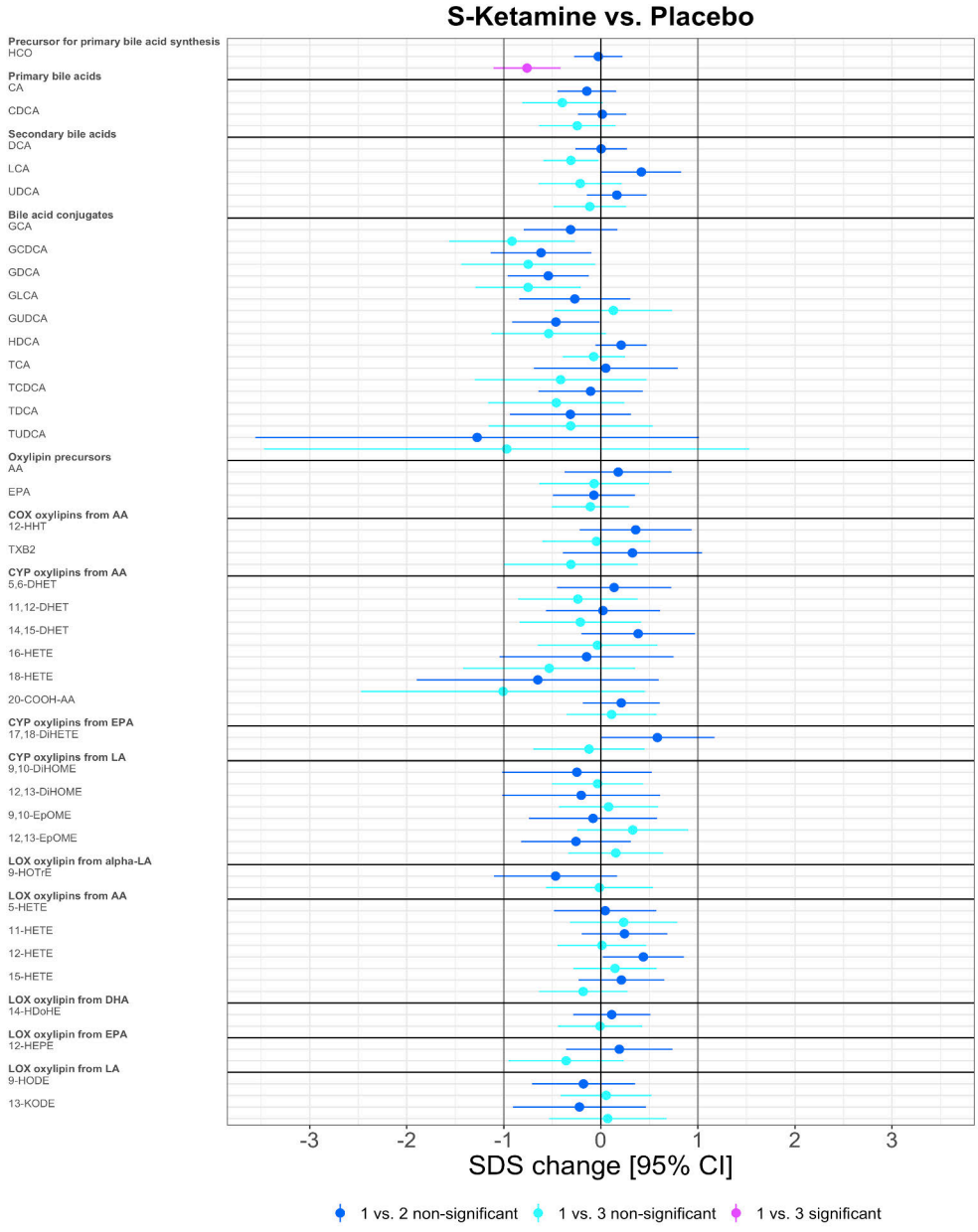

Figure 23: Forest plot of S-ketamine vs. placebo, all analysed metabolites in the LC-MS/MS profile, as modified from original publication II. Change is reported in SDS with 95% CI. The vertical lines depict 0 and +/- 1 SD thresholds. The colour coding represents the changes in time points 1 vs. 2 and 1 vs. 3, the significant changes are highlighted. HCO, 7α-Hydroxy-4-cholesten-3-one; CA, cholic acid; CDCA, chenodeoxycholic acid; DCA, deoxycholic acid; LCA, lithocholic acid; UDCA, ursodesoxycholic acid; GCA, glycocholic acid; GCDCA, glycochenodeoxycholic acid; GDCA, glycodeoxycholic acid; GLCA, glycolithocholic acid; GUDCA, glycoursodeoxycholic acid; HDCA, hyodeoxycholic acid; TCA, taurocholic acid; TCDCA, taurochenodeoxycholic acid acid; TDCA, taurodeoxycholic acid; TUDCA, tauroursodeoxycholic acid; AA, arachidonic acid; EPA, eicosapentaeonic acid; 12-HHT, 12-hydroxy-5,8,10-heptadecatrienoic acid; PGD2, prostaglandin D2; PGE2, prostaglandin E2; TXB2, thromboxane B2; 5,6-DHET, 5,6-dihydroxy-8,11,14-eicosatrienoic acid; 8,9-DHET, 8,9-dihydroxy-5,11,14-eicosatrienoic acid; 11,12-DHET, 11,12-dihydroxy-5,8,14-eicosatrienoic acid; 14,15-DHET, 14,15-dihydroxy-5,8,11-eicosatrienoic acid; 16-HETE, 16-hydroxy-5,8,11,14-eicosatetraenoic acid; 18-HETE, 18-hydroxy-5,8,11,14-eicosatetraenoic acid; 20-COOH-AA, 5,8,11,14-eicosatetraenedioic acid; 5,6-DiHETE, 5,6-dihydroxy-8,11,14,17-eicosatetraenoic acid; 17,18-DiHETE, 17,18-dihydroxy-5,8,11,14-eicosatetraenoic acid; 9,10-DiHOME, 9,10-dihydroxy-12-octadecenoic acid; 12,13-DiHOME, 12,13-dihydroxyoctadec-9-enoic acid; 9,10-EpOME, 9,10-epoxy-12-octadecenoic acid; 12,13-EpOME, 12,13-epoxy-9-octadecenoic acid; 9-HOTrE, 9-hydroxy-10,12,15-octadecatrienoic acid; 5-HETE, 5-hydroxy-6,8,11,14-eicosatetraenoic acid; 11-HETE, 11-hydroxy-5,8,12,14-eicosatetraenoic acid; 12-HETE, 12-hydroxy-5,8,10,14-eicosatetraenoic acid; 15-HETE, 15-hydroxy-5,8,11,13-eicosatetraenoic acid; 14-HDoHE, 14-hydroxy docosahexaenoic acid; 12-HEPE, 12-hydroxy-5,8,10,14,17-eicosapentaenoic acid; 9-HpODE, 9-hydroperoxyoctadeca-10,12-dienoic acid; 9-HODE, 9-hydroxy-10,12-octadecadienoic acid; 13-KODE, 13-keto-9,11,-octadecadienoic acid; LA, linoleic acid; alpha-LA, alpha-linoleic acid; DHA, docosahexaenoic acid.

5.1.4 Sevoflurane

Sevoflurane was the most inert of the examined anaesthetics based on the NMR metabolic profile. Only an increase in the level of alanine reached statistical significance 0.6 [0.4; 0.81], $P<0.001$ (Figs. 20-22).

In the LC-MS/MS experiment, the concentration of an EPA derived CYP epoxygenase oxylipin 17,18-DiHETE was slightly increased 1.18 [0.66; 1.7], $P=0.01$. A decrease was observed in tauroursodeoxycholic acid (TUDCA) -2.7 [-3.84; -1.55], $P=0.015$, a bile acid conjugate of ursodeoxycholic acid (Fig. 23). Importantly, in the sevoflurane and placebo groups respectively, exact quantification of TUDCA was available for only 19.0% and 17.1% of the analysed samples.

In comparison to dexmedetomidine, the change in DiHETE remained significant.

Figure 20. The sevoflurane-placebo comparison of the NMR profile, part 1

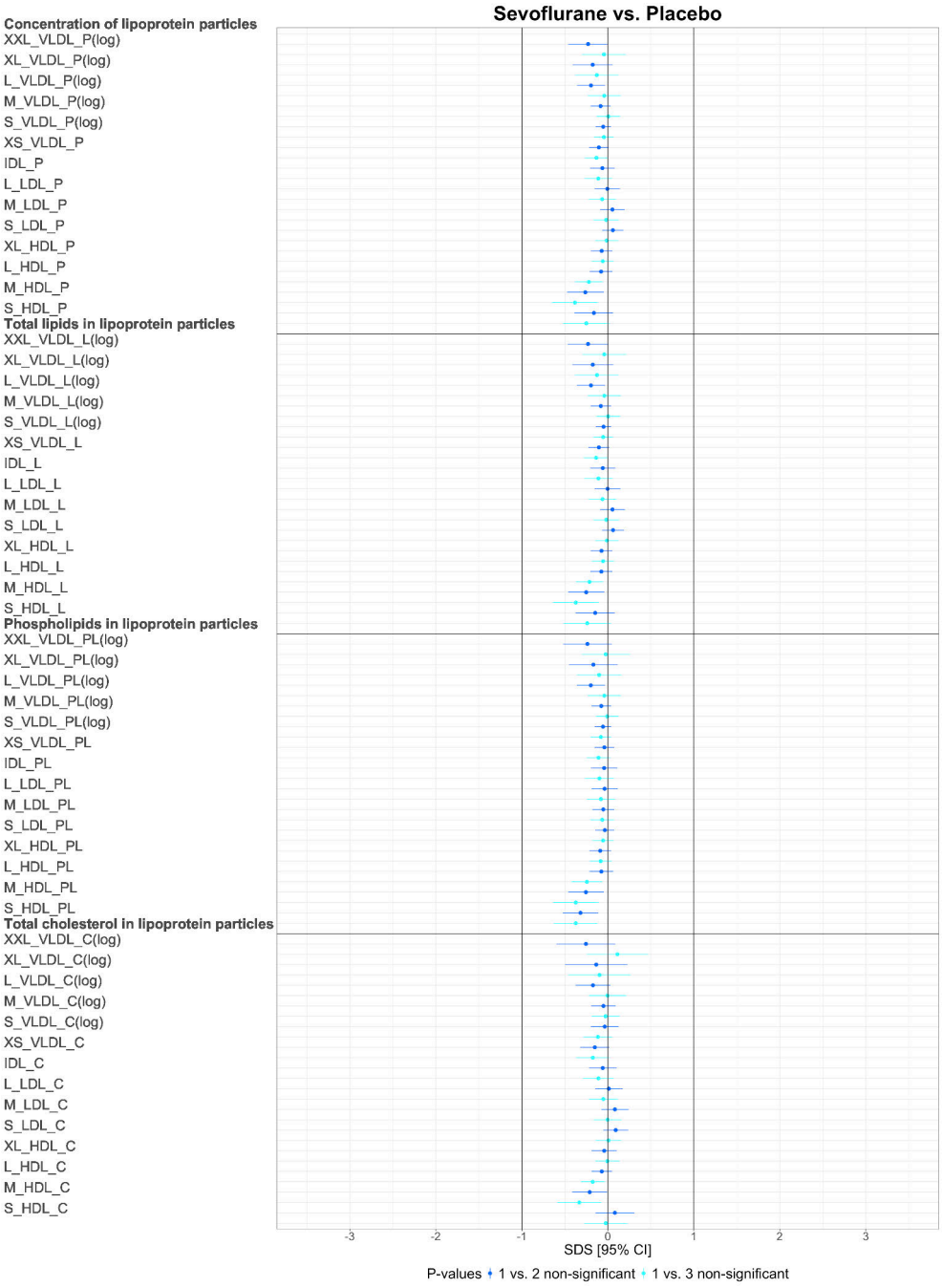

Figure 21. The sevoflurane-placebo comparison of the NMR profile, part 2

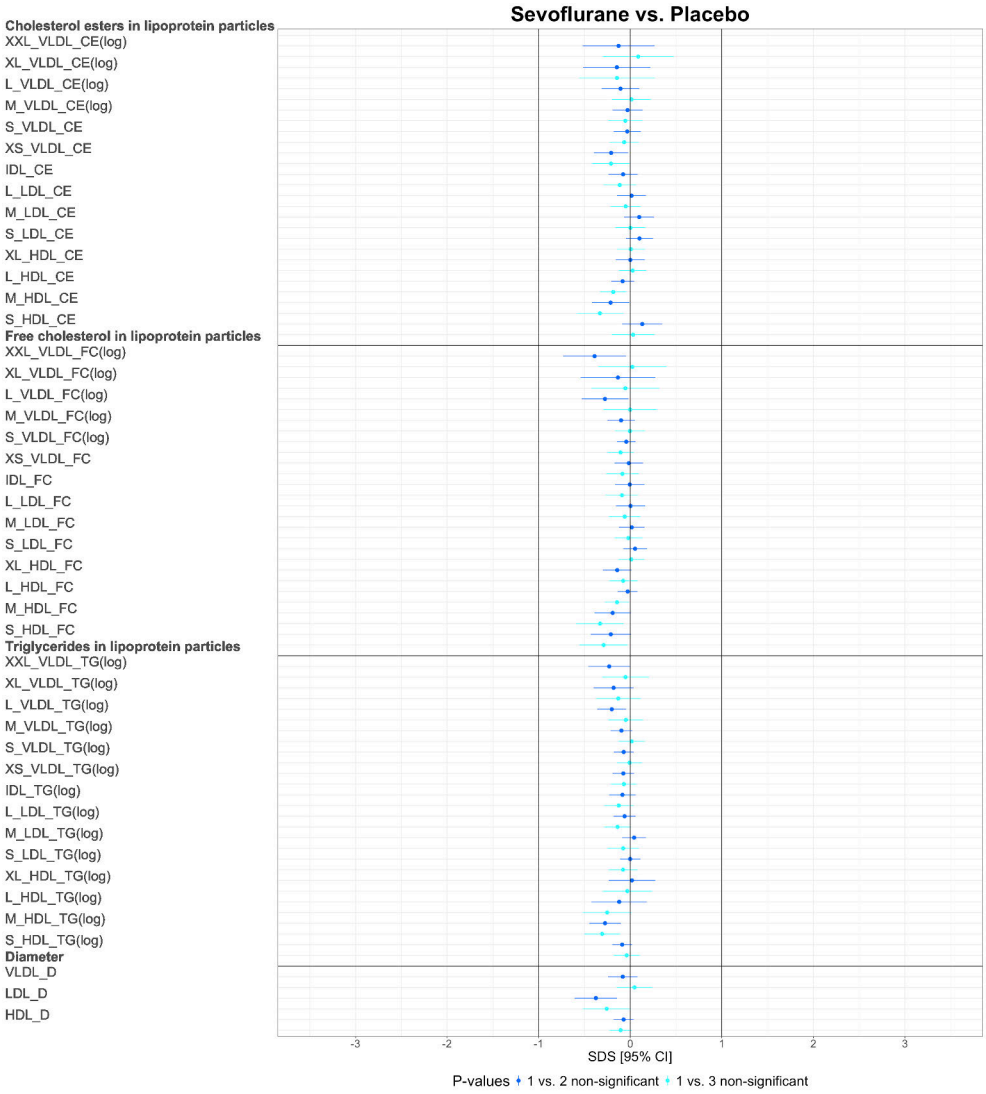

Figures 20-22: Forest plots of the sevoflurane-placebo comparison of the NMR profile, as modified from study I. Data are reported as SDS and 95% CI. The vertical lines depict 0 and +/- 1 SDS thresholds. Positive values (to the right) depict an increase in metabolite concentration compared to placebo, while negative values (to the left) represent a decrease compared to placebo. The colour coding represents the changes during anaesthetic administration (in timepoints 1 vs. 2) and from baseline to 70 minutes after anaesthetic administration (in timepoints 1 vs. 3). Statistically significant changes are highlighted in red and pink (timepoints 1 vs. 2 and 1 vs. 3, respectively). Logarithmic transformation was carried out for skewed metabolites; these metabolites are marked with (log). All the metabolite abbreviations of the NMR metabolic profile can be found in study I, Appendix A.

Figure 22. The sevoflurane-placebo comparison of the NMR profile, part 3

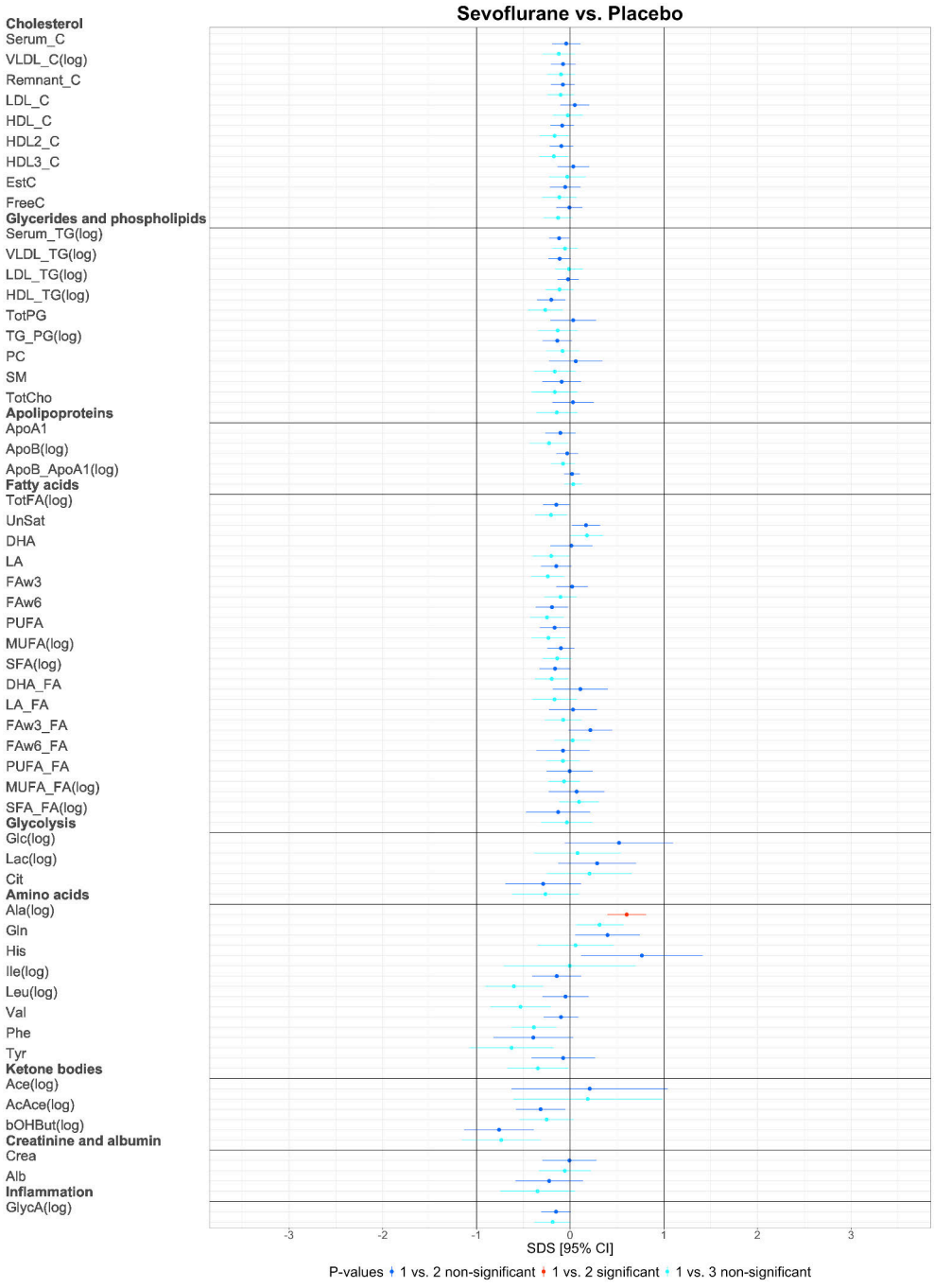

Figure 23. Forest plot of sevoflurane *vs.* placebo, LC-MS/MS

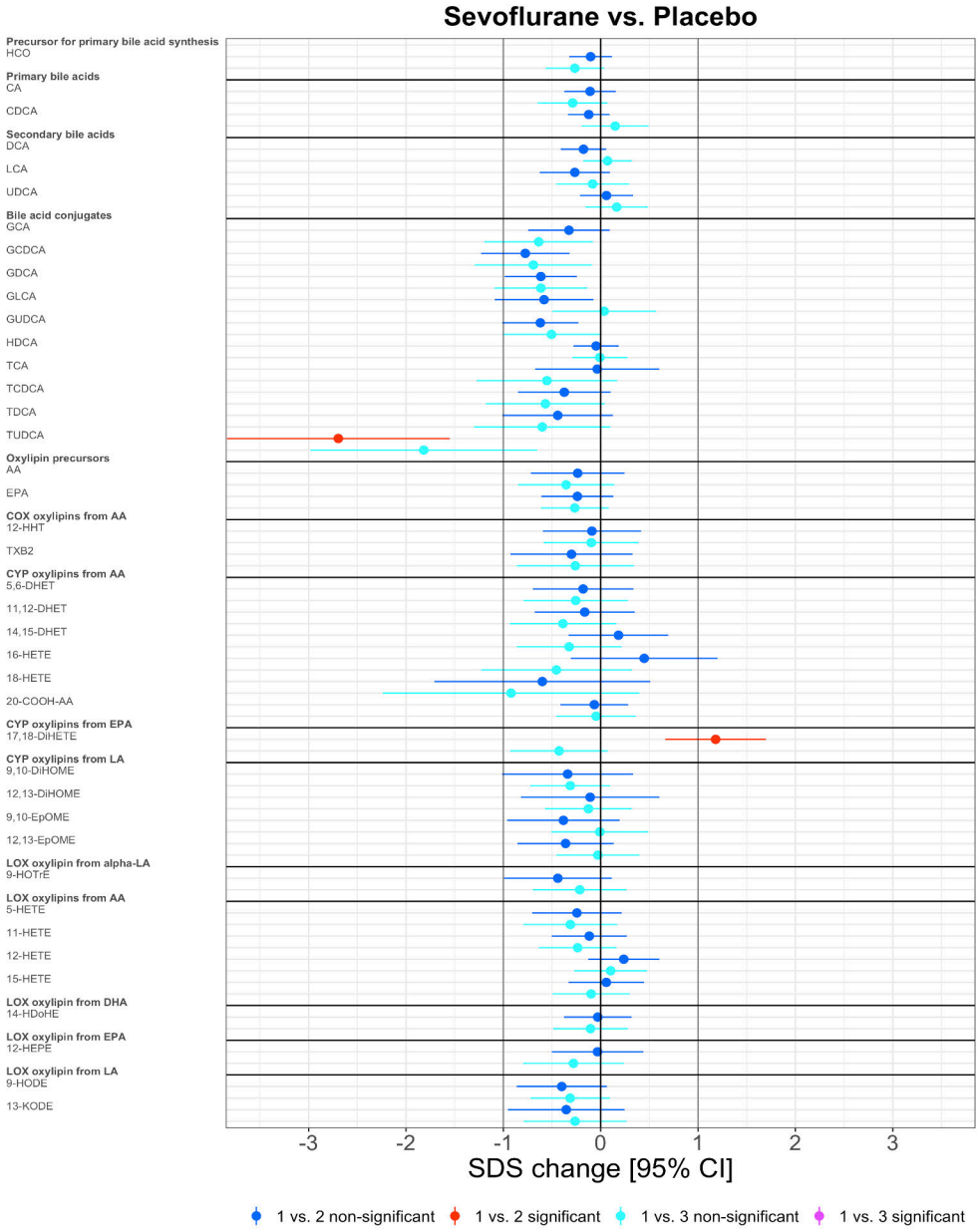

Figure 19: Forest plot of sevoflurane vs. placebo, all analysed metabolites in the LC-MS/MS profile, as modified from original publication II. Change is reported in SDS with 95% CI. The vertical lines depict 0 and +/- 1 SD thresholds. The colour coding represents the changes in time points 1 vs. 2 and 1 vs. 3, the significant changes are highlighted. HCO, 7α-Hydroxy-4-cholesten-3-one; CA, cholic acid; CDCA, chenodeoxycholic acid; DCA, deoxycholic acid; LCA, lithocholic acid; UDCA, ursodesoxycholic acid; GCA, glycocholic acid; GCDCA, glycochenodeoxycholic acid; GDCA, glycodeoxycholic acid; GLCA, glycolithocholic acid; GUDCA, glycoursodeoxycholic acid; HDCA, hyodeoxycholic acid; TCA, taurocholic acid; TCDCA, taurochenodeoxycholic acid acid; TDCA, taurodeoxycholic acid; TUDCA, tauroursodeoxycholic acid; AA, arachidonic acid; EPA, eicosapentaeonic acid; 12-HHT, 12-hydroxy-5,8,10-heptadecatrienoic acid; PGD2, prostaglandin D2; PGE2, prostaglandin E2; TXB2, thromboxane B2; 5,6-DHET, 5,6-dihydroxy-8,11,14-eicosatrienoic acid; 8,9-DHET, 8,9-dihydroxy-5,11,14-eicosatrienoic acid; 11,12-DHET, 11,12-dihydroxy-5,8,14-eicosatrienoic acid; 14,15-DHET, 14,15-dihydroxy-5,8,11-eicosatrienoic acid; 16-HETE, 16-hydroxy-5,8,11,14-eicosatetraenoic acid; 18-HETE, 18-hydroxy-5,8,11,14-eicosatetraenoic acid; 20-COOH-AA, 5,8,11,14-eicosatetraenedioic acid; 5,6-DiHETE, 5,6-dihydroxy-8,11,14,17-eicosatetraenoic acid; 17,18-DiHETE, 17,18-dihydroxy-5,8,11,14-eicosatetraenoic acid; 9,10-DiHOME, 9,10-dihydroxy-12-octadecenoic acid; 12,13-DiHOME, 12,13-dihydroxyoctadec-9-enoic acid; 9,10-EpOME, 9,10-epoxy-12-octadecenoic acid; 12,13-EpOME, 12,13-epoxy-9-octadecenoic acid; 9-HOTrE, 9-hydroxy-10,12,15-octadecatrienoic acid; 5-HETE, 5-hydroxy-6,8,11,14-eicosatetraenoic acid; 11-HETE, 11-hydroxy-5,8,12,14-eicosatetraenoic acid; 12-HETE, 12-hydroxy-5,8,10,14-eicosatetraenoic acid; 15-HETE, 15-hydroxy-5,8,11,13-eicosatetraenoic acid; 14-HDoHE, 14-hydroxy docosahexaenoic acid; 12-HEPE, 12-hydroxy-5,8,10,14,17-eicosapentaenoic acid; 9-HpODE, 9-hydroperoxyoctadeca-10,12-dienoic acid; 9-HODE, 9-hydroxy-10,12-octadecadienoic acid; 13-KODE, 13-keto-9,11,-octadecadienoic acid; LA, linoleic acid; alpha-LA, alpha-linoleic acid; DHA, docosahexaenoic acid.

5.2 Metabolomics after out-of-hospital cardiac arrest

Patient demographics are shown in Table 11. Of the 224 patients who were screened for eligibility, 110 patients were randomised 1:1 to the xenon and control groups. The metabolic profiles of 105 patients were evaluable. The 6-month mortality within this group was 30.5% (32/105), the mean ± SD age of survivors and non-survivors was 57.8 ± 11.9 and 64.6 ± 7.8 years and 67.1% of survivors and 84.4% of non-survivors were male. The Kaplan-Meier survival estimate of the intention to treat population of 110 patients after 6-months was 27.3% and 34.5% in xenon *vs.* control, respectively, adjusted HR [95% CI], 0.49 [0.23, 1.01], p=0.053, as previously reported[115].

No significant intergroup differences between xenon *vs.* control were identified (Figs. 24-26).

Upon hospital admission at baseline, no metabolites were significantly associated with mortality at 6 months. At 24 hours, lactate 2.25 [1.53; 3.30], $P<0.001$ and two BCAAs i.e. leucine 0.64 [0.5; 0.82], P=0.007 and valine 0.37 [0.22; 0.63], $P=0.003$ showed a significant adjusted HR with 6-month mortality. At 72 hours, the adjusted HR of lactate increased to 2.77 [1.76; 4.36], $P<0.001$. Similarly at 72 h, significant adjusted HR were observed for alanine 2.43 [1.56; 3.78], $P = 0.001$ and small high-density lipoprotein cholesteryl ester content (S-HDL-CE) 0.36 [0.19; 0.68], $P= 0.021$ (Fig. 27).

Table 11. Patient demographics, study III

	Control (n=53)	Xenon (n=52)	P-value
Age, median (IQR), y	60 (55-67)	63 (56-69)	0.52[b]
Male sex	38 (71.7)	38 (73.1)	0.87[c]
Coronary artery disease	39(73.6)	36 (69.2)	0.62[c]
Hypertension	25 (47.2)	20 (38.5)	0.37[c]
Congestive heart failure	3 (5.7)	6 (11.5)	0.32[d]
Diabetes	7 (13.2)	8(15.4)	0.75[c]
Asthma or chronic obstructive pulmonary disease	8 (15.1)	6(11.5)	0.59[c]
Dyslipidemia	21 (39.6)	15(28.9)	0.24[c]
Smoker*	21 (40.4)	15(30)	0.27[c]
ST elevation myocardial infarction	19 (35.9)	16 (30.8)	0.58[c]
Previous stroke^	13 (26.0)	11 (22.9)	0.72[c]
Resuscitation details			
Bystander resuscitation	39 (73.6)	36 (69.2)	0.62[c]
EMS delay, mean (SD), min	8.8 (3.4)	8.3 (3.4)	0.58[a]
ROSC, mean (SD), min	22.0 (7.0)	22.0 (7.6)	0.99[a]
No flow, median (IQR), min	0 (0-0)	0 (0-6)	0.47[b]
Treatment and sampling			
Core temperature before cooling, median (IQR), °C	35.4 (34.0-36.3)	34.9 (34.3-35.8)	0.22[b]
Time from OHCA to target temperature, median (IQR), h	5.6 (4.35-6.58)	4.9 (4.24-5.67)	0.09[b]
Cooling rate, median (IQR), °C/h	0.43 (0.22-0.50)	0.42 (0.28-0.50)	0.79[b]
Time from OHCA to initiation of xenon, median (IQR), min		251 (210-282)	
Time from OHCA to baseline metabolic sampling, median (IQR), h	3.0 (1.8-4.3)	3.3 (1.8-4.3)	0.84[b]

Data are expressed as No. (%) unless otherwise stated. From original publication III. Abbreviations: IQR, interquartile range; SD, standard deviation; EMS, emergency medical services; ROSC, return of the spontaneous circulation; OHCA, out-of-hospital cardiac arrest. [a]Two sample t-test. [b]Mann-Whitney U-test. [c]Chi-square. [d]Fisher's exact test. *Data missing: 1 patient in control, 2 in xenon. ^Data missing: 3 patients in control, 5 in xenon.

Figure 24. The comparison of the NMR profile xenon *vs.* control, part 1

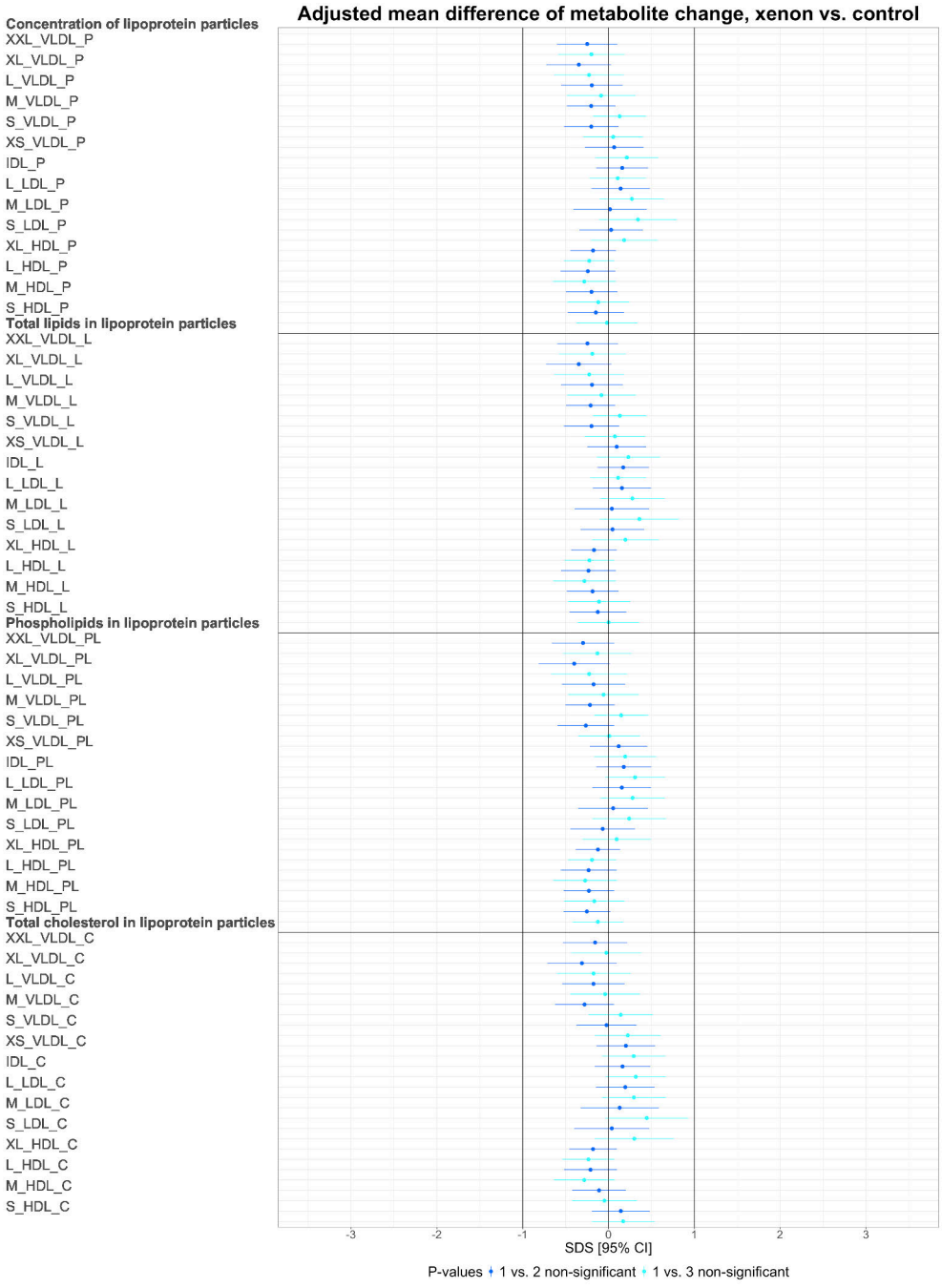

Figure 25. The comparison of the NMR profile xenon *vs.* control, part 2

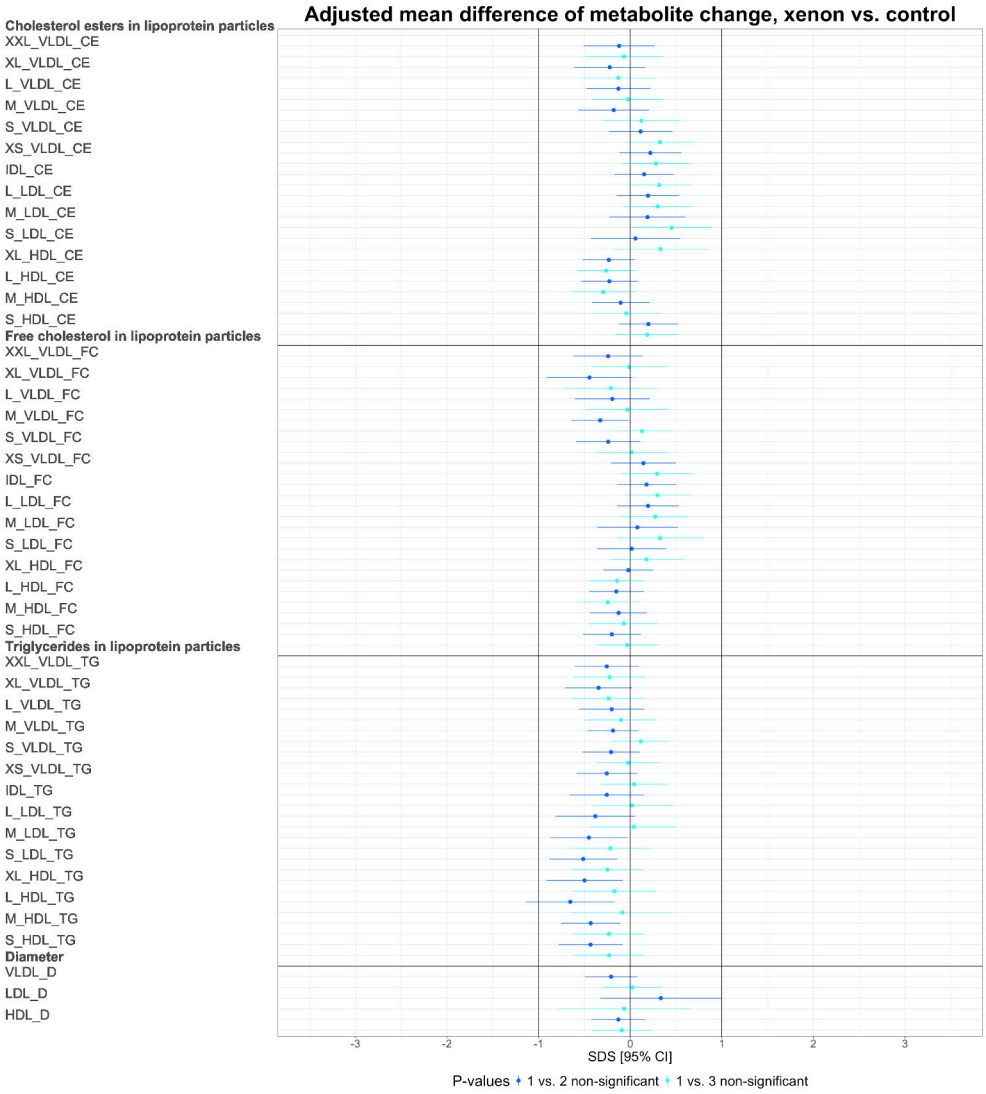

Figures 24-26: Forest plots depicting the intergroup comparison of the xenon and control groups, as modified from study III. There was no statistically significant difference between groups. Data are reported as adjusted mean difference of metabolite change from baseline to 24 and 72 hours in SDS and 95% CI. Negative values (to the left) indicate that the change in metabolite concentration from baseline was lower in xenon treated patients vs. the change observed in control group. All the metabolite abbreviations of the NMR metabolic profile can be found in study I, Appendix A.

Figure 26. The comparison of the NMR profile xenon *vs.* control, part 3

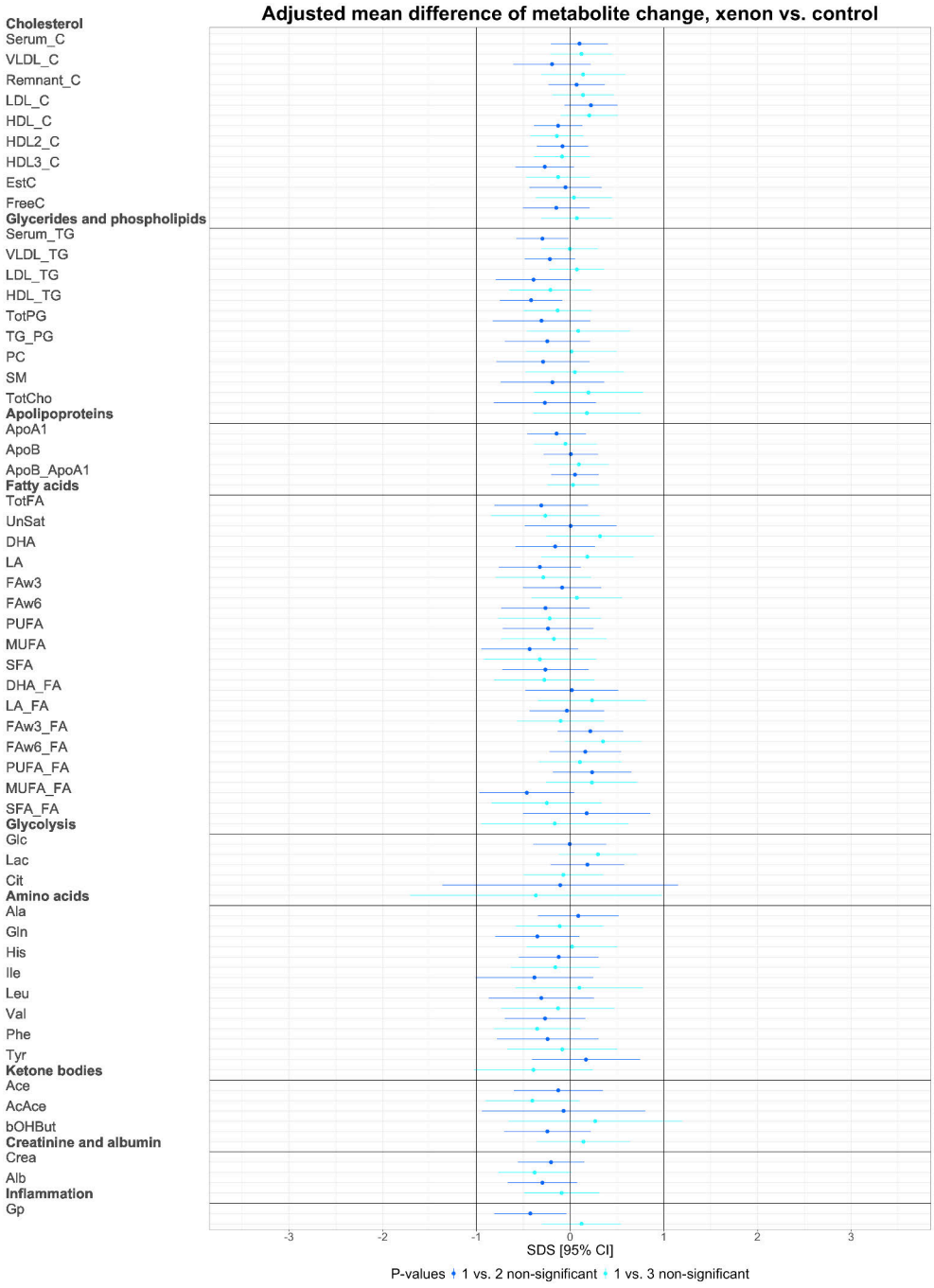

Figure 27. Metabolites associated with 6-month mortality after OHCA

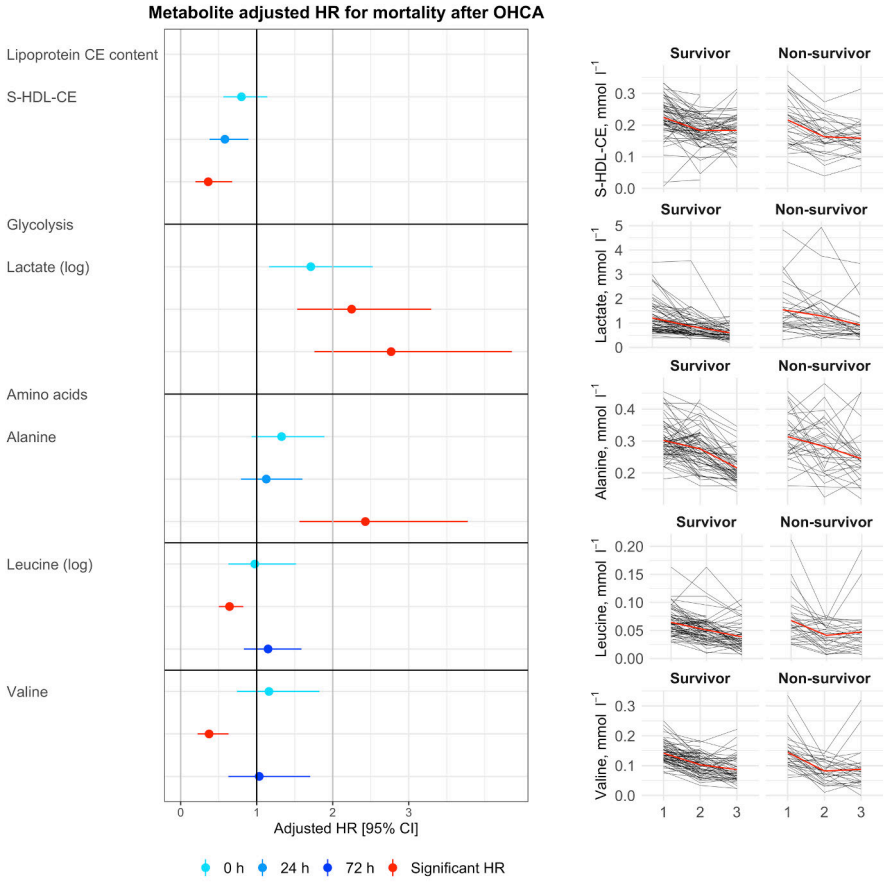

Summary of metabolites with statistically significant association with mortality at 6 months after out-of-hospital cardiac arrest, from original study III. Forest plots summarising selected metabolites with statistically significant adjusted HRs for mortality at 6 months, at one or more time points (left). Line graphs depict individual metabolite concentrations within each patient grouped by survival (right). In forest plots (left), data are reported as an adjusted HR and 95% CI. Statistically significant results after correction for multiple testing are highlighted in red. Logarithmic transformation was carried out for skewed metabolites, these metabolites are marked with (log). In the line graphs (right), data are reported as measured metabolite concentration in mmol l-1, time point means are depicted as red lines. Abbreviations: Ala, alanine; HR, hazard ratio; Lac, lactate; Leu, leucine: OHCA, out-of-hospital cardiac arrest; S-HDL-CE, small high-density lipoprotein cholesteryl ester content; Val, valine.

6 Discussion

As far as we are aware, this is the first investigation in which NMR spectroscopy and LC-MS/MS metabolomics has been implemented to assess the effects of specific anaesthetic/sedative agents in healthy human volunteers. Similarly, there are no previous studies on the effects of inhaled xenon on the circulating metabolic profile in OHCA patients.

There are several key findings; a relatively brief exposure to anaesthetics/sedatives, regardless of the moderate dose used (EC_{50} for verbal command), induced numerous unique alterations in the metabolic profiles of healthy male subjects. Furthermore, by implementing NMR targeted metabolic profiling in OHCA patients, several metabolites were observed to be associate with the 6-month mortality. Importantly, inhaled xenon did not seem to alter the current metabolic profile in the context of OHCA patients.

6.1 Pharmacometabolic profiles

6.1.1 Dexmedetomidine

In the NMR metabolic profile, changes in the levels of glucose, ketone bodies and to some extent the lipoprotein composition were detected. As expected, a 29% increase in the glucose concentration was observed, an observation reflecting dexmedetomidine-induced inhibition of insulin excretion due to α_2-adrenoceptor agonism[83,193]. A concomitant decrease in the amounts of ketone bodies was observed. Furthermore, a trend towards a decrease in HDL measurements was evident, e.g. a statistically significant decrease in the very large HDL concentration and a change in composition was determined. The total lipids, phospholipid and free cholesterol content decreased. Similarly, there were decreases in the phospholipid content in medium to small HDL, the triglyceride content in medium HDL and cholesteryl esters in large HDL. With the exception of the reduction in LDL diameter, the changes in lipoprotein concentration and composition were restricted to HDL. The

ratio of apolipoprotein B to A1 was slightly but significantly increased, suggesting a relative decrease in the ApoA1 concentration, a major structural component of HDL. The estimated degree of unsaturation of fatty acids increased. Indeed, it has been reported that adrenergic receptors contribute to lipid metabolism, with the role of α_2-adrenoceptor being antilipolytic[45,46]. For example, the α_2-adrenoceptor agonist, clonidine, caused significant reductions in the levels of HDL and ApoA1 (And ApoA2)[47]. Moreover, the concentration of one amino acid (alanine) increased, reaching statistical significance after the study drug administration had ended.

In the LC-MS/MS assessment, dexmedetomidine induced a wide-ranging decrease in the levels of the bile acids and oxylipins. The level of the primary bile acid precursor HCO declined, as did those of the primary bile acid chenodeoxycholic acid and many of the measured secondary bile acids and their conjugates. Metabolites of hepatic origin might decrease in response to a decrease in the hepatic blood flow. Although dexmedetomidine has a substantial hepatic extraction ratio and a decrease in cardiac output has been shown to reduce its rate of elimination, in animal models no significant reduction in hepatic blood has been demonstrated[194,195]. Alternatively, dexmedetomidine has been shown to increase the discharge frequency of vagal nerve and maintain acetylcholine levels in rodent models during a lipopolysaccharide (LPS) challenge and a vagal cholinergic stimulus is known to increases the rate of gall bladder emptying[73,105,196]. Possibly, dexmedetomidine-mediated vagal effects could contribute to the observed reduction of bile acids in the circulation[197]. Alternatively, vagal and/or α_2-adrenoceptor mediated effects might evoke alterations in gastrointestinal motility, which could affect the enterohepatic circulation of bile-acids and bile-acid metabolism being performed by the intestinal microbiota. In healthy male volunteers, dexmedetomidine markedly inhibited gastric emptying and gastronintestinal transit as demonstrated by the paracetamol absorbtion test and the hydrogen breath test, respectively[104]. It is an open question if slower transit time induced by dexmedetomidine promotes metabolism of bile acids by the intestinal microbiota resulting in decreased concentration of serum bile acids.

Moreover, marked decreases were observed in the levels of many of the measured oxylipins in response to dexmedetomidine. Decreases were evident in oxylipin precursors EPA and AA, CYP-derived oxylipins from AA (5,6-DHET, 11,12-DHET, 14,15-DHET), AA derived LOX oxylipin 5-HETE and EPA derived CYP oxylipin 17,18-DiHETE. Furthermore, CYP-derived oxylipins from LA (9,10- and 12,13-DiHOMEs and 9,10- and 12,13-EpOMEs), LOX oxylipins from LA (9-HODE, 13-KODE) and from α-LA (9-HOTrE) were reduced.

Soluble epoxide hydrolase (sEH) is a common denominator for DHET, DiHOME and EpOME metabolism. The main catabolic pathway of EETs is the conversion to their corresponding DHET, a reaction catalysed by sEH, with 14,15-EET being the preferred substrate followed by 11,12 EET. However, 5,6-EET has

been described as a poor substrate for sEH[198]. The conversion of EET to DHET by sEH has been considered to attenuate the biologic effects of EETs. Thus, a reduction in the circulating DHET level might be reflected in an increased effect of EETs, e.g. protection against a reperfusion injury in cardiomyocytes, anti-inflammatory properties and inhibition NF-κB signalling[79,198–200]. Similarly, the conversion of EpOME to DiHOME occurs via sEH. Understandably, sEH inhibition has been studied extensively due to its possibly favourable cardiovascular and anti-inflammatory effects[198,201]. Interestingly, LPS-induced inflammation in sEH null mice resulted in decreased DHETs without affecting EET levels and a decrease in the levels of 5-HETE and thromboxane B_2 was observed[202]. Similarly, in the context of LPS-induced inflammation, the concentrations of both DiHOME, DHET and prostaglandin D2 decreased in mice with targeted disruption of the sEH coding Ephx2 gene (sEH null) *vs.* wild-type, whereas EpOME and 5-HETE were unaffected while the decreases in 9- and 13-HODE were non-significant. The 60.5% decrease in 13-HODE, a precursor of 13-KODE, was not statistically significant[203]. In another LPS challenge in murine models, sEH inhibition increased the levels of EpOME, decreased those of DiHOME, increased the EET/DHET ratio and eventually decreased the 5-HETE concentration[204]. Importantly, in the current study there was no inflammatory state present. As discussed, the levels of EpOMEs, DiHOMEs, DHETs, 5-HETE, 9-HODE and 13-KODE were significantly decreased in the current study. The dexmedetomidine-induced effects on prostaglandin D2 (and 8,9-DHET) could not be reliably quantified due to the high number of values under the detection limit of the current methodology. Although dexmedetomidine induced decreases in the aforementioned oxylipins share some resemblance to sEH inhibition in animal models, one would have expected to observe an increase, rather than a decrease in the amounts EpOMEs. This was the case in an experiment where sEH-null mice were compared to their wild-type counterparts without LPS provocations[203]. Moreover, one would have predicted that there would have been an increase, rather than a decrease in HDL markers[205].

Alternatively, CYP-mediated effects might contribute to DHET, EpOME, and DiHOME[49,206]. It is well known that the CYP2C family of enzymes is responsible for the generation of the majority of epoxide metabolites in mammals, and minor contributions to the hepatic metabolism of dexmedetomidine have been reported via CYP2C19 and CYP2C9[207]. However, changes were observed in LOX metabolites as well. Prior to the current study, there was only limited knowledge on the effects of dexmedetomidine, and of α_2-adrenoceptor agonism, on circulating levels of oxylipins, further research may clarify the mechanisms underlying the present observations.

Specific oxylipins may have pro- and antithrombotic, and vasoactive properties. 9-HODE displays pro-thrombotic properties in human saphenous vein endothelial

cells, whilst previous research on the role of 13-HODE in thrombosis has been inconclusive, suggesting both pro- and anti-thrombotic properties. In animal models, 13-HODE has been shown to cause vasorelaxation[208]. Here, while dexmedetomidine decreased 9-HODE and 13-KODE (a derivative of 13-HODE), the physiological relevance of these findings remains to be established.

The observed decreases in 9,10- and 12,13-DiHOME seem especially interesting. A decrease in EPOMEs (1 *vs.* 2) preceded the reduction of DiHOMEs. Initially, EpOME had been identified as a possible culprit underlying mitochondrial toxicity in burn patients developing an acute respiratory distress syndrome (ARDS). Later, it was discovered that mitochondrial toxicity was driven by an EpOME derivative, DiHOME[209]. DiHOME-mediated mitochondrial dysfunction is elicited at high concentrations of the compound and its administration in animal models caused mortality and histopathologic changes resembling those of ARDS[210,211]. However, DiHOME has physiological roles at low concentrations[212,213]. Due to the association with DiHOME, mitochondrial toxicity and ARDS, it is worth considering whether a reduction in DiHOME might prove beneficial in patients with or at risk of ARDS. Indeed, a reduction in the inflammatory markers in response to dexmedetomidine has been described in an animal model of acute lung injury. For example, the mechanisms included decreases in the activities of the myeloid differentiation primary response gene 88 (MyD88) and NF-κB[214]. In patients with or at risk of ARDS, sedation with dexmedetomidine reduced in-hospital mortality *vs.* propofol or midazolam sedation. Dexmedetomidine-related reductions in the levels of inflammatory mediators, which is supported by the current results, along with a lack of suppression of the respiratory drive, reduced the incidence as well as the duration of delirium, and organoprotection was thought to be a factor contributing to the observed reduction in mortality[215].

Dexmedetomidine-induced organoprotection has been an area on intense research and the cholinergic anti-inflammatory pathway (CAP) is considered to contribute to this property. The CAP can be considered an inflammatory reflex wherein the CNS receives an input via both humoral and afferent vagal neural fibers and responds via efferent activity of the vagus nerve leading to ACh release in organs of the reticuloendothelial system (e.g. the liver, heart, spleen and the gastrointestinal tract) eventually suppressing peripheral cytokine release from tissue macrophages.[216] ACh binds to the α7 subunit of the nicotinic ACh receptor (α7nAChR), triggering many signalling cascades e.g. leading to an inhibition of cytokine release and inhibition of TNF synthesis in macrophages[217]. α7nAChR agonists exhibit inhibitory effects on TLR mediated inflammatory pathways[218]. A dexmedetomidine-induced increase in myocardial α7nAChR has been reported, and an antagonist of the α7nAChR blocked the cardioprotective effect of dexmedetomidine[219]. CAP mediated dexmedetomidine-induced effects have been reported to alleviate renal

ischemia-reperfusion injury and LPS-induced acute lung injury in murine models. Disrupting CAP either by vagotomy, splenectomy or administration of atipamezole, an α_2-adrenoceptor antagonist, abolished the beneficial effect of dexmedetomidine[73,105].

In the context of dexmedetomidine-induced hepatoprotection, CAP contributes to the observed downregulation of TLR4/MyD88/NF-κB[152]. Indeed, many of the measured oxylipins are connected to the TLR/MyD88/NF-κB pathway. TLRs are expressed widely in immune (macrophages, dendritic cells, B-cells and neutrophils) and non-immune cells (fibroblast cells, epithelial cells and keratinocytes)[220]. TLRs play a key role in inflammation via the detection of pathogen-associated molecular patterns and damage associated molecular patterns, the latter may be produced in the setting of IRI[168,220]. Briefly, upon TLR activation, an innate immune response is elicited, including recruitment of MyD88 and activation of transcription factor NF-κB resulting in a pro-inflammatory response mediated by the production of cytokines, chemokines and co-stimulatory molecules on dendritic cells. This cascade of events is essential for T-cell activation[220]. Oxylipins possess immunomodulatory properties and are produced in response to acute inflammation as well as during the resolution of inflammation[79,206]. Several studies in animal models, often in the context of LPS-induced inflammatory provocation, support the role of NF-κB signalling in dexmedetomidine-induced organoprotection[70,74,151–153]. The current findings on oxylipins may support these observations, as the reduction in DiHOMEs, EpOMEs and possibly increased effects of EETs (possibly reflected here by a reduction in DHETs) would elicit inhibitory effects on the NF-κB pathway[79,199,221]. In contrast, 9-HODE and 13-HODE (precursor for 13-KODE) have been reported to elicit inhibitory effects on NF-κB and in the current study, the levels of these compounds were decreased by dexmedetomidine[222]. Based on the previous literature, it is worth considering whether the observed reductions in oxylipins, and quite possibly a vagally-mediated decrease in bile acids, might reflect the effects of dexmedetomidine on CAP. The current findings encourage further research to resolve this matter.

6.1.2 Propofol

Propofol induced wide ranging changes in the NMR metabolic profile, whereas in the LC-MS/MS metabolic profile substantial increases in concentration were focused on a few specific oxylipins. The *in vitro* analysis of the NMR metabolic profile hinted at the accumulation of propofol emulsion constituents during continuous infusion *in vivo*, whereas *in vitro* analysis of the LC-MS/MS profile

showed increases in the amounts of 9,10- and 12,13-DiHOME in the *in vitro* samples corresponding to the observed increases *in vivo*.

When one views the NMR metabolic profile, marked alterations were evident in the lipoprotein and fatty acid markers. The concentrations of XXL-M VLDL and very large HDL were elevated, while decreases were observed in the small to medium sized HDL. There were also changes observed in the content and diameter of lipoproteins. The ratio of total triglycerides to phosphoglycerides was increased as total triglycerides were elevated. The SFA/FA substantially increased. The estimated degree of unsaturation of fatty acids decreased, and saturated fatty acids increased. Although the ratios of PUFA, n-3 and n-6 fatty acids to total fatty acids decreased, there were no significant changes in PUFA, n-3 and n-6 concentrations. Furthermore, an increase in the level of GlycA was observed.

Propofol and the accompanying lipid emulsion are the strongest risk-factors for hypertriglyceridemia in ICU treated patients[42]. Regardless of the extensive alterations observed in the lipid metabolism in response propofol infusion, the actual increase in triglyceride levels remained quite modest. The total triglycerides increased by approximately 9% during one hour of propofol administration (in timepoints 1 *vs.* 2, difference in timepoint means), e.g. a change that is minor in comparison to a PUFA rich meal which was reported to increased total triglyceride concentrations by 75% from baseline within 2 hours[223]. Importantly, the *in vitro* analysis showed that the concentration of VLDL markers in the propofol group *in vivo* corresponded to the VLDL values observed at a 10-fold higher propofol concentration in the *in vitro* analysis. A further analysis of the NMR difference spectra suggested that there had been an accumulation of the propofol emulsion constituents e.g. soybean oil. A study comparing propofol and Intralipid, an often used proxy for the lipid emulsion of propofol, evoked similiar changes in selected blood lipids when the soybean oil content was equal between groups[156].

In the present data, the SFA/FA was markedly increased in the propofol group. As soybean oil and Intralipid both contain mostly unsaturated fatty acids, this finding seems relatively surprising. In the *in vitro* analysis at approximately 10-fold propofol dosing to the *in vivo* target concentration, the changes observed in the estimated degree of unsaturation (2.1% decrease from baseline) and saturated fatty acids (6.1% increase from baseline), and triglycerides (8.2% increase from baseline) were similar to the *in vivo* measurements with lower propofol target (1.7% decrease in unsaturation and 6.1% increase in saturated fatty acids, 9.0% increase in total triglycerides, based on timepoint means 1 *vs.* 2, respectively). However, with respect to total fatty acids, the elevation in *in vitro* with 10-fold propofol dosing was 4.2% whereas *in vivo* it was much less, 0.89%. The main difference between the *in vitro* and *in vivo* analysis was considered to be attributable to the absence of active metabolism in the *in vitro* measurement. Previously, propofol-induced bioenergetic

changes have been studied *in vitro*, demonstrating a profound inhibitory effect of propofol on FAO in human skeletal and heart muscle cells[44,78]. Considering the absence of active metabolism in *in vitro* samples, an inhibition of FAO might be expected to result in higher relative concentrations of triglyceride and fatty acid markers *in vivo vs. in vitro* comparisons, when the accumulation of propofol emulsion constituents is taken into account. However, this may be an oversimplification. After an overnight fast, FAO may account for up to 70% of total body energy expenditure. In most circumstances, even in the post-absorptive state, the regulation of lipolysis provides an ample supply of lipid fuel, far exceeding the rate of whole body lipid oxidation[224]. It could be argued that changes in the entry of specific chain length fatty acids to FAO (e.g. as mediated by carnitine transportation as discussed earlier), would not be reflected in the systemic levels of circulating free fatty acids, as the availability of free fatty acids exceeds by a substantial amount the need for FAO. A metabolic profile targeted to detect changes in FAO, e.g. specific chain length fatty acids and the carnitine transport system, might offer more information on this matter.

As demonstrated by the current data, a relatively brief 60-minute propofol administration led to marked changes in lipid metabolism, possibly due to the accumulation of propofol emulsion constituents. Furthermore, there were changes in the fatty acid pool, with a tendency towards an increase in the amounts of saturated fatty acids. Moreover, the previous literature describes changes in fatty acid utilisation in FAO[44,78]. Understandably, known complications of prolonged propofol infusions have included hypertriglyceridemia and hypertriglyceridemia-associated pancreatitis[42,155]. In the ICU, triglyceride levels are routinely screened for the early detection of propofol-induced hypertriglyceridemia, which has been reported to develop after a median of 7 days[42]. The observed relatively moderate increase in the triglyceride concentration raises the question about whether propofol-induced hypertriglyceridemia might be better predicted with other markers reflecting propofol-induced alterations in the lipid profile. Evidently, whether alterations in SFA/FA precede the rise in circulating triglycerides remains an open question.

It is worth briefly discussing the observation on the subtle elevation of the inflammatory marker GlycA induced by propofol. As discussed earlier in detail, GlycA is an NMR signal arising from the N-acetyl groups in multiple acute phase metabolites. Even though chronically elevated levels of GlycA have been associated with gene networks of neutrophil functions, long-term risk of infection and even all-cause mortality, less is known about the impacts of acute GlycA alterations[3,4,7]. The clinical relevance of this observation is uncertain.

To some extent, the LC-MS/MS oxylipin profile echoed the changes observed in the NMR profile and were probably related to the accumulation of lipid emulsion constituents. In the propofol group, the amounts of LA derivatives 9,10- and 12,13-

DiHOME substantially increased, up to 7.6- and 4.5-fold from baseline, respectively (1 *vs*. 2), with approximately the same fold-difference in propofol *vs*. placebo at timepoint 2 (7.7 and 4.5, 9,10- and 12,13-DiHOME, respectively). This is likely a repercussion of the lipid emulsion used for delivering propofol, as demonstrated by the *in vitro* analysis. Accordingly, 12,13-DiHOME has been detected by LC-MS/MS in response to an Intralipid infusion in healthy human subjects[157]. However, increases were also observed in other LA and α-LA derivatives, LOX oxylipins 9-HODE and 9-HOTrE, respectively. The levels of 9-HODE and 9-HOTrE remained unaffected in the *in vitro* analysis, whereas those of DiHOME were elevated. Soybean oil, a propofol emulsion constituent, is an excellent source of LA and α-LA. Regardless of their presence, the LA concentration remained unchanged in the NMR metabolic profile. One possible explanation for the observed changes is increased substrate availability for 9-HODE and 9-HOTrE synthesis in the *in vivo* experiment. However, in the *in vitro* analysis, as propofol was directly added to the previously stored pooled serum samples, the possibility of ongoing metabolism of LA and α-LA towards DiHOMEs seems less likely.

As discussed previously, propofol has the capability to alter FAO[44,78]. These effects in combination with the observed increases of DiHOME may be of interest concerning cellular bioenergetics. Especially during catabolic states, fatty acids are broken down to yield energy via mitochondrial FAO. As discussed, the entry to FAO of fatty acids with specific chain lengths requires active transportation, e.g. the fatty acids abundant in the propofol emulsion such as LA and α-LA require carnitine transportation in order to gain access to mitochondria and FAO[225]. An inhibition of this transport mechanism has been described in animal models in response to propofol administration. Furthermore, a similar inhibition has been suspected in the context of the propofol infusion syndrome (PRIS)[43]. *In vitro* studies in human heart and skeletal muscle demonstrated that propofol in a clinically relevant concentration inhibited FAO and mitochondrial respiration. This inhibition was thought to occur between CPT II and the entry of electrons from FAO into the electron transport chain via complex II, rather than inhibition at CPT I as previously described[44,78]. Interestingly, oxylipin metabolism is controlled by FAO in the context of bacterial inflammation: Blocking FAO with a CPT I inhibitor, etomoxir, during an LPS challenge, resulted in higher DiHOME precursor EpOME concentrations *vs.* LPS alone[226]. Physiologically, it is known that exercise increases the level of 12,13-DiHOME leading to elevations in fatty acid uptake into cardiac and skeletal muscle cells and increasing mitochondrial respiration[213]. However, when high DiHOME concentrations are present i.e. in excess of physiological concentrations, the compound has triggered a mitochondrial dysfunction[79,82,211]. As an interesting detail, fat accumulation in heart and skeletal muscle has been described in a case report of PRIS[227]. Indeed, in a mouse cardiac cell line, administration of either 9,10- or 12,13-

DiHOME resulted in a concentration-dependent decline in cell viability, a collapse in mitochondrial respiratory function and a massive release of certain pro-inflammatory cytokines such as TNF-α and monocyte chemoattractant protein-1[203]. Furthermore, mitochondrial dysfunction and inhibition of FAO have been suggested as possible pathophysiological mechanisms for PRIS[43]. Although these prior publications could in theory represent a basis for a vicious cycle of mitochondrial dysfunction, it is important to remember that propofol is a routinely used anaesthetic whereas PRIS is an exceedingly rare phenomenon. In contrast, the elevation of DiHOME was a common occurrence in the current data. Nonetheless, the behaviour of DiHOMEs during prolonged propofol infusions should be established in the future. Based on the previous literature and the current observations, it would be of interest to quantify DiHOME in the context of PRIS.

6.1.3 S-Ketamine

In the NMR metabolic profile, S-ketamine elevated the concentrations of glucose and lactate were, whereas a decrease in the circulating levels of BCAAs isoleucine, leucine and valine was observed. When compared with the placebo group, the lactate concentration was 53.8% higher in the S-ketamine group at timepoint 2. In the LC-MS/MS profile, only a decrease in the level of the bile-acid precursor HCO was observed.

The magnitude of the lactate increase seems biologically significant, as the mean concentration of lactate at timepoint 2 in the S-ketamine group was approximately 53% and 10.6% of the lactate concentrations present during moderate- and high-intensity exercise, respectively[228]. Racemic ketamine has been shown to increase circulating adrenaline and noradrenaline levels[48,123]. Moreover, the preconditioning effects on isolated human myocardium by racemic ketamine were abolished by blockade of α and β adrenoceptors, suggesting that the ketamine effects are directly mediated via adrenoceptors[229]. Similarly, S-ketamine anaesthesia in human subjects approximately doubled the plasma noradrenaline concentration in comparison to the level at awake baseline[230]. In human subjects, administration of noradrenaline resulted in an approximately 15% elevation in the plasma glucose and lactate levels and furthermore the lactate levels in smooth muscle and adipose tissue exceeded the plasma concentrations[231]. It seems likely that the hyperadrenergic state induced by S-ketamine contributes to the current observations of increases in the glucose and lactate concentrations.

Furthermore, S-ketamine induced changes in the concentrations of metabolites of several amino acids with those of the BCAAs, isoleucine, leucine and valine decreasing during study drug administration. Interestingly, the decline in the level of

the AAA tyrosine reached statistical significance after study drug administration had ended at timepoint 3. Similarly, a further decrease in the valine, isoleucine and leucine concentrations occurred after S-ketamine infusion had ended. It is an interesting question if the active metabolites of S-ketamine could have contributed to these findings[124]. This kind of modulation of amino acid profiles is especially interesting as S-ketamine has been approved as a drug for treatment-resistant depression. BCAA and AAA share a competitive transport mechanism across the BBB, which is almost fully saturated at physiological concentrations as discussed earlier. Thus, changes in the ratio of available BCAA and AAA will affect their intake into the CNS. Specific BCAAs and AAAs serve as precursors for neurotransmitter synthesis in the CNS e.g. the AAA, tryptophan, is a precursor for serotonin synthesis and tyrosine for noradrenaline synthesis via transformation to dopamine. Increases in circulating BCAA concentrations lead to a reduction in the synthesis of AAA-derived neurotransmitters such as serotonin and noradrenaline in the brain[94]. In theory, a reduction in the amounts of circulating BCAA concentrations might result in increased AAA entry to the CNS and a subsequent increase in the synthesis of neurotransmitters of AAA origin e.g. serotonin and noradrenaline. This might be of interest concerning the established role of S-ketamine in treatment-resistant depression, as the mechanism of action of many of the commonly used antidepressants is based on selective inhibition of serotonin and serotonin-noradrenaline reuptake. Sertraline is a selective serotonin reuptake inhibitor and the sertraline-induced reduction in symptoms of major depressive disorder has been associated with decreases in the amounts of BCAAs valine, leucine and isoleucine in serum samples. Furthermore, previous research on the metabolomics of S-ketamine in patients with a major depressive disorder showed a decrease in the tyrosine concentration[89]. Considering the role of tyrosine in noradrenaline synthesis, the gradual decrease observed in the tyrosine concentration in the current study might also be a reflection of the hyperadrenergic state induced by S-ketamine[230].

The LC-MS/MS oxylipin and bile acid profiles were relatively unaffected by S-ketamine. Only a decrease in the level of the primary bile acid precursor HCO was observed without changes in other bile acid metabolites. As such, the isolated decrease in the HCO level likely has no clinical relevance.

6.1.4 Sevoflurane

Based on the current NMR and LC-MS/MS profiles, sevoflurane was the most inert of the studied anaesthetics/sedatives. In the NMR profile, an elevation in the alanine concentration was observed; this might be the result of increased motor restlessness during the study period[232]. LC-MS/MS profile detected increases in the

amounts of TUDCA and an EPA derived CYP oxylipin DiHETE. The reduction in the circulating level TUDCA, a secondary bile acid with putative neuroprotective effects in animal models of ischemic stroke, might be of interest[111]. Rather surprisingly, a single study in a murine model, where the neonatal animals were repeatedly exposed to sevoflurane suggested that administration of TUDCA resulted in an amelioration of both hippocampal endoplasmic reticulum stress and caused a reduction in the extent of the cognitive impairment. However, due to the high number of missing values in the TUDCA measurements in the sevoflurane group, the current findings remain uncertain and will need to be verified in future studies.

In contrast to a previous study conducted in primates, no statistically significant alterations were observed in triglyceride levels, ketone bodies, PUFA, n-3 or n-6 fatty acids. However, in contrast to the values in the referenced study, the anaesthetic administration was markedly shorter in our current study (1 h *vs.* 9 h)[25]. The observed reduction in levels of cholic acid and the increase in the levels of DHA when neonatal mice were exposed to sevoflurane were not evident in the current data[29].

6.2 Metabolomics after out-of-hospital cardiac arrest

In OHCA patients randomised to receive TTM alone or in combination with inhaled xenon, NMR metabolomics demonstrated significant HR for 6-month mortality for lactate at 24 and 72 h, alanine at 72 h, leucine and valine at 24 h, and S-HDL-CE at 72 h. No significant metabolite associations were observed upon admission. The NMR profile did not significantly differ between xenon *vs.* control.

In a targeted metabolomics analysis of OHCA patients, Beske et al. demonstrated that most of the variation between OHCA survivors and non-survivors at 2-3 hours after OHCA was explained by metabolites associated with the TCA cycle i.e. malic, fumaric and succinic acid. These observations were thought to reflect the transient global ischaemia induced by OHCA. Moreover, concentrations of lactate, amino acids (e.g. alanine, leucine, isoleucine, tyrosine, phenylalanine) and acylcarnitines were elevated, whereas those of LA and 12,13-DiHOME were decreased in non-survivors. While the concentration of valine was higher in non-survivors, it did not reach statistical significance. It is important to be aware that in that experiment the metabolites were only analysed upon admission[37]. Notably, the current NMR profile was not focused on TCA cycle intermediates as the only TCA cycle intermediate assessed was citrate. Moreover, in the current study neither creatinine nor albumin showed an association with mortality upon admission, a finding which is in contrast with the previous literature[98,99]. However, in the present study, the levels of lactate,

alanine, two BCAAs i.e. leucine and valine, and S-HDL-CE associated with 6-month mortality in the days following OHCA.

The current observation on the association between 6-month mortality after OHCA and the alanine concentration at 72 hours, may be a consequence of the metabolic connection between lactate and alanine as discussed earlier: The alanine cycle is connected to the Cori cycle via pyruvate[87]; this linkage has been described earlier in a small sample of human patients. In the same study, when rat liver was perfused with high levels of lactate and pyruvate, a reduction in hepatic uptake of alanine was observed, whereas the concentrations of BCAAs i.e. leucine, isoleucine and valine, remained relatively unaffected *vs.* control[233].

Previous research has demonstrated that elevated lactate levels upon admission are associated with patient mortality after OHCA[37]. This would be expected, as the sudden circulation standstill which occurs in OHCA results in global hypoperfusion, i.e. the tissues are deprived of oxygen and the removal of metabolic waste products is abruptly terminated. This results in a depletion of O_2 within 20 seconds and ATP within 4-6 minutes[100]. Rather surprisingly, the initial lactate level upon admission did not show any association with mortality in the current study, unlike the relatively modest elevation of lactate evident at both 24 and 72 h. The current observation that a long-term elevation in lactate concentration is associated with 6-month mortality after OHCA is in line with previous studies[84,85]. Similar findings on lactate have been reported at 48 hours post-OHCA in patients receiving TTM[38]. The current findings suggest that, rather than the initial OHCA-induced transient global hypoperfusion and ischaemia, it is the subsequent pathophysiological processes e.g. PCAS and IRI, that may contribute to the persistent lactatemia and the observed association with mortality. Quite possibly, the median no flow of 0 minutes as reported in Table 11 may have contributed to the current observations upon admission.

In the present material, decreases in the levels of two BCAAs, valine and leucine, associated with an increased risk of 6-month mortality at 24 h after admission i.e. at the end of the 24-hour randomised study treatment of TTM alone or in combination with xenon. This signifies that prior to sampling, patients were under sedation with a RASS target of -4 to -5, i.e. nutritional differences are unlikely to be the explaining factor for the observations on the levels of the BCAAs. Moreover, had nutritional status prior to OHCA exerted a decisive factor in survival, the BCAA observations would be expected to present already at baseline. The current observation is in line with previous research in OHCA and TTM, as higher leucine and valine levels at 48 hours after OHCA were associated with a favourable outcome[38]. However, these results are in contrast with previous observations in the context of ST elevation myocardial infarction (STEMI) treated with PCI, wherein high levels of circulating BCAAs were correlated with several in-hospital adverse events: cardiovascular mortality and acute heart failure with abnormal catabolism of the BCAAs in the

pathologically-stressed myocardium being thought to underlie these observations[21]. In the present material, the incidence of cardiovascular disease was high e.g. STEMI was diagnosed in 30.8% of patients in the xenon group and 35.9% in the control group[114]. These contrasting observations suggest that the metabolic processes giving rise to the observed alterations in the circulating BCAAs in STEMI and OHCA may be quite different. Notably, BCAA metabolism is intertwined with many of the metabolic processes of particular interest in the context of OHCA and TTM.

First, considering the current findings on lactate, it is relevant to discuss previous research on metabolic acidosis and its role in BCAA degradation. Although not directly comparable to the current context of adult OHCA patients, in pediatric patients with end-stage renal disease, research has demonstrated that chronic metabolic acidosis induces a decrease in plasma BCAA levels[234]. In rodent models, it was hypothesised that the acidosis would need to be chronic in order to cause the observed reduction in BCAA, at least via the mechanism of BCAA decarboxylation which was not acutely stimulated by incubation of rat muscle in acidified media[235,236]. As discussed earlier, when rat liver was perfused with high concentrations of lactate and pyruvate, the amounts of the BCAA:s were relatively unaffected[233]. In contrast, when leucine turnover was studied in 7 healthy volunteers with ammonium chloride-induced acidosis, it was observed that leucine appearance from and its incorporation into proteins, and leucine oxidation were increased in times of acidosis. However, this resulted in an increase in the circulating levels of valine and leucine, whereas those of isoleucine were unaffected[237]. This is in contrast with the current findings of decreased levels of BCAAs associating with 6-month mortality, as acidosis would be expected to be linked with an unfavourable prognosis.

Second, as discussed, three BCAAs i.e. leucine, isoleucine and valine, are essential amino acids with a central supporting role in cellular bioenergetics in the TCA cycle, with the potential to replenish TCA cycle intermediates. Carbons originating from leucine enter the TCA cycle as acetyl-CoA (in the context of TCA cycle, a precursor of citrate), whereas isoleucine and valine mainly provide carbon to the TCA cycle via anaplerotic conversion of propionyl-coenzyme A to succinyl-coenzyme A (precursor of succinate)[90]. Beske et al. demonstrated that the circulating concentration of many TCA cycle metabolites i.e. citrate, 2-oxoglutaric acid (i.e. α-ketoglutarate), succinic, fumaric and malic acid were increased in OHCA non-survivors in comparison to survivors[37]. Two models have been proposed to explain succinate (anion of succinic acid) accumulation in patients with ischaemia. One involves the reversal of mitochondrial complex II with fumarate (anion of fumaric acid) serving as the electron acceptor yielding succinate (in the absence of oxygen as a teminal electron acceptor), whereas another posits that there is an inhibition of mitochondrial complex II together with canonical TCA cycle activity, partly

supported by aminotransferase anaplerosis. The latter proposal was supported by an extensive study in mitochondria sampled from mouse cardiomyocytes, and in perfused mouse hearts. The central finding was that the majority of ischaemic succinate is generated by the canonical TCA cycle activity. With reperfusion, most of the succinate is washed out and may serve a signalling role. A depletion of immediate succinate precursors i.e. succinyl-coenzyme A and α-ketoglutarate was observed during ischaemia, while a repletion of α-ketoglutarate increased ischaemic succinate production. Interestingly, the authors discussed the possibility that ALAT mediated deamidation of glutamate might be required to generate alanine and anaplerotic α-ketoglutarate for TCA cycle, as alanine is known to accumulate during ischaemia[238]. This is interesting concerning the current finding on alanine. However, had the anaplerotic roles of leucine and valine contributed to the current observations, it might be expected to see similar results in other anaplerotic amino acids as well[239]. Moreover, due to the initial OHCA-induced global ischaemia and subsequent reperfusion after ROSC, alterations in circulating metabolites would likely be evident upon admission.

Third, BAT thermogenesis can be fueled by the BCAAs. This might be of interest in the context of TTM at the target temperature of 33 °C. BAT primarily relies on triglyceride stores in order to perform thermogenesis[240]. Indeed, cold-exposure is considered to increase thermogenic utilisation of BCAA in BAT, leading to enhanced BCAA clearance from the circulation[241]. Interestingly, a reduction in anaesthesia-induced hypothermia and shivering has been demonstrated in response to intravenous amino acid supplementation prior to anaesthesia, supporting a role for the BCAAs in thermoregulation in humans[242,243]. Indeed, the previous study conducted by Beske et al. demonstrated that 48 hours after OHCA, TTM at 33 °C initiated upon ICU admission resulted in a greater decrease in both leucine and valine concentrations in comparison to TTM at 36 °C. In the same study, lower leucine and valine concentrations at 48 hours were associated with 6-month mortality. Importantly, the association with mortality was independent of the TTM group[38]. Additionally, in OHCA patients, neither TTM with normothermic target of 36 °C *vs.* 33 °C, nor a normothermic target of 37.5 °C or less (TTM initiated if the body temperature reached 37.8 °C or higher) *vs.* 33 °C was associated with any significant difference in survival, regardless of the observed increase in hemodynamically significant arrhythmia with the hypothermic target (24 *vs.* 17%) in the latter study. Moreover, the hypothermic target did not confer any benefit *vs.* normothermic target[244,245]. Even though the thermogenic utilisation might lower circulating BCAA concentrations in response to TTM, this mechanism alone would seem to be insufficient to explain the observed association between BCAAs and mortality in OHCA patients.

Fourth, in the CNS, the metabolisms of alanine, leucine and valine are intertwined with the metabolism of the neurotransmitter glutamate, e.g. as demonstrated in multiple ^{15}N labelling studies[96,246–249]. Indeed, in human and rat brain slices incubated with ^{15}N labelled leucine, isoleucine and valine, ^{15}N-incorporation occurred in glutamate, glutamine, alanine, and aspartate, indicating nitrogen incorporation into these amino acids was supported by BCAA metabolism[247]. Similarly, in mouse cerebellar astrocytes, ^{15}N leucine and ^{15}N isoleucine-derived labels were identified in glutamate, glutamine, aspartate, and alanine[95].

In OHCA patients who achieve ROSC and survive to hospital admission, post-cardiac arrest brain injury is the likely cause for mortality[171]. As discussed earlier, aberrant CNS glutamate metabolism, namely glutamate excitotoxicity, is one of the central mechanisms of post-cardiac arrest brain injury. In glutamate excitotoxicity, a bioenergetic failure terminates neuronal Na^+/K^+-ATPase activity, leading to anoxic depolarisation and a loss of ionic gradients. A dramatic influx of Na^+, Cl^- and Ca^{2+}, and efflux of K^+ ensues, triggering an extensive presynaptic release of glutamate. Concurrently, astrocytic compensatory glutamate reuptake and cycling fails under this severe bioenergetic strain, potentially reversing glutamate transport. This cascade of events leads to a supraphysiological accumulation of glutamate in the synaptic cleft, resulting in a propagation of neuronal damage which is exacerbated by many secondary mechanisms such as inflammation, oxidative stress and mitochondrial dysfunction[166,169].

Under physiological conditions, the astrocytic processes intricately ensheathing synapses facilitate the removal of up to 90% of synaptic glutamate maintaining neuronal homeostasis[166]. Once taken up by astrocytes, glutamate's carbon skeleton can undergo TCA cycle mediated oxidative metabolism via either complete oxidation to CO_2 i.e. complete pyruvate cycling, or it can produce lactate via partial pyruvate cycling; *in vitro*, the latter route is favoured. Prior to entry into the TCA cycle as α-ketoglutarate, glutamate undergoes transamination of which 75%–90% is considered to occur mainly via ALAT and aspartate aminotransferase. In the context of alanine, ALAT catalyses the reversible interconversion of glutamate and pyruvate to α-ketoglutarate and alanine. Later the roles of BCAT and glutamate dehydrogenase were elucidated. Moreover, glutamate can be recycled via the glutamate-glutamine-cycle, wherein the carbon skeleton of glutamate is returned to the presynaptic neuron as the non-excitatory amino acid glutamine[239,249,250]. Schousboe et al. have illustrated the enzymes and reactions governing astrocytic glutamate handling[250]. In astrocytes, the label from ^{13}C labelled glutamate was found to a larger extent in lactate than in glutamine. Moreover, in response to elevated exogenous glutamate concentrations, the metabolism to lactate predominated[249]. It has been hypothesised that lactate produced in the CNS may be exported outside the CNS under physiological conditions[239].

The metabolism of BCAAs in relation to glutamate has been reviewed in detail by Yudkoff, where a connection between the glutamine-glutamate cycle and the proposed glutamate-BCAA cycle was discussed. This coupling would serve two purposes; e.g. it would offer a mechanism for BCAA importation to the CNS in exchange for glutamine and provide a means for the transient buffering of the rapidly rising synaptic glutamate levels. In simplified terms, the latter would be achieved by utilising the bidirectional reaction converting BCAA and α-ketoglutarate to glutamate and BCKA catalysed by BCAT, and the concomitant transport of BCAA and BCKA between neurons and astrocytes[246]. Interestingly, the predicted uptake of leucine to the CNS via the aforementioned exchange mechanism exceeds that of any other amino acid at physiologic plasma concentrations. Furthermore, *in vitro,* the concentration of glutamine augmented leucine transportation into astrocytes. In an *in vitro* study of mouse cerebellar astrocytes, incorporation of ^{15}N label into intracellular glutamate from ^{15}N labelled leucine, isoleucine, or valine amounted to approximately 40-50% with the contribution of each individual BCAA differing only marginally. Interestingly, in contrast to the other BCAAs, the label in glutamate from ^{15}N labelled valine was not decreased upon exposure to exogenous glutamate, suggesting an up-regulation of transamination involving only valine during repetitive exposure to glutamate[95].

Indeed, the prior literature has described similar associations between circulating BCAA concentrations and neuronal damage. Metabolic profiling has identified reduced plasma BCAA valine, isoleucine and leucine concentrations not only in animal models, but also in human patients with cardioembolic stroke. Moreover in patients, reduced plasma levels of BCAAs correlated with poor neurological outcome in these patients as measured by the modified Ranking Scale[20]. Similar reports have been published in a systematic review of patients with traumatic brain injury (TBI)[251]. A significant reduction in plasma BCAAs leucine, isoleucine and valine was observed in both mild and severe TBI *vs.* healthy controls. No significant difference in BCAAs was observed in the comparison of mild TBI *vs.* orthopaedic trauma without TBI. However, severe TBI led to a significant decrease in the levels of leucine and valine *vs.* orthopaedic trauma without TBI[252].

However, it is important to note that in animal models under physiological conditions, approximately 86% of BCAA catabolism occurred in skeletal muscle, brown fat or the liver; e.g. the contribution of the CNS was relatively modest[93]. This raises an important question: Is BCAA metabolism redistributed in the context of severe neuronal damage and if so, to what extent? The aforementioned study on TBI *vs.* orthopaedic trauma may well indicate that in the context of tissue trauma, extracranial metabolism likely affects circulating BCAAs as well. Furthermore, considering the exchange mechanism of BCAA entry into the CNS, neither the

current study nor the previously discussed report on cardioembolic stroke, detected any significant changes in the plasma glutamine concentration[20].

Nevertheless, out of the mechanisms known to drive mortality in OHCA patients, neuronal damage could have the potential to induce a decrease in the circulating BCAA levels. Moreover, the well-established metabolic connections between the BCAAs, alanine, lactate and the excitatory neurotransmitter glutamate exist in the CNS. In the light of the previous literature, it is worth considering whether the current findings on BCAAs, alanine and lactate might reflect OHCA-induced neuronal damage. However, further research will be needed to answer this question.

Lastly, the higher S-HDL-CE at 72 h associated with decreased mortality after OHCA. As described earlier, cholesteryl esters are formed by LCAT in HDL after the initial uptake of free cholesterol in the peripheral tissues, a process central in RCT[50]. However, the current study evaluated mortality at 6 months post-OHCA, which is a relatively brief period of time to achieve a survival benefit based on RCT alone. Lipoprotein metabolites including HDL are known to decrease in the days following myocardial injury, and this decline correlated with surrogate markers of infarct size[50]. One could speculate that this might contribute to the observed association between S-HDL-CE and mortality.

In the current study, no significant difference was observed in the metabolic profile in the comparison of xenon *vs.* control. Xenon as a noble gas is not metabolised; it possesses very rapid induction and recovery characteristics and it has been observed to be safe in various clinical settings[253]. Due to these attributes, xenon has been recognised to be close to the "ideal anaesthetic". Consequently, it might be suspected that inhaled xenon would be a relatively inert anaesthetic in the context of metabolic profiling. However, in the present material, it has been earlier demonstrated that less cerebral white matter damage occurred in the xenon group *vs.* control as measured by fractional anisotropy of diffusion tensor MRI[115]. Similarly in the present material, xenon attenuated the myocardial injury as measured by troponin-T levels[114]. In theory, both of these protective effects might be reflected on the circulating metabolic profile as discussed earlier. Moreover, based on the metabolic profile observed in response to propofol infusion in study I, it might have been expected to see some intergroup differences in study III due to the propofol-sparing effect of inhaled xenon within the first 24 hours but nonetheless, no changes were observed in the between-group comparison of the metabolic profiles. Importantly, the sample size for the study had been calculated based on a power analysis of fractional anisotropy values as discussed earlier[115]. As such, it may be that the study was not powered to detect a difference in the metabolic profile between the two treatment groups. However, considering prolonged sedation of vulnerable ICU patients e.g. in the context of post-resuscitation OHCA, the trait of metabolical inertness might be a desired attribute for an ICU anaesthetic/sedative.

7 Study limitations

The present study has some important limitations. First, in studies I-II, the doses of anaesthetics/sedatives were moderate (EC_{50} for verbal command) and the duration relatively short resulting in smaller anaesthetic/sedative exposure when compared with the doses administered in clinical anaesthesia. Second, *a priori* power analysis for metabolic profiling was not conducted due to the exploratory nature of the study as explained previously. Third, only healthy male ASA I volunteers were studied as pre-specified in the trial protocol. The study population was limited to males due to the subsequent PET study of human consciousness. As such, comorbidities and accompanying medications that usually are present in clinical anaesthesia were absent. Although limiting the generalizability of the results, the absence of these confounding factors which are usually present in clinical anaesthesia allowed an unhindered depiction of the metabolic response to each of the studied anesthetics/sedatives. Clearly, more pragmatic studies will be needed to assess the clinical impact of the newly discovered properties of these anaesthetics/sedatives. Fourth, the statistical analysis was not separately adjusted for age, BMI, sex, smoking or diet. However, it is worth noting that the subject groups were relatively homogenous as is evident from the inclusion and exclusion criteria e.g. non-smoking ASA I (ASA I refers to healthy, BMI<30) males of 18–30 years of age. This decision was made in agreement with the biostatistician responsible for the statistical analysis. Fifth, both NMR and LC-MS/MS markers may be affected by recent diet. Thus, the study was conducted in fasted subjects removing possible effects of recent meals. Sixth, propofol is administered in a lipid emulsion, which understandably affects the circulating metabolic profile. Lacking a control group for propofol-free lipid emulsion, the effects of propofol cannot be distinguished from those of the formulation. However, as propofol is currently administered exclusively in a lipid emulsion in clinical practise, the combined effects are of clinical interest. Seventh, the TUDCA quantification resulted in a relatively high number of missing values in the sevoflurane group, further research will be needed to verify the observed effect. Sixth, considering the findings of decreased DHET levels in the dexmedetomidine group, the quantification of their biochemically more active precursors, i.e. EETs, would have proven useful.

A few limitiations are to be discussed concerning study III. First, due to the well-established role of TTM in the context of OHCA, a control group without TTM was not a viable possibility. At the time, TTM with a hypothermic target of 33 °C was the mainstay of post-OHCA treatment and as such, there was no control group with normothermic TTM[244,245]. This limits our ability to assess the role of possible thermogenic BCAA metabolism. Second, there were no significant associations between metabolites measured upon hospital admission and 6-month mortality, a finding in contrast with previous research[37]. There may be several factors contributing to this discrepancy. The targeted NMR metabolomics was not focused on TCA cycle metabolites which have been shown to associate with OHCA mortality upon admission. Moreover, the sample size of the current study was smaller (105 *vs.* 163), the number of metabolite variables was higher (155 *vs.* 61) and metabolites were quantified at several timepoints (3 *vs.* 1)[37]. Third, the sample size for the current study had been calculated based on a power analysis of fractional anisotropy values as discussed earlier[115]. Thus, the sample size may have limited our ability to detect differences between the treatment groups.

As overall limitations, studies I-III were restricted to targeted metabolomics, i.e. due to the chosen methodology, the results and interpretations are based on the metabolic pathways covered by the targeted analysis. Moreover, metabolic markers that share metabolic routes are to some extent correlated[254]. Importantly, measurement of the circulating metabolic profile produces a snapshot into the current metabolic state of an organism. Due to the complexity of metabolic compensatory mechanisms, extensive extrapolation of the study results has inherent limitations, and further experiments will be needed to assess the metabolic changes occurring in different clinical scenarios. Furthermore, the current data did not allow us to pinpoint the origin of metabolic processes underlying the current observations, e.g. whether the metabolic changes had occurred in the heart, the CNS or skeletal muscle.

8 Summary/Conclusions

The main results and conclusions according to the aims of the current study are as follows:

1. We demonstrated that dexmedetomidine, propofol, S-ketamine and sevoflurane in equipotent moderate doses (EC_{50} for verbal command) induced acute metabolic changes as measured by targeted NMR and LC-MS/MS metabolic profiles, a previously uncharacterised attribute of these routinely used anaesthetics/sedatives.
2. The metabolic response was unique to each anaesthetic/sedative used. Dexmedetomidine caused a wide-ranging decrease in the levels of both bile acids and oxylipins. The drug's known effects on vagal activity and intestinal motility may contribute to the observed decrease in bile acid concentrations. Similarly, prior research indicates that vagal activity through the CAP appears to contribute to the drug's organoprotective effects in animal models. Whether the observed decrease in oxylipins reflects modulation of the CAP remains an interesting question for future research. S-ketamine decreased circulating BCAAs, a finding of possible interest concerning the antidepressant effects of S-ketamine. The propofol emulsion extensively altered the lipid profile as expected. Especially, the markedly increased concentrations of 9,10- and 12,13-DiHOME warrant further research due to their potential interactions with cellular bioenergetics. In contrast to other anaesthetics/sedatives, sevoflurane showed relative inertness.
3. In OHCA patients, the NMR metabolic profile demonstrated that the concentrations of alanine, lactate, leucine, valine and S-HDL-CE were associated with 6-month mortality. As described, these metabolites are known to be connected to several metabolic processes of potential interest in the context of OHCA and TTM e.g. cellular bioenergetics, thermoregulation and the metabolism of the neurotransmitter glutamate.
4. In the present data, the targeted NMR metabolic profile in OHCA patients did not significantly differ between the xenon and control groups.

Acknowledgements

These studies were carried out during the years 2016–2017 at Turku PET-centre and 2009–2014 in Turku and Helsinki University Hospitals (studies I-II and III, respectively). Both studies were funded by the Academy of Finland. Additionally, studies I-II were funded by The Jane and Aatos Erkko Foundation, Helsinki, Finland. This research has been supported by researcher specific grants from The Finnish Medical Foundation, Helsinki, Finland; The Emil Aaltonen Foundation, Tampere, Finland; The Paulo Foundation, Espoo, Finland; Orion Research Foundation, Espoo, Finland; and Signe and Ane Gyllenberg Foundation, Helsinki, Finland. My thesis work was also supported by the The Finnish Medical Foundation, Eero Matti Raninen Fund, Helsinki; University of Turku Graduate School, University of Turku; and University of Turku and Turku PET centre. Both of these studies were investigator-originated, and the funders had no role in the study.

First, I would like to express my sincere gratitude to the volunteers of studies I-II for their participation in the study of human consciousness, and the study of metabolomics in the context of anaesthesia. Your participation has provided the scientific community with new knowledge in many facets of anaesthesia research. Furthermore, my deepest gratitude goes to the OHCA patients and their next of kin, for their decision to participate in a randomised clinical trial in the wake of a sudden and serious medical emergency. Prior preclinical and clinical studies had demonstrated the safety of inhaled xenon, yet no cardiac arrest patient had previously been exposed to it. Their brave actions made possible the characterisation of neuro- and cardioprotective properties of inhaled xenon in OHCA and offered new knowledge in the context of the metabolomics after OHCA.

As a part of my M.D. degree, I was first interviewed by Anna-Lotta Scheinin and accepted as a trainee to complete my advanced studies in medicine in the “The Neural Mechanisms of Anaesthesia and Human Consciousness”-project. I am thankful to Anna-Lotta for seeing the potential in me as a young M.D. student. Eventually, this interview set me on a demanding, yet extremely rewarding, path towards my PhD. My way forward was aided by my mentor Anu Maksimow, who supervised my advanced studies and during this process introduced me to the principles of science in medicine. Upon my graduation in 2017, I was contacted by

Harry Scheinin, the principal investigator of studies I-II, who encouraged me to pursue a PhD in metabolomics in anaesthesia. Later on, Harry introduced me to Timo Laitio, the principal investigator of study III. I will be forever grateful for this opportunity, and for the responsibility entrusted to me.

During my journey towards the PhD, I have had the privilege to work in two exceptional research groups. The studies were vastly different, the first being a clinical drug trial in healthy subjects whereas the second involved ICU-treated OHCA patients. As a PhD student, I was warmly welcomed in both research groups. I was offered guidance, support and the opportunity to learn from several leading professionals in their respective fields. As an internist, this support and guidance, especially in the context of anaesthesia, was warmly welcomed. Both studies required extraordinary expertise from all of the personnel involved, my warmest gratitude goes to the radiographers in the Turku PET centre, study nurses, nurse anaesthetists, "xenon nurses", ICU staff, and colleagues, who with their precise and unrelenting work turned these intricately planned studies into reality.

I want to extend my gratitude to all the co-authors and collaborators. Your tireless and meticulous work on metabolite quantification, ongoing support during the revision processes and expertise in metabolomics and clinical pharmacology have been of immense value. I want to thank Mikko Neuvonen for his work in oxylipin and bile acid quantification with LC-MS/MS and Harri Koskela and Viljami Aittomäki who worked at Nightingale Health at the time of NMR metabolite analysis. Furthermore, I want to extend my gratitude to Anni Joensuu, who helped with the early statistical analysis of the xenon data, sparked my enthusiasm towards R and taught me the basics. I want to thank our collaborators Markus Perola and Mikko Niemi who have kindly offered their expertise on metabolomics and clinical pharmacology.

I am grateful to our professional statistician MSc Tero Vahlberg from the Department of Biostatics, University of Turku, whose vital contribution to this thesis is warmly acknowledged. Your expertise has been of the utmost importance.

I express my deepest gratitude to my mentors and thesis supervisors, Associate Professor Harry Scheinin and Professor Timo Laitio. Harry and Timo, your ungoing support during the PhD process has been irreplacable. Harry, your warm and welcoming personality, pedagogic approach to medical research and leadership skills have been something to look up to. Timo, you too lead by example, as exemplified by the late evening you helped me gather data from the case report forms for the latest revision. I have always been able to rely on your boundless expertise on xenon and clinical research. Both of you possess an extraordinary ability to manage complex research projects, leading them efficiently while creating a positive and inspiring atmosphere for your students and co-workers. Timo and Harry, you have always found the time to answer my questions and, when needed, the time to

sit down in a meeting and discuss the best course of action. Your honest feedback and continued encouragement to proceed forward have been of the utmost value and shaped me to be the researcher I am today. It has been a pleasure working with you.

I am extremely privileged to have such unwavering support from my family. My mother Susan and my father Jarmo, you have created for me a solid foundation on which to build my future. My brother Elias with whom we have tirelessly pondered the philosophy of existence and consciousness on our hikes and travels. My sister Mandi, who has always cheered me up with her phone calls and offered her help as a babysitter for my firstborn. I want to thank my grandfather Jussi who told me once, that no time will ever be wasted reading a book. My grandmother Lea, who has always showed interest in my scientific aspirations. And my grandmother Paula and great aunt Ruut, who with their never-ending care for their loved ones taught me many valuable lessons in life. Thank you, uncle Juha, for sparking my interest in science. And thank you, Kimmo, for always being there for us when we needed your help.

Lastly, to my beloved wife Marika, who has tirelessly supported me throughout this process. The laughs and adventures we have shared, the beautiful places we have witnessed, and most importantly, the home we have built together has brought me boundless happiness. I am grateful that I will have you beside me on our next adventure, the adventure of a lifetime: This work is dedicated to our firstborn Eino.

16.5.2025

Aleksi Nummela

References

1. Pray L. Discovery of DNA Double Helix: Watson and Crick | Learn Science at Scitable. *Nat Educ*. 2008;1(1):100.
2. Würtz P, Tiainen M, Mak̈inen VP, et al. Circulating metabolite predictors of glycemia in middle-aged men and women. *Diabetes Care*. 2012;35(8):1749-1756. doi:10.2337/dc11-1838
3. Fischer K, Kettunen J, Würtz P, et al. Biomarker Profiling by Nuclear Magnetic Resonance Spectroscopy for the Prediction of All-Cause Mortality: An Observational Study of 17,345 Persons. Minelli C, ed. *PLoS Med*. 2014;11(2):e1001606. doi:10.1371/journal.pmed.1001606
4. Jaurila H, Koivukangas V, Koskela M, et al. 1H NMR based metabolomics in human sepsis and healthy serum. *Metabolites*. 2020;10(2):70. doi:10.3390/metabo10020070
5. Han X, Rozen S, Boyle SH, et al. Metabolomics in Early Alzheimer's Disease: Identification of Altered Plasma Sphingolipidome Using Shotgun Lipidomics. Wang Y, ed. *PLoS ONE*. 2011;6(7):e21643. doi:10.1371/journal.pone.0021643
6. Guo L, Milburn MV, Ryals JA, et al. Plasma metabolomic profiles enhance precision medicine for volunteers of normal health. *Proc Natl Acad Sci*. 2015;112(35):E4901-E4910. doi:10.1073/pnas.1508425112
7. Ritchie SC, Würtz P, Nath AP, et al. The Biomarker GlycA is Associated with Chronic Inflammation and Predicts Long-Term Risk of Severe Infection. *Cell Syst*. 2015;1(4):293-301. doi:10.1016/j.cels.2015.09.007
8. Tynkkynen J, Chouraki V, van der Lee SJ, et al. Association of branched-chain amino acids and other circulating metabolites with risk of incident dementia and Alzheimer's disease: A prospective study in eight cohorts. *Alzheimers Dement J Alzheimers Assoc*. 2018;14(6):723-733. doi:10.1016/j.jalz.2018.01.003
9. Würtz P, Raiko JR, Magnussen CG, et al. High-throughput quantification of circulating metabolites improves prediction of subclinical atherosclerosis. *Eur Heart J*. 2012;33(18):2307-2316. doi:10.1093/eurheartj/ehs020
10. Guo Y, Li Y, Zhang Y, et al. Postoperative Delirium Development Associated with Metabolic Alterations Following Hemi-Arthroplasty in Elderly. *unpublished*. Published online September 19, 2018. Accessed February 18, 2019. https://papers.ssrn.com/sol3/papers.cfm?abstract_id=3252687
11. Holmes MV, Millwood IY, Kartsonaki C, et al. Lipids, Lipoproteins, and Metabolites and Risk of Myocardial Infarction and Stroke. *J Am Coll Cardiol*. 2018;71(6):620-632. doi:10.1016/j.jacc.2017.12.006
12. Shah SH, Kraus WE, Newgard CB. Metabolomic Profiling for the Identification of Novel Biomarkers and Mechanisms Related to Common Cardiovascular Diseases. *Circulation*. 2012;126(9):1110-1120. doi:10.1161/CIRCULATIONAHA.111.060368
13. Serkova NJ, Standiford TJ, Stringer KA. The Emerging Field of Quantitative Blood Metabolomics for Biomarker Discovery in Critical Illnesses. *Am J Respir Crit Care Med*. 2011;184(6):647-655. doi:10.1164/rccm.201103-0474CI

14. Würtz P, Havulinna AS, Soininen P, et al. Metabolite profiling and cardiovascular event risk: A prospective study of 3 population-based cohorts. *Circulation*. 2015;131(9):774-785. doi:10.1161/CIRCULATIONAHA.114.013116
15. Widmer M, Thommen EB, Becker C, et al. Association of acyl carnitines and mortality in out-of-hospital-cardiac-arrest patients: Results of a prospective observational study. *J Crit Care*. 2020;58:20-26. doi:10.1016/j.jcrc.2020.03.009
16. Welsh P, Rankin N, Li Q, et al. Circulating amino acids and the risk of macrovascular, microvascular and mortality outcomes in individuals with type 2 diabetes: results from the ADVANCE trial. *Diabetologia*. 2018;61(7):1581-1591. doi:10.1007/s00125-018-4619-x
17. Parent BA, Seaton M, Sood RF, et al. Use of metabolomics to trend recovery and therapy after injury in critically ill trauma patients. *JAMA Surg*. 2016;151(7):e160853. doi:10.1001/jamasurg.2016.0853
18. Varvarousis D, Xanthos T, Ferino G, et al. Metabolomics profiling reveals different patterns in an animal model of asphyxial and dysrhythmic cardiac arrest. *Sci Rep*. 2017;7(1):16575. doi:10.1038/s41598-017-16857-6
19. Bajaj JS, Garcia-Tsao G, Reddy KR, et al. Admission Urinary and Serum Metabolites Predict Renal Outcomes in Hospitalized Patients With Cirrhosis. *Hepatology*. 2021;74(5):2699-2713. doi:10.1002/hep.31907
20. Kimberly WT, Wang Y, Pham L, Furie KL, Gerszten RE. Metabolite Profiling Identifies a Branched Chain Amino Acid Signature in Acute Cardioembolic Stroke. *Stroke*. 2013;44(5):1389-1395. doi:10.1161/STROKEAHA.111.000397
21. Du X, You H, Li Y, et al. Relationships between circulating branched chain amino acid concentrations and risk of adverse cardiovascular events in patients with STEMI treated with PCI. *Sci Rep*. 2018;8(1):1-8. doi:10.1038/s41598-018-34245-6
22. Kofink D, Eppinga RN, Gilst WHV, et al. Statin Effects on Metabolic Profiles: Data from the PREVEND IT (Prevention of Renal and Vascular End-stage Disease Intervention Trial). *Circ Cardiovasc Genet*. 2017;10(6). doi:10.1161/CIRCGENETICS.117.001759
23. Dinis-Oliveira RJ. Metabolism and metabolomics of ketamine: a toxicological approach. *Forensic Sci Res*. 2017;2(1):2-10. doi:10.1080/20961790.2017.1285219
24. Sliz E, Kettunen J, Holmes MV, et al. Metabolomic Consequences of Genetic Inhibition of PCSK9 Compared with Statin Treatment. *Circulation*. 2018;138(22):2499-2512. doi:10.1161/CIRCULATIONAHA.118.034942
25. Wang C, Liu F, Frisch-Daiello JL, et al. Lipidomics reveals a systemic energy deficient state that precedes neurotoxicity in neonatal monkeys after sevoflurane exposure. *Analytica Chimica Acta*. December 11, 2018:87-96.
26. Wang Q, Würtz P, Auro K, et al. Effects of hormonal contraception on systemic metabolism: Cross-sectional and longitudinal evidence. *Int J Epidemiol*. 2016;45(5):1445-1457. doi:10.1093/ije/dyw147
27. Beger RD, Sun J, Schnackenberg LK. Metabolomics approaches for discovering biomarkers of drug-induced hepatotoxicity and nephrotoxicity. *Toxicol Appl Pharmacol*. 2010;243(2):154-166. doi:10.1016/j.taap.2009.11.019
28. Ghini V, Unger FT, Tenori L, Turano P, Juhl H, David KA. Metabolomics profiling of pre-and post-anesthesia plasma samples of colorectal patients obtained via Ficoll separation. *Metabolomics*. 2015;11(6):1769-1778. doi:10.1007/s11306-015-0832-5
29. Jiang J, Li S, Wang Y, et al. Potential neurotoxicity of prenatal exposure to sevoflurane on offspring: Metabolomics investigation on neurodevelopment and underlying mechanism. *Int J Dev Neurosci*. 2017;62:46-53. doi:10.1016/j.ijdevneu.2017.08.001
30. Kaddurah-Daouk R, Bogdanov MB, Wikoff WR, et al. Pharmacometabolomic mapping of early biochemical changes induced by sertraline and placebo. *Transl Psychiatry*. 2013;3(1):e223-e223. doi:10.1038/tp.2012.142

31. Würtz P, Wang Q, Soininen P, et al. Metabolomic Profiling of Statin Use and Genetic Inhibition of HMG-CoA Reductase. *J Am Coll Cardiol*. 2016;67(10):1200-1210. doi:10.1016/j.jacc.2015.12.060
32. Villaseñor A, Ramamoorthy A, Silva Dos Santos M, et al. A pilot study of plasma metabolomic patterns from patients treated with ketamine for bipolar depression: Evidence for a response-related difference in mitochondrial networks. *Br J Pharmacol*. 2014;171(8):2230-2242. doi:10.1111/bph.12494
33. Kaddurah-Daouk R, Weinshilboum R. Metabolomic signatures for drug response phenotypes: Pharmacometabolomics enables precision medicine. *Clin Pharmacol Ther*. 2015;98(1):71-75. doi:10.1002/cpt.134
34. Weckmann K, Deery MJ, Howard JA, et al. Ketamine's antidepressant effect is mediated by energy metabolism and antioxidant defense system. *Sci Rep*. 2017;7(1). doi:10.1038/s41598-017-16183-x
35. Kudenchuk PJ, Sandroni C, Drinhaus HR, et al. Breakthrough in cardiac arrest: reports from the 4th Paris International Conference. *Ann Intensive Care*. 2015;5:22. doi:10.1186/s13613-015-0064-x
36. Nolan JP, Sandroni C, Böttiger BW, et al. European Resuscitation Council and European Society of Intensive Care Medicine Guidelines 2021: Post-resuscitation care. *Resuscitation*. 2021;161:220-269. doi:10.1016/j.resuscitation.2021.02.012
37. Paulin Beske R, Henriksen HH, Obling L, et al. Targeted plasma metabolomics in resuscitated comatose out-of-hospital cardiac arrest patients. *Resuscitation*. 2022;179:163-171. doi:10.1016/j.resuscitation.2022.06.010
38. Beske RP, Obling LER, Bro-Jeppesen J, et al. The Effect of Targeted Temperature Management on the Metabolome Following Out-of-Hospital Cardiac Arrest. *Ther Hypothermia Temp Manag*. 2023;13(4):208-215. doi:10.1089/ther.2022.0065
39. Rankin NJ, Preiss D, Welsh P, Sattar N. Applying metabolomics to cardiometabolic intervention studies and trials: past experiences and a roadmap for the future: Table 1. *Int J Epidemiol*. 2016;45(5):1351-1371. doi:10.1093/ije/dyw271
40. Eppinga RN, Kofink D, Dullaart RPF, et al. Effect of Metformin on Metabolites and Relation with Myocardial Infarct Size and Left Ventricular Ejection Fraction after Myocardial Infarction. *Circ Cardiovasc Genet*. 2017;10(1):e001564. doi:10.1161/CIRCGENETICS.116.001564
41. Mattes WB, Kamp HG, Fabian E, et al. Prediction of Clinically Relevant Safety Signals of Nephrotoxicity through Plasma Metabolite Profiling. *BioMed Res Int*. 2013;2013:1-12. doi:10.1155/2013/202497
42. Devaud JC, Berger MM, Pannatier A, et al. Hypertriglyceridemia: A potential side effect of propofol sedation in critical illness. *Intensive Care Med*. 2012;38(12):1990-1998. doi:10.1007/s00134-012-2688-8
43. Krajčová A, Waldauf P, Anděl M, Duška F. Propofol infusion syndrome: a structured review of experimental studies and 153 published case reports. *Crit Care*. 2015;19(1):398. doi:10.1186/s13054-015-1112-5
44. Krajčová A, Løvsletten NG, Waldauf P, et al. Effects of Propofol on Cellular Bioenergetics in Human Skeletal Muscle Cells. *Crit Care Med*. 2017;46(3):1. doi:10.1097/CCM.0000000000002875
45. Grabner GF, Xie H, Schweiger M, Zechner R. Lipolysis: cellular mechanisms for lipid mobilization from fat stores. *Nat Metab*. 2021;3(11):1445-1465. doi:10.1038/s42255-021-00493-6
46. Langin D. Adipose tissue lipolysis as a metabolic pathway to define pharmacological strategies against obesity and the metabolic syndrome. *Pharmacol Res*. 2006;53(6):482-491. doi:10.1016/j.phrs.2006.03.009

47. Houston MC, Burger C, Hays JT, et al. The effects of clonidine hydrochloride versus atenolol monotherapy on serum lipids, lipid subfractions, and apolipoproteins in mild hypertension. *Am Heart J*. 1990;120(1):172-179. doi:10.1016/0002-8703(90)90175-W
48. Baraka A, Harrison T, Kachachi T. Catecholamine levels after ketamine anesthesia in man. *Anesth Analg*. 1973;52(2):198-200.
49. Weerink MAS, Struys MMRF, Hannivoort LN, Barends CRM, Absalom AR, Colin P. Clinical pharmacokinetics and pharmacodynamics of dexmedetomidine. *Clin Pharmacokinet*. 2017;56(8):893-913. doi:10.1007/s40262-017-0507-7
50. S. Rosenson R. Myocardial injury: The acute phase response and lipoprotein metabolism. *J Am Coll Cardiol*. 1993;22(3):933-940. doi:10.1016/0735-1097(93)90213-K
51. Luo J, Yang H, Song BL. Mechanisms and regulation of cholesterol homeostasis. *Nat Rev Mol Cell Biol*. 2020;21(4):225-245. doi:10.1038/s41580-019-0190-7
52. Altmann SW, Davis HR, Zhu LJ, et al. Niemann-Pick C1 Like 1 Protein Is Critical for Intestinal Cholesterol Absorption. *Science*. 2004;303(5661):1201-1204. doi:10.1126/science.1093131
53. Anurag M, Shapiro MD. Apolipoproteins in vascular biology and atherosclerotic disease. *Nat Rev Cardiol*. 2022;19(3):168-179. doi:10.1038/s41569-021-00613-5
54. Gotto AM. *Interrelationship of Triglycerides with Lipoproteins and High-Density Lipoproteins*. Vol 66.
55. Goldstein JL, Brown MS. The LDL receptor. *Arterioscler Thromb Vasc Biol*. 2009;29(4):431-438. doi:10.1161/ATVBAHA.108.179564
56. Chang TY, Li BL, Chang CCY, Urano Y. Acyl-coenzyme A:cholesterol acyltransferases. *Am J Physiol - Endocrinol Metab*. 2009;297(1). doi:10.1152/ajpendo.90926.2008
57. Phillips MC. Molecular Mechanisms of Cellular Cholesterol Efflux. *J Biol Chem*. 2014;289(35):24020. doi:10.1074/jbc.R114.583658
58. Ouimet M, Barrett TJ, Fisher EA. HDL and Reverse Cholesterol Transport. *Circ Res*. 2019;124(10):1505-1518. doi:10.1161/CIRCRESAHA.119.312617
59. Barter PJ, Brewer HB, Chapman MJ, Hennekens CH, Rader DJ, Tall AR. Cholesteryl ester transfer protein: A novel target for raising HDL and inhibiting atherosclerosis. *Arterioscler Thromb Vasc Biol*. 2003;23(2):160-167. doi:10.1161/01.ATV.0000054658.91146.64
60. Alves-Bezerra M, Cohen DE. Triglyceride metabolism in the liver. *Compr Physiol*. 2017;8(1):1. doi:10.1002/cphy.c170012
61. Sim KG, Hammond J, Wilcken B. Strategies for the diagnosis of mitochondrial fatty acid β-oxidation disorders. *Clin Chim Acta*. 2002;323(1-2):37-58. doi:10.1016/S0009-8981(02)00182-1
62. Schug ZT, Vande Voorde J, Gottlieb E. The metabolic fate of acetate in cancer. *Nat Rev Cancer*. 2016;16(11):708-717. doi:10.1038/nrc.2016.87
63. Puchalska P, Crawford PA. Multi-dimensional Roles of Ketone Bodies in Fuel Metabolism, Signaling, and Therapeutics. *Cell Metab*. 2017;25(2):262-284. doi:10.1016/j.cmet.2016.12.022
64. Dyall SC, Balas L, Bazan NG, et al. Polyunsaturated fatty acids and fatty acid-derived lipid mediators: Recent advances in the understanding of their biosynthesis, structures, and functions. *Prog Lipid Res*. 2022;86:101165. doi:10.1016/j.plipres.2022.101165
65. O'Donnell VB, Rossjohn J, Wakelam MJO. Phospholipid signaling in innate immune cells. *J Clin Invest*. 2018;128(7):2670-2679. doi:10.1172/JCI97944
66. Quinville BM, Deschenes NM, Ryckman AE, Walia JS. A Comprehensive Review: Sphingolipid Metabolism and Implications of Disruption in Sphingolipid Homeostasis. *Int J Mol Sci*. 2021;22(11):5793. doi:10.3390/ijms22115793
67. Hannun YA, Obeid LM. Sphingolipids and their metabolism in physiology and disease. *Nat Rev Mol Cell Biol*. 2018;19(3):175-191. doi:10.1038/nrm.2017.107
68. Ackerman RS, Luddy KA, Icard BE, Piñeiro Fernández J, Gatenby RA, Muncey AR. The Effects of Anesthetics and Perioperative Medications on Immune Function: A Narrative Review. *Anesth Analg*. 2021;133(3):676-689. doi:10.1213/ANE.0000000000005607

69. Ueki M, Kawasaki T, Habe K, Hamada K, Kawasaki C, Sata T. The effects of dexmedetomidine on inflammatory mediators after cardiopulmonary bypass. *Anaesthesia*. 2014;69(7):693-700. doi:10.1111/anae.12636
70. Bao N, Tang B. Organ-Protective Effects and the Underlying Mechanism of Dexmedetomidine. *Mediators Inflamm*. 2020;2020:1-11. doi:10.1155/2020/6136105
71. Yang YF, Peng K, Liu H, Meng XW, Zhang JJ, Ji FH. Dexmedetomidine preconditioning for myocardial protection in ischaemia-reperfusion injury in rats by downregulation of the high mobility group box 1-toll-like receptor 4-nuclear factor κB signalling pathway. *Clin Exp Pharmacol Physiol*. 2017;44(3):353-361. doi:10.1111/1440-1681.12711
72. Zhang H, Sha J, Feng X, et al. Dexmedetomidine ameliorates LPS induced acute lung injury via GSK-3β/STAT3-NF-κB signaling pathway in rats. *Int Immunopharmacol*. 2019;74. doi:10.1016/j.intimp.2019.105717
73. Ma J, Chen Q, Li J, et al. Dexmedetomidine-mediated prevention of renal ischemia-reperfusion injury depends in part on cholinergic anti-inflammatory mechanisms. *Anesth Analg*. 2020;130(4):1054-1062. doi:10.1213/ANE.0000000000003820
74. Jin YH, Li ZT, Chen H, Jiang XQ, Zhang YY, Wu F. Effect of dexmedetomidine on kidney injury in sepsis rats through TLR4/MyD88/ NF-κB/iNOS signaling pathway. *Eur Rev Med Pharmacol Sci*. 2019;23(11):5020-5025. doi:10.26355/eurrev_201906_18094
75. Wang ZX, Huang CY, Hua YP, Huang WQ, Deng LH, Liu KX. Dexmedetomidine reduces intestinal and hepatic injury after hepatectomy with inflow occlusion under general anaesthesia: A randomized controlled trial. *Br J Anaesth*. 2014;112(6):1055-1064. doi:10.1093/bja/aeu132
76. Visvabharathy L, Xayarath B, Weinberg G, Shilling RA, Freitag NE. Propofol increases host susceptibility to microbial infection by reducing subpopulations of mature immune effector cells at sites of infection. *PLoS ONE*. 2015;10(9). doi:10.1371/journal.pone.0138043
77. Yang B, Fung A, Pac-Soo C, Ma D. Vascular surgery-related organ injury and protective strategies: Update and future prospects. *Br J Anaesth*. 2016;117:ii32-ii43. doi:10.1093/bja/aew211
78. Urban T, Waldauf P, Krajčová A, et al. Kinetic characteristics of propofol-induced inhibition of electron-transfer chain and fatty acid oxidation in human and rodent skeletal and cardiac muscles. *PLOS ONE*. 2019;14(10):e0217254. doi:10.1371/journal.pone.0217254
79. Gabbs M, Shan Leng, Devassy JG, Monirujjaman M, Aukema HM. Advances in our understanding of oxylipins derived from dietary PUFAs. *Adv Nutr*. 2015;6(5):513-540. doi:10.3945/an.114.007732
80. Murakami M, Sato H, Taketomi Y. Updating phospholipase a2 biology. *Biomolecules*. 2020;10(10):1-33. doi:10.3390/biom10101457
81. Shearer GC, Walker RE. An overview of the biologic effects of omega-6 oxylipins in humans. *Prostaglandins Leukot Essent Fatty Acids*. 2018;137:26-38. doi:10.1016/j.plefa.2018.06.005
82. Hildreth K, Kodani SD, Hammock BD, Zhao L. Cytochrome P450-derived linoleic acid metabolites EpOMEs and DiHOMEs: A review of recent studies. *J Nutr Biochem*. 2020;86:108484. doi:10.1016/j.jnutbio.2020.108484
83. Ghimire LV, Muszkat M, Sofowora GG, et al. Variation in the α2A adrenoceptor gene and the effect of dexmedetomidine on plasma insulin and glucose. *Pharmacogenet Genomics*. 2013;23(9):479-486. doi:10.1097/FPC.0b013e3283642f93
84. Donnino MW, Miller J, Goyal N, et al. Effective lactate clearance is associated with improved outcome in post-cardiac arrest patients. *Resuscitation*. 2007;75(2):229-234. doi:10.1016/j.resuscitation.2007.03.021
85. Laurikkala J, Skrifvars MB, Bäcklund M, et al. Early Lactate Values after Out-of-Hospital Cardiac Arrest: Associations with One-Year Outcome. *Shock*. 2019;51(2):168-173. doi:10.1097/SHK.0000000000001145
86. Patil N, Howe O, Cahill P, Byrne HJ. Monitoring and modelling the dynamics of the cellular glycolysis pathway: A review and future perspectives. *Mol Metab*. 2022;66:101635. doi:10.1016/j.molmet.2022.101635

87. Gray LR, Tompkins SC, Taylor EB. Regulation of pyruvate metabolism and human disease. *Cell Mol Life Sci CMLS*. 2013;71(14):2577. doi:10.1007/s00018-013-1539-2
88. Liemburg-Apers DC, Imamura H, Forkink M, et al. Quantitative Glucose and ATP Sensing in Mammalian Cells. *Pharm Res*. 2011;28(11):2745-2757. doi:10.1007/s11095-011-0492-8
89. Rotroff DM, Corum DG, Motsinger-Reif A, et al. Metabolomic signatures of drug response phenotypes for ketamine and esketamine in subjects with refractory major depressive disorder: new mechanistic insights for rapid acting antidepressants. *Transl Psychiatry*. 2016;6(9):e894. doi:10.1038/tp.2016.145
90. Bifari F, Nisoli E. Branched-chain amino acids differently modulate catabolic and anabolic states in mammals: a pharmacological point of view. *Br J Pharmacol*. 2017;174(11):1366-1377. doi:10.1111/bph.13624
91. Holeček M. The BCAA–BCKA cycle: its relation to alanine and glutamine synthesis and protein balance. *Nutrition*. 2001;17(1):70. doi:10.1016/S0899-9007(00)00483-4
92. Fernstrom JD. Aromatic amino acids and monoamine synthesis in the central nervous system: influence of the diet. *J Nutr Biochem*. 1990;1(10):508-517. doi:10.1016/0955-2863(90)90033-H
93. Neinast MD, Jang C, Hui S, et al. Quantitative Analysis of the Whole-Body Metabolic Fate of Branched-Chain Amino Acids. *Cell Metab*. 2019;29(2):417-429.e4. doi:10.1016/j.cmet.2018.10.013
94. Fernstrom JD. Branched-Chain Amino Acids and Brain Function. *J Nutr*. 2005;135(6):1539S-1546S. doi:10.1093/jn/135.6.1539S
95. Bak LK, Johansen ML, Schousboe A, Waagepetersen HS. Among the branched-chain amino acids, only valine metabolism is up-regulated in astrocytes during glutamate exposure. In: *Journal of Neuroscience Research*. Vol 85. J Neurosci Res; 2007:3465-3470. doi:10.1002/jnr.21347
96. García-Espinosa MA, Wallin R, Hutson SM, Sweatt AJ. Widespread neuronal expression of branched-chain aminotransferase in the CNS: Implications for leucine/glutamate metabolism and for signaling by amino acids. *J Neurochem*. 2007;100(6):1458-1468. doi:10.1111/j.1471-4159.2006.04332.x
97. Hull J, Hindy ME, Kehoe PG, Chalmers K, Love S, Conway ME. Distribution of the branched chain aminotransferase proteins in the human brain and their role in glutamate regulation. *J Neurochem*. 2012;123(6):997-1009. doi:10.1111/jnc.12044
98. Adrie C, Cariou A, Mourvillier B, et al. Predicting survival with good neurological recovery at hospital admission after successful resuscitation of out-of-hospital cardiac arrest: the OHCA score. *Eur Heart J*. 2006;27(23):2840-2845. doi:10.1093/eurheartj/ehl335
99. Matsuyama T, Iwami T, Yamada T, et al. Effect of Serum Albumin Concentration on Neurological Outcome After Out-of-Hospital Cardiac Arrest (from the CRITICAL [Comprehensive Registry of Intensive Cares for OHCA Survival] Study in Osaka, Japan). *Am J Cardiol*. 2018;121(2):156-161. doi:10.1016/j.amjcard.2017.10.005
100. Mongardon N, Dumas F, Ricome S, et al. Postcardiac arrest syndrome: from immediate resuscitation to long-term outcome. *Ann Intensive Care*. 2011;1(1):45. doi:10.1186/2110-5820-1-45
101. Wyss M, Kaddurah-Daouk R. Creatine and Creatinine Metabolism. *Physiol Rev*. 2000;80(3):1107-1213. doi:10.1152/physrev.2000.80.3.1107
102. Otvos JD, Shalaurova I, Wolak-Dinsmore J, et al. GlycA: A composite nuclear magnetic resonance biomarker of systemic inflammation. *Clin Chem*. 2015;61(5):714-723. doi:10.1373/clinchem.2014.232918
103. Ala-Korpela M. Serum nuclear magnetic resonance spectroscopy: One more step toward clinical utility. *Clin Chem*. 2015;61(5):681-683. doi:10.1373/clinchem.2015.238279
104. Iirola T, Vilo S, Aantaa R, et al. Dexmedetomidine inhibits gastric emptying and oro-caecal transit in healthy volunteers. *Br J Anaesth*. 2011;106(4):522-527. doi:10.1093/bja/aer004

105. Li Y, Wu B, Hu C, et al. The role of the vagus nerve on dexmedetomidine promoting survival and lung protection in a sepsis model in rats. *Eur J Pharmacol*. 2022;914. doi:10.1016/j.ejphar.2021.174668
106. Russell DW. The enzymes, regulation, and genetics of bile acid synthesis. *Annu Rev Biochem*. 2003;72:137-174. doi:10.1146/annurev.biochem.72.121801.161712
107. Fiorucci S, Biagioli M, Zampella A, Distrutti E. Bile acids activated receptors regulate innate immunity. *Front Immunol*. 2018;9(AUG):1853. doi:10.3389/fimmu.2018.01853
108. Khurana S, Raufman JP, Pallone TL. Bile Acids Regulate Cardiovascular Function. *Clin Transl Sci*. 2011;4(3):210-218. doi:10.1111/j.1752-8062.2011.00272.x
109. Chiang JYL. Regulation of bile acid synthesis: Pathways, nuclear receptors, and mechanisms. *J Hepatol*. 2004;40(3):539-551. doi:10.1016/j.jhep.2003.11.006
110. Mertens KL, Kalsbeek A, Soeters MR, Eggink HM. Bile acid signaling pathways from the enterohepatic circulation to the central nervous system. *Front Neurosci*. 2017;11(NOV). doi:10.3389/fnins.2017.00617
111. Ackerman HD, Gerhard GS. Bile acids in neurodegenerative disorders. *Front Aging Neurosci*. 2016;8:263. doi:10.3389/fnagi.2016.00263
112. Hemmings HC, Riegelhaupt PM, Kelz MB, et al. Towards a Comprehensive Understanding of Anesthetic Mechanisms of Action: A Decade of Discovery. *Trends Pharmacol Sci*. 2019;40(7):464-481. doi:10.1016/j.tips.2019.05.001
113. Scheinin A, Kantonen O, Alkire M, et al. Foundations of Human Consciousness: Imaging the Twilight Zone. *J Neurosci*. 2021;41(8):1769-1778. doi:10.1523/JNEUROSCI.0775-20.2020
114. Arola O, Saraste A, Laitio R, et al. Inhaled Xenon Attenuates Myocardial Damage in Comatose Survivors of Out-of-Hospital Cardiac Arrest. *J Am Coll Cardiol*. 2017;70(21):2652-2660. doi:10.1016/j.jacc.2017.09.1088
115. Laitio R, Hynninen M, Arola O, et al. Effect of inhaled xenon on cerebral white matter damage in comatose survivors of out-of-hospital cardiac arrest: A randomized clinical trial. *JAMA - J Am Med Assoc*. 2016;315(11):1120-1128. doi:10.1001/jama.2016.1933
116. Preckel B, Weber NC, Sanders RD, Maze M, Schlack W. Molecular mechanisms transducing the anesthetic, analgesic, and organ-protective actions of xenon. *Anesthesiology*. 2006;105(1):187-197. doi:10.1097/00000542-200607000-00029
117. Baker MT, Naguib M. Propofol: The challenges of formulation. *Anesthesiology*. 2005;103(4):860-876. doi:10.1097/00000542-200510000-00026
118. Trapani G, Altomare C, Sanna E, Biggio G, Liso G. *Medicinal Chemistry Feature Molecule Propofol in Anesthesia. Mechanism of Action, Structure-Activity Relationships, and Drug Delivery*. Vol 7.; 2000:249-271.
119. Sahinovic MM, Struys MMRF, Absalom AR. Clinical Pharmacokinetics and Pharmacodynamics of Propofol. *Clin Pharmacokinet*. 2018;57(12):1539-1558. doi:10.1007/s40262-018-0672-3
120. Hiraoka H, Yamamoto K, Miyoshi S, et al. Kidneys contribute to the extrahepatic clearance of propofol in humans, but not lungs and brain. *Br J Clin Pharmacol*. 2005;60(2):176-182. doi:10.1111/j.1365-2125.2005.02393.x
121. Peltoniemi MA, Hagelberg NM, Olkkola KT, Saari TI. Ketamine: A Review of Clinical Pharmacokinetics and Pharmacodynamics in Anesthesia and Pain Therapy. *Clin Pharmacokinet*. 2016;55(9):1059-1077. doi:10.1007/s40262-016-0383-6
122. Kohrs R, Durieux ME. Ketamine: Teaching an Old Drug New Tricks. *Anesth Analg*. 1998;87(5):1186-1193. doi:10.1213/00000539-199811000-00039
123. Takki S, Nikki P, Jäättelä A, Tammisto T. Ketamine and plasma catecholamines. *Br J Anaesth*. 1972;44(12):1318-1322. doi:10.1093/bja/44.12.1318
124. Zanos P, Moaddel R, Morris PJ, et al. Ketamine and Ketamine Metabolite Pharmacology: Insights into Therapeutic Mechanisms. *Pharmacol Rev*. 2018;70(3):621-660. doi:10.1124/pr.117.015198
125. Palanca BJA, Avidan MS, Mashour GA. Human neural correlates of sevoflurane-induced unconsciousness. *Br J Anaesth*. 2017;119(4):573-582. doi:10.1093/bja/aex244

126. Kharasch ED, Karol MD, Lanni C, Sawchuk R. Clinical Sevoflurane Metabolism and Disposition: I. Sevoflurane and Metabolite Pharmacokinetics. *Anesthesiology*. 1995;82(6):1369. doi:10.1097/00000542-199506000-00008
127. Mervyn M, Timo L. Neuroprotective Properties of Xenon. *Mol Neurobiol*. 2020;57(1):118-124. doi:10.1007/s12035-019-01761-z
128. Behnke AR, Yarbrough OD. Respiratory resistance, oil-water solubility, and mental effects of argon, compared with helium and nitrogen. *Am J Physiol-Leg Content*. 1939;126(2):409-415. doi:10.1152/ajplegacy.1939.126.2.409
129. Cullen SC, Gross EG. The anesthetic properties of xenon in animals and human beings, with additional observations on krypton. *Science*. 1951;113(2942):580-582. doi:10.1126/science.113.2942.580
130. Dickinson R, Peterson BK, Banks P, et al. Competitive Inhibition at the Glycine Site of the N -Methyl-d-aspartate Receptor by the Anesthetics Xenon and Isoflurane: Evidence from Molecular Modeling and Electrophysiology. *Anesthesiology*. 2007;107(5):756-767. doi:10.1097/01.anes.0000287061.77674.71
131. Banks P, Franks NP, Dickinson R. Competitive Inhibition at the Glycine Site of the N -Methyl-d-Aspartate Receptor Mediates Xenon Neuroprotection against Hypoxia–Ischemia. *Anesthesiology*. 2010;112(3):614. doi:10.1097/ALN.0b013e3181cea398
132. Dinse A, Fo¨hr KJ, Georgieff M, Beyer C, Bulling A, Weigt HU. Xenon reduces glutamate-, AMPA-, and kainate-induced membrane currents in cortical neurones. *Br J Anaesth*. 2005;94(4):479-485. doi:10.1093/bja/aei080
133. Gruss M, Bushell TJ, Bright DP, Lieb WR, Mathie A, Franks NP. Two-pore-domain K+ channels are a novel target for the anesthetic gases xenon, nitrous oxide, and cyclopropane. *Mol Pharmacol*. 2004;65(2):443-452. doi:10.1124/mol.65.2.443
134. Bantel C, Maze M, Trapp S. Noble Gas Xenon Is a Novel Adenosine Triphosphate-sensitive Potassium Channel Opener. *Anesthesiology*. 2010;112(3):623. doi:10.1097/ALN.0b013e3181cf894a
135. Wilhelm S, Ma D, Maze M, Franks NP. Effects of Xenon on In Vitro and In Vivo Models of Neuronal Injury. *Anesthesiology*. 2002;96(6):1485. doi:10.1097/00000542-200206000-00031
136. Ma D, Hossain M, Chow A, et al. Xenon and hypothermia combine to provide neuroprotection from neonatal asphyxia. *Ann Neurol*. 2005;58(2):182-193. doi:10.1002/ana.20547
137. Homi HM, Yokoo N, Ma D, et al. The Neuroprotective Effect of Xenon Administration during Transient Middle Cerebral Artery Occlusion in Mice. *Anesthesiology*. 2003;99(4):876. doi:10.1097/00000542-200310000-00020
138. Dingley J, Tooley J, Porter H, Thoresen M. Xenon Provides Short-Term Neuroprotection in Neonatal Rats When Administered After Hypoxia-Ischemia. *Stroke*. 2006;37(2):501-506. doi:10.1161/01.STR.0000198867.31134.ac
139. David HN, Haelewyn B, Risso JJ, Colloc'h N, Abraini JH. Xenon is an Inhibitor of Tissue-Plasminogen Activator: Adverse and Beneficial Effects in a Rat Model of Thromboembolic Stroke. *J Cereb Blood Flow Metab*. 2010;30(4):718-728. doi:10.1038/jcbfm.2009.275
140. David HN, Leveille F, Chazalviel L, et al. Reduction of Ischemic Brain Damage by Nitrous Oxide and Xenon. *J Cereb Blood Flow Metab*. 2003;23(10):1168-1173. doi:10.1097/01.WCB.0000087342.31689.18
141. Schmidt M, Marx T, Glöggl E, Reinelt H, Schirmer U. Xenon Attenuates Cerebral Damage after Ischemia in Pigs. *Anesthesiology*. 2005;102(5):929. doi:10.1097/00000542-200505000-00011
142. Fries M, Nolte KW, Coburn M, et al. Xenon reduces neurohistopathological damage and improves the early neurological deficit after cardiac arrest in pigs*. *Crit Care Med*. 2008;36(8):2420. doi:10.1097/CCM.0b013e3181802874
143. Fries M, Brücken A, Çizen A, et al. Combining xenon and mild therapeutic hypothermia preserves neurological function after prolonged cardiac arrest in pigs*. *Crit Care Med*. 2012;40(4):1297. doi:10.1097/CCM.0b013e31823c8ce7

144. Sheng SP, Lei B, James ML, et al. Xenon Neuroprotection in Experimental Stroke: Interactions with Hypothermia and Intracerebral Hemorrhage. *Anesthesiology*. 2012;117(6):1262-1275. doi:10.1097/ALN.0b013e3182746b81
145. Hobbs C, Thoresen M, Tucker A, Aquilina K, Chakkarapani E, Dingley J. Xenon and hypothermia combine additively, offering long-term functional and histopathologic neuroprotection after neonatal hypoxia/ischemia. *Stroke*. 2008;39(4):1307-1313. doi:10.1161/STROKEAHA.107.499822
146. Chakkarapani E, Dingley J, Liu X, et al. Xenon enhances hypothermic neuroprotection in asphyxiated newborn pigs. *Ann Neurol*. 2010;68(3):330-341. doi:10.1002/ana.22016
147. Thoresen M, Hobbs CE, Wood T, Chakkarapani E, Dingley J. Cooling Combined with Immediate or Delayed Xenon Inhalation Provides Equivalent Long-Term Neuroprotection after Neonatal Hypoxia—Ischemia. *J Cereb Blood Flow Metab*. 2009;29(4):707-714. doi:10.1038/jcbfm.2008.163
148. Schwiebert C, Huhn R, Heinen A, et al. Postconditioning by xenon and hypothermia in the rat heart in vivo. *Eur J Anaesthesiol EJA*. 2010;27(8):734. doi:10.1097/EJA.0b013e328335fc4c
149. Roehl AB, Funcke S, Becker MM, et al. Xenon and Isoflurane Reduce Left Ventricular Remodeling after Myocardial Infarction in the Rat. *Anesthesiology*. 2013;118(6):1385-1394. doi:10.1097/ALN.0b013e31828744c0
150. Baumert JH, Hein M, Hecker KE, Satlow S, Neef P, Rossaint R. Xenon or propofol anaesthesia for patients at cardiovascular risk in non-cardiac surgery. *Br J Anaesth*. 2008;100(5):605-611. doi:10.1093/bja/aen050
151. Gao JM, Meng XW, Zhang J, et al. Dexmedetomidine Protects Cardiomyocytes against Hypoxia/Reoxygenation Injury by Suppressing TLR4-MyD88-NF- B Signaling. *BioMed Res Int*. 2017;2017. doi:10.1155/2017/1674613
152. Zi S feng, Li J hui, Liu L, et al. Dexmedetomidine-mediated protection against septic liver injury depends on TLR4/MyD88/NF-κB signaling downregulation partly via cholinergic anti-inflammatory mechanisms. *Int Immunopharmacol*. 2019;76:105898. doi:10.1016/j.intimp.2019.105898
153. Meng L, Li L, Lu S, et al. The protective effect of dexmedetomidine on LPS-induced acute lung injury through the HMGB1-mediated TLR4/NF-κB and PI3K/Akt/mTOR pathways. *Mol Immunol*. 2018;94:7-17. doi:10.1016/j.molimm.2017.12.008
154. Kallio A, Scheinin M, Koulu M, et al. Effects of dexmedetomidine, a selective α2-adrenoceptor agonist, on hemodynamic control mechanisms. *Clin Pharmacol Ther*. 1989;46(1):33-42. doi:10.1038/clpt.1989.103
155. Devlin JW, Lau AK, Tanios MA. Propofol-Associated Hypertriglyceridemia and Pancreatitis in the Intensive Care Unit: An Analysis of Frequency and Risk Factors. *Pharmacotherapy*. 2005;25(10):1348-1352. doi:10.1592/phco.2005.25.10.1348
156. De Sommer MR, Driessen JH, Willems CM, Lust PC. A comparative study on the effects of propofol in emulsion and Intralipid on fat metabolism. *Acta Anaesthesiol Belg*. 1990;41(2):133-138.
157. Edwards LM, Lawler NG, Nikolic SB, et al. Metabolomics reveals increased isoleukotoxin diol (12,13-DHOME) in human plasma after acute Intralipid infusion. *J Lipid Res*. 2012;53(9):1979-1986. doi:10.1194/jlr.P027706
158. Lacoumenta S, Walsh ES, Waterman AE, Ward I, Paterson JL, Hall GM. Effects of ketamine anaesthesia on the metabolic response to pelvic surgery. *Br J Anaesth*. 1984;56(5):493-497.
159. Myat A, Kyoung-Jun S, Rea T. Out-of-hospital cardiac arrest: current concepts. *The Lancet*. 2018;391(10124):970-979. doi:10.1016/S0140-6736(18)30472-0
160. Huikuri HV, Castellanos A, Myerburg RJ. Sudden Death Due to Cardiac Arrhythmias. *N Engl J Med*. 2001;345(20):1473-1482. doi:10.1056/NEJMra000650
161. Atwood C, Eisenberg MS, Herlitz J, Rea TD. Incidence of EMS-treated out-of-hospital cardiac arrest in Europe. *Resuscitation*. 2005;67(1):75-80. doi:10.1016/j.resuscitation.2005.03.021

162. Hiltunen P, Kuisma M, Silfvast T, Rutanen J, Vaahersalo J, Kurola J. Regional variation and outcome of out-of-hospital cardiac arrest (ohca) in Finland - the Finnresusci study. *Scand J Trauma Resusc Emerg Med*. 2012;20. doi:10.1186/1757-7241-20-80
163. The epidemiology of out-of-hospital 'sudden' cardiac arrest. *Resuscitation*. 2002;52(3):235-245. doi:10.1016/S0300-9572(01)00464-6
164. Spaulding CM, Joly LM, Rosenberg A, et al. Immediate Coronary Angiography in Survivors of Out-of-Hospital Cardiac Arrest. *N Engl J Med*. 1997;336(23):1629-1633. doi:10.1056/NEJM199706053362302
165. Kitamura T, Kiyohara K, Sakai T, et al. Epidemiology and outcome of adult out-of-hospital cardiac arrest of non-cardiac origin in Osaka: a population-based study. *BMJ Open*. 2014;4:6462. doi:10.1136/bmjopen-2014
166. Daniele SG, Trummer G, Hossmann KA, et al. Brain vulnerability and viability after ischaemia. *Nat Rev Neurosci*. 2021;22(9):553-572. doi:10.1038/s41583-021-00488-y
167. Stepanova A, Kahl A, Konrad C, Ten V, Starkov AS, Galkin A. Reverse electron transfer results in a loss of flavin from mitochondrial complex I: Potential mechanism for brain ischemia reperfusion injury. *J Cereb Blood Flow Metab*. 2017;37(12):3649. doi:10.1177/0271678X17730242
168. Eltzschig HK, Eckle T. Ischemia and reperfusion-from mechanism to translation. *Nat Med*. 2011;17(11):1391-1401. doi:10.1038/nm.2507
169. Hertz L. Bioenergetics of cerebral ischemia: A cellular perspective. *Neuropharmacology*. 2008;55(3):289-309. doi:10.1016/j.neuropharm.2008.05.023
170. Neumar RW, Nolan JP, Adrie C, et al. Post-cardiac arrest syndrome: Epidemiology, pathophysiology, treatment, and prognostication a consensus statement from the International Liaison Committee on Resuscitation. In: *Circulation*. Vol 118. ; 2008:2452-2483. doi:10.1161/CIRCULATIONAHA.108.190652
171. Laver S, Farrow C, Turner D, Nolan J. Mode of death after admission to an intensive care unit following cardiac arrest. *Intensive Care Med*. 2004;30(11):2126-2128. doi:10.1007/s00134-004-2425-z
172. Herzog N, Laager R, Thommen E, et al. Association of Taurine with In-Hospital Mortality in Patients after Out-of-Hospital Cardiac Arrest: Results from the Prospective, Observational COMMUNICATE Study. *J Clin Med*. 2020;9(5):1405. doi:10.3390/jcm9051405
173. Isenschmid C, Kalt J, Gamp M, et al. Routine blood markers from different biological pathways improve early risk stratification in cardiac arrest patients: Results from the prospective, observational COMMUNICATE study. *Resuscitation*. 2018;130:138-145. doi:10.1016/j.resuscitation.2018.07.021
174. Laaksonen L, Kallioinen M, Långsjö J, et al. Comparative effects of dexmedetomidine, propofol, sevoflurane, and S-ketamine on regional cerebral glucose metabolism in humans: A positron emission tomography study. *Br J Anaesth*. 2018;121(1):281-290. doi:10.1016/j.bja.2018.04.008
175. Domino EF, Domino SE, Smith RE, et al. Ketamine kinetics in unmedicated and diazepam-premedicated subjects. *Clin Pharmacol Ther*. 1984;36(5):645-653.
176. Talke P, Lobo E, Brown R. Systemically administered alpha2-agonist-induced peripheral vasoconstriction in humans. *Anesthesiology*. 2003;99(1):65-70.
177. Marsh B, White M, Morton N, Kenny GN. Pharmacokinetic model driven infusion of propofol in children. *Br J Anaesth*. 1991;67(1):41-48.
178. Långsjö JW, Maksimow A, Salmi E, et al. S-ketamine anesthesia increases cerebral blood flow in excess of the metabolic needs in humans. *Anesthesiology*. 2005;103(2):258-268. doi:10.1097/00000542-200508000-00008
179. Kaskinoro K, Maksimow A, Långsjö J, et al. Wide inter-individual variability of bispectral index and spectral entropy at loss of consciousness during increasing concentrations of dexmedetomidine, propofol, and sevoflurane. *Br J Anaesth*. 2011;107(4):573-580. doi:10.1093/bja/aer196

180. Kaskinoro K, Revonsuo A, Langsjo JW, et al. Returning from oblivion: Imaging the neural core of consciousness. *J Neurosci*. 2012;32(14):4935-4943. doi:10.1523/jneurosci.4962-11.2012
181. Bothwell JHF, Griffin JL. An introduction to biological nuclear magnetic resonance spectroscopy. *Biol Rev*. 2011;86(2):493-510. doi:10.1111/j.1469-185X.2010.00157.x
182. Würtz P, Kangas AJ, Soininen P, Lawlor DA, Davey Smith G, Ala-Korpela M. Quantitative Serum Nuclear Magnetic Resonance Metabolomics in Large-Scale Epidemiology: A Primer on -Omic Technologies. *Am J Epidemiol*. 2017;186(9):1084-1096. doi:10.1093/aje/kwx016
183. Soininen P, Kangas AJ, Würtz P, Suna T, Ala-Korpela M. Quantitative Serum Nuclear Magnetic Resonance Metabolomics in Cardiovascular Epidemiology and Genetics. *Circ Cardiovasc Genet*. 2015;8(1):192-206. doi:10.1161/CIRCGENETICS.114.000216
184. Pitt JJ. Principles and Applications of Liquid Chromatography-Mass Spectrometry in Clinical Biochemistry. *Clin Biochem Rev*. 2009;30(1):19.
185. Finehout EJ, Lee KH. An introduction to mass spectrometry applications in biological research. *Biochem Mol Biol Educ*. 2004;32(2):93-100. doi:10.1002/bmb.2004.494032020331
186. Rodriguez-Aller M, Gurny R, Veuthey JL, Guillarme D. Coupling ultra high-pressure liquid chromatography with mass spectrometry: Constraints and possible applications. *J Chromatogr A*. 2013;1292:2-18. doi:10.1016/j.chroma.2012.09.061
187. Ho CS, Lam CWK, Chan MHM, et al. Electrospray ionisation mass spectrometry: principles and clinical applications. *Clin Biochem Rev*. 2003;24(1):3-12.
188. Xiang X, Han Y, Neuvonen M, Laitila J, Neuvonen PJ, Niemi M. High performance liquid chromatography-tandem mass spectrometry for the determination of bile acid concentrations in human plasma. *J Chromatogr B*. 2010;878(1):51-60. doi:10.1016/j.jchromb.2009.11.019
189. Yamada M, Kita Y, Kohira T, et al. A comprehensive quantification method for eicosanoids and related compounds by using liquid chromatography/mass spectrometry with high speed continuous ionization polarity switching. *J Chromatogr B*. 2015;995-996:74-84. doi:10.1016/j.jchromb.2015.05.015
190. Ren S, Hinzman AA, Kang EL, Szczesniak RD, Lu LJ. Computational and statistical analysis of metabolomics data. *Metabolomics*. 2015;11(6):1492-1513. doi:10.1007/s11306-015-0823-6
191. Kanehisa M, Goto S. KEGG: kyoto encyclopedia of genes and genomes. *Nucleic Acids Res*. 2000;28(1):27-30. doi:10.1093/nar/28.1.27
192. Kujala UM, Mäkinen VP, Heinonen I, et al. Long-term leisure-time physical activity and serum metabolome. *Circulation*. 2013;127(3):340-348. doi:10.1161/CIRCULATIONAHA.112.105551
193. Peterhoff M, Sieg A, Brede M, Chao C, Hein L, Ullrich S. Inhibition of insulin secretion via distinct signaling pathways in alpha2-adrenoceptor knockout mice. *Eur J Endocrinol*. 2003;149(4):343-350. doi:10.1530/eje.0.1490343
194. Dutta S, Lal R, Karol MD, Cohen T, Ebert T. Influence of cardiac output on dexmedetomidine pharmacokinetics. *J Pharm Sci*. 2000;89(4):519-527. doi:10.1002/(SICI)1520-6017(200004)89:4<519::AID-JPS9>3.0.CO;2-U
195. Lawrence CJ, Prinzen FW, de Lange S. The effect of dexmedetomidine on nutrient organ blood flow. *Anesth Analg*. 1996;83(6):1160-1165. doi:10.1097/00000539-199612000-00005
196. Fisher RS, Rock E, Malmud LS. *Cholinergic Effects on Gallbladder Emptying in Humans*. Vol 89.; 1985:716-738.
197. Xiang H, Hu B, Li Z, Li J. Dexmedetomidine controls systemic cytokine levels through the cholinergic anti-inflammatory pathway. *Inflammation*. 2014;37(5):1763-1770. doi:10.1007/s10753-014-9906-1
198. Imig JD. Epoxides and soluble epoxide hydrolase in cardiovascular physiology. *Physiol Rev*. 2012;92(1):101-130. doi:10.1152/physrev.00021.2011
199. Node K, Huo Y, Ruan X, et al. Anti-inflammatory properties of cytochrome P450 epoxygenase-derived eicosanoids. *Science*. 1999;285:1276-1279. doi:10.1126/science.285.5431.1276

200. O'Connell TD, Mason RP, Budoff MJ, Navar AM, Shearer GC. Mechanistic insights into cardiovascular protection for omega-3 fatty acids and their bioactive lipid metabolites. *Eur Heart J Suppl*. 2020;22:J3-J20. doi:10.1093/EURHEARTJ/SUAA115
201. Harris TR, Li N, Chiamvimonvat N, Hammock BD. The Potential of Soluble Epoxide Hydrolase Inhibition in the Treatment of Cardiac Hypertrophy. *Congest Heart Fail*. 2008;14(4):219-224. doi:10.1111/j.1751-7133.2008.08430.x
202. Liu JY, Yang J, Inceoglu B, et al. Inhibition of soluble epoxide hydrolase enhances the anti-inflammatory effects of aspirin and 5-lipoxygenase activation protein inhibitor in a murine model. *Biochem Pharmacol*. 2010;79(6):880-887. doi:10.1016/j.bcp.2009.10.025
203. Samokhvalov V, Jamieson KL, Darwesh AM, et al. Deficiency of soluble epoxide hydrolase protects cardiac function impaired by LPS-induced acute inflammation. *Front Pharmacol*. 2019;9:1572. doi:10.3389/fphar.2018.01572
204. Schmelzer KR, Kubala L, Newman JW, Kim IH, Eiserich JP, Hammock BD. Soluble epoxide hydrolase is a therapeutic target for acute inflammation. *Proc Natl Acad Sci*. 2005;102(28):9772-9777. doi:10.1073/pnas.0503279102
205. Shen L, Peng H, Peng R, et al. Inhibition of soluble epoxide hydrolase in mice promotes reverse cholesterol transport and regression of atherosclerosis. *Atherosclerosis*. 2015;239(2):557-565. doi:10.1016/j.atherosclerosis.2015.02.014
206. Gilroy DW, Edin ML, De Maeyer RPH, et al. CYP450-derived oxylipins mediate inflammatory resolution. *Proc Natl Acad Sci*. 2016;113(23):E3240-E3249. doi:10.1073/pnas.1521453113
207. O'Kane A, Quinney SK, Kinney E, Bergstrom RF, Tillman EM. A systematic review of dexmedetomidine pharmacology in pediatric patients. *Clin Transl Sci*. 2024;17(12):e70020. doi:10.1111/cts.70020
208. Du Y, Taylor CG, Aukema HM, Zahradka P. Role of oxylipins generated from dietary PUFAs in the modulation of endothelial cell function. *Prostaglandins Leukot Essent Fatty Acids*. 2020;160:102160. doi:10.1016/j.plefa.2020.102160
209. Aoyama H, Suzuki K, Izawa Y, Kobashashi M, Ozawa T. Mitochondria-toxic activity in burned human skin: relation to severity of burn and period after burn. *Burns*. 1982;9(1):13-16. doi:10.1016/0305-4179(82)90129-2
210. Zheng J, Plopper CG, Lakritz J, Storms DH, Hammock BD. Leukotoxin-Diol: A putative toxic mediator involved in acute respiratory distress syndrome. *Am J Respir Cell Mol Biol*. 2001;25(4):434-438. doi:10.1165/ajrcmb.25.4.4104
211. Sisemore MF, Zheng J, Yang JC, et al. Cellular characterization of leukotoxin diol-induced mitochondrial dysfunction. *Arch Biochem Biophys*. 2001;392:32-37. doi:10.1006/abbi.2001.2434
212. Stanford KI, Lynes MD, Takahashi H, et al. 12,13-diHOME: An exercise-induced lipokine that increases skeletal muscle fatty acid uptake. *Cell Metab*. 2018;27(5):1111-1120.e3. doi:10.1016/j.cmet.2018.03.020
213. Pinckard KM, Shettigar VK, Wright KR, et al. A Novel Endocrine Role for the BAT-Released Lipokine 12,13-diHOME to Mediate Cardiac Function. *Circulation*. 2021;143(2):145-159. doi:10.1161/CIRCULATIONAHA.120.049813
214. Flanders CA, Rocke AS, Edwardson SA, Baillie JK, Walsh TS. The effect of dexmedetomidine and clonidine on the inflammatory response in critical illness: A systematic review of animal and human studies. *Crit Care*. 2019;23:402. doi:10.1186/s13054-019-2690-4
215. Hu AM, Zhong XX, Li Z, Zhang ZJ, Li HP. Comparative effectiveness of midazolam, propofol and dexmedetomidine in patients with or at risk for acute respiratory distress syndrome: A propensity score-matched cohort study. *Front Pharmacol*. 2021;12:352. doi:10.3389/fphar.2021.614465
216. Tracey KJ. The inflammatory reflex. *Nature*. 2002;420(6917):853-859. doi:10.1038/nature01321
217. Pavlov VA, Wang H, Czura CJ, Friedman SG, Tracey KJ. The Cholinergic Anti-inflammatory Pathway: A Missing Link in Neuroimmunomodulation. *Mol Med*. 2003;9(5-8):125-134. doi:10.1007/bf03402177

218. Wu Y jin, Wang L, Ji C fan, Gu S fei, Yin Q, Zuo J. The Role of α7nAChR-Mediated Cholinergic Anti-inflammatory Pathway in Immune Cells. *Inflammation*. 2021;44(3):821-834. doi:10.1007/s10753-020-01396-6
219. Kong W, Kang K, Gao Y, et al. Dexmedetomidine alleviates LPS-induced septic cardiomyopathy via the cholinergic anti-inflammatory pathway in mice. *Am J Transl Res*. 2017;9(11):5040-5047.
220. Kawai T, Akira S. Signaling to NF-κB by Toll-like receptors. *Trends Mol Med*. 2007;13(11):460-469. doi:10.1016/j.molmed.2007.09.002
221. Viswanathan S, Hammock BD, Newman JW, Meerarani P, Toborek M, Hennig B. Involvement of CYP 2C9 in mediating the proinflammatory effects of linoleic acid in vascular endothelial cells. *J Am Coll Nutr*. 2003;22(6):502-510. doi:10.1080/07315724.2003.10719328
222. Chung SW, Kang BY, Kim SH, et al. Oxidized low density lipoprotein inhibits interleukin-12 production in lipopolysaccharide-activated mouse macrophages via direct interactions between peroxisome proliferator-activated receptor-γ and nuclear factor-κB. *J Biol Chem*. 2000;275(42):32681-32687. doi:10.1074/jbc.M002577200
223. Oyri LKL, Hansson P, Bogsrud MP, et al. Delayed postprandial TAG peak after intake of SFA compared with PUFA in subjects with and without familial hypercholesterolaemia: A randomised controlled trial. *Br J Nutr*. 2018;119(10):1142-1150. doi:10.1017/S0007114518000673
224. Coppack SW, Jensen MD, Miles JM. In vivo regulation of lipolysis in humans. *J Lipid Res*. 1994;35(2):177-193. doi:10.1016/S0022-2275(20)41207-6
225. Clouet P, Niot I, Bézard J. Pathway of α-linolenic acid through the mitochondrial outer membrane in the rat liver and influence on the rate of oxidation. Comparison with linoleic and oleic acids. *Biochem J*. 1989;263(3):867-873. doi:10.1042/bj2630867
226. Misheva M, Kotzamanis K, Davies LC, et al. Oxylipin metabolism is controlled by mitochondrial β-oxidation during bacterial inflammation. *Nat Commun*. 2022;13(1):139. doi:10.1038/s41467-021-27766-8
227. Jorens PG, Van den Eynden GG. Propofol infusion syndrome with arrhythmia, myocardial fat accumulation and cardiac failure. *Am J Cardiol*. 2009;104(8):1160-1162. doi:10.1016/j.amjcard.2009.05.065
228. Peake JM, Tan SJ, Markworth JF, Broadbent JA, Skinner TL, Cameron-Smith D. Metabolic and hormonal responses to isoenergetic high-intensity interval exercise and continuous moderate-intensity exercise. *Am J Physiol - Endocrinol Metab*. 2014;307(7):E539-E552. doi:10.1152/ajpendo.00276.2014
229. Hanouz JL, Zhu L, Persehaye E, et al. Ketamine Preconditions Isolated Human Right Atrial Myocardium: Roles of Adenosine Triphosphate–sensitive Potassium Channels and Adrenoceptors. *Anesthesiology*. 2005;102(6):1190-1196. doi:10.1097/00000542-200506000-00019
230. Kienbaum P, Heuter T, Pavlakovic G, Michel MC, Peters J. S (+)-Ketamine Increases Muscle Sympathetic Activity and Maintains the Neural Response to Hypotensive Challenges in Humans. *Anesthesiology*. 2001;94(2):252-258. doi:10.1097/00000542-200102000-00014
231. Qvisth V, Hagström-Toft E, Enoksson S, Bolinder J. Catecholamine Regulation of Local Lactate Production in Vivo in Skeletal Muscle and Adipose Tissue: Role of β-Adrenoreceptor Subtypes. *J Clin Endocrinol Metab*. 2008;93(1):240-246. doi:10.1210/jc.2007-1313
232. Pitkänen H, Mero A, Oja SS, et al. Serum amino acid responses to three different exercise sessions in male power athletes. *J Sports Med Phys Fitness*. 2002;42(4):472-480.
233. Marliss EB, Aoki TT, Toews CJ, et al. Amino acid metabolism in lactic acidosis. *Am J Med*. 1972;52(4):474-481. doi:10.1016/0002-9343(72)90038-1
234. Mak RHK. Effect of metabolic acidosis on branched-chain amino acids in uremia. *Pediatr Nephrol*. 1999;13(4):319-322. doi:10.1007/s004670050617
235. Hara Y, May RC, Kelly RA, Mitch WE. Acidosis, not azotemia, stimulates branched-chain, amino acid catabolism in uremic rats. *Kidney Int*. 1987;32(6):808-814. doi:10.1038/ki.1987.280

236. May RC, Hara Y, Kelly RA, Block KP, Buse MG, Mitch WE. Branched-chain amino acid metabolism in rat muscle: abnormal regulation in acidosis. *Am J Physiol-Endocrinol Metab*. 1987;252(6):E712-E718. doi:10.1152/ajpendo.1987.252.6.E712
237. Reaich D, Channon SM, Scrimgeour CM, Goodship TH. Ammonium chloride-induced acidosis increases protein breakdown and amino acid oxidation in humans. *Am J Physiol-Endocrinol Metab*. 1992;263(4):E735-E739. doi:10.1152/ajpendo.1992.263.4.E735
238. Zhang J, Wang YT, Miller JH, Day MM, Munger JC, Brookes PS. Accumulation of Succinate in Cardiac Ischemia Primarily Occurs via Canonical Krebs Cycle Activity. *Cell Rep*. 2018;23(9):2617-2628. doi:10.1016/j.celrep.2018.04.104
239. Sonnewald U. Glutamate synthesis has to be matched by its degradation - where do all the carbons go? *J Neurochem*. 2014;131(4):399-406. doi:10.1111/jnc.12812
240. Blondin DP, Frisch F, Phoenix S, et al. Inhibition of Intracellular Triglyceride Lipolysis Suppresses Cold-Induced Brown Adipose Tissue Metabolism and Increases Shivering in Humans. *Cell Metab*. 2017;25(2):438-447. doi:10.1016/j.cmet.2016.12.005
241. Yoneshiro T, Wang Q, Tajima K, et al. BCAA catabolism in brown fat controls energy homeostasis through SLC25A44. *Nature*. 2019;572(7771):614-619. doi:10.1038/s41586-019-1503-x
242. Selldén E, Lindahl SGE. Amino Acid-Induced Thermogenesis Reduces Hypothermia During Anesthesia and Shortens Hospital Stay. *Anesth Analg*. 1999;89(6):1551. doi:10.1097/00000539-199912000-00045
243. Selldén E, Bränström R, Brundin T. *Preoperative Infusion of Amino Acids Prevents Postoperative Hypothermia*. Vol 76.; 1996:227-234. doi:10.1093/bja/76.2.227
244. Nielsen N, Wetterslev J, Cronberg T, et al. Targeted Temperature Management at 33°C versus 36°C after Cardiac Arrest. *N Engl J Med*. 2013;369(23):2197-2206. doi:10.1056/nejmoa1310519
245. Dankiewicz J, Cronberg T, Lilja G, et al. Hypothermia versus Normothermia after Out-of-Hospital Cardiac Arrest. *N Engl J Med*. 2021;384(24):2283-2294. doi:10.1056/nejmoa2100591
246. Yudkoff M. Interactions in the Metabolism of Glutamate and the Branched-Chain Amino Acids and Ketoacids in the CNS. *Neurochem Res*. 2017;42(1):10-18. doi:10.1007/s11064-016-2057-z
247. Salcedo C, Andersen JV, Vinten KT, et al. Functional Metabolic Mapping Reveals Highly Active Branched-Chain Amino Acid Metabolism in Human Astrocytes, Which Is Impaired in iPSC-Derived Astrocytes in Alzheimer's Disease. *Front Aging Neurosci*. 2021;13:553. doi:10.3389/fnagi.2021.736580
248. Yudkoff M, Nissim I, Hummeler K, Medow M, Pleasure D. Utilization of [15N]glutamate by cultured astrocytes. *Biochem J*. 1986;234(1):185-192. doi:10.1042/bj2340185
249. McKenna MC, Stridh MH, McNair LF, Sonnewald U, Waagepetersen HS, Schousboe A. Glutamate oxidation in astrocytes: Roles of glutamate dehydrogenase and aminotransferases. *J Neurosci Res*. 2016;94(12):1561-1571. doi:10.1002/jnr.23908
250. Schousboe A, Scafidi S, Bak LK, Waagepetersen HS, McKenna MC. Glutamate Metabolism in the Brain Focusing on Astrocytes. *Adv Neurobiol*. 2014;11:13-30. doi:10.1007/978-3-319-08894-5_2
251. Sharma B, Lawrence DW, Hutchison MG. Branched Chain Amino Acids (BCAAs) and Traumatic Brain Injury: A Systematic Review. *J Head Trauma Rehabil*. 2018;33(1):33-45. doi:10.1097/HTR.0000000000000280
252. Jeter CB, Hergenroeder GW, Ward NH, Moore AN, Dash PK. Human mild traumatic brain injury decreases circulating branched-chain amino acids and their metabolite levels. *J Neurotrauma*. 2013;30(8):671-679. doi:10.1089/neu.2012.2491
253. Dickinson R, Franks NP. Bench-to-bedside review: Molecular pharmacology and clinical use of inert gases in anesthesia and neuroprotection. *Crit Care*. 2010;14(4):229. doi:10.1186/cc9051
254. Nummela AJ, Laaksonen LT, Laitio TT, et al. Effects of dexmedetomidine, propofol, sevoflurane and S-ketamine on the human metabolome: A randomised trial using nuclear magnetic resonance spectroscopy. *Eur J Anaesthesiol*. 2021;39(6):521-532. doi:10.1097/EJA.0000000000001591

List of Figures and Tables

Figures

Tables

TURUN
YLIOPISTO
UNIVERSITY
OF TURKU

Painosalama, Turku, Finland 2025

ISBN 978-952-02-0219-4 (PRINT)
ISBN 978-952-02-0220-0 (PDF)
ISSN 0355-9483 (Print)
ISSN 2343-3213 (Online)